KING FAHD UNIVERSITY OF PETROLEUM AND MINERALS

DEPARTMENT OF PHYSICS

INSTRUCTOR'S/COORDINATOR'S REPORT

Course: **Phys 503** No. of Sections: **7** Term: **142**
Instructor's/Coordinator's Name: Dr. Abdulaziz M. Al-Jalal

I. STUDENTS

The following information should be supplied based on the ***FINAL ROSTER*** of grades issued by the Registrar:

No. of the students who received	W	1
No. of the students who received	WP	0
No. of the students who received	WF	0
No. of the students who received	DN	0
No. of the students who received	Z	0
No. of the students who received	AU	0
No. of the students (excluding the above) who took the Final Examination		0
No. of the students (excluding the above) who missed the Final Examination		0
	TOTAL	11

II. RANGE OF EACH LETTER GRADE

Range	A+≥83	83>A≥80.5	80.5>B+≥76	76>B≥70	
Range	70>C+≥65	65>C≥60	60>D+≥55	55>D≥50	50≥F

Course overall average: **78.5 %** Std. Dev.: **3.6**

III. DISTRIBUTION OF GRADES

	A+	**A**	**B+**	**B**	**C+**	**C**	**D+**	**D**	**F**	**IC**	**TOTALS OF A+, A, B+, B, C+, C, D+, D, F, IC**
No. of students	1	2	4	3							10
% of students	10	20	40	30							**100%**

$$\text{GRADE POINT AVERAGE} = \frac{4A^{+} + 3.75A + 3.5B^{+} + 3B + 2.5C^{+} + 2C + 1.5D^{+} + D}{A^{+} + A + B^{+} + B + C^{+} + C + D^{+}} = 3.45$$

PLEASE ATTACH FINAL ROSTER OF GRADES.

IV. SAMPLES

Homework assignments ( )
Quizzes ( )
Examinations ( )
Projects ( )
Samples of graded student work, including computer assignments (√)

(Please put a tick in the parenthesis if copies are attached)

V. **“IC” GRADES**

Number of students given the “IC” grade: 0.

Attach a report on each “IC” grade providing the following information:

(a) Student’s ID #, Name, Section #, and Instructor’s Name.
(b) Reason for giving an “IC” grade.
(c) Precise requirements for the removal of “IC” grade, including time and method.

VI. **SYLLABUS**

A copy of the course syllabus **covered** should be attached.

VII. **FINAL EXAMINATION**

A copy of the final exam should be attached (a copy of the key solution is recommended).

VIII. **USE OF COMPUTER IN THE COURSE**

Describe the use of computers in the course e.g. description of the problem, software used, etc.

Students have used computers in data collection, data analysis, reports writing and presentations.

IX. **STUDENTS’ REMARKS** (BASED ON COURSE EVALUATION OR OTHER SOURCES).

Please see the next page.

X. **INSTRUCTOR’S REMARKS**

1- This course is demanding and a lot of time is spent in helping the students to perform their experiments, advise them in writing their reports and making their presentations. Also, the course requires grading many reports and attending many presentations. The load for teaching this course should be counted as 3 graduate course credit hours. Currently it seems the teaching load for this course is treated as the load of teaching a physics 101 lab.
2- Some students do not start their experiments at the beginning of the experiment period.
3- Many old reports available to students and some students are copying from these reports. Use Authenticate to check reports.

XI. **RECOMMENDATIONS**

1- The load for teaching this course should be counted as 3 graduate course credit hours.
2- There should be a fixed time for attending this lab for all students and for all experiments. This might solve the problem of starting the experiment on time.
3- Use Authenticate to check reports or give more weight on presentations.

Students’ comments from course evaluation

Instructor	**Students’ Comments**
Dwaikat	He should come with preparation to distribute his time. It happened in other time he kept us in the Lab for one hour with no much work and the work in the course for 2 hours or less. In the future, I will not take course with this instructor.
Dwaikat	We spend 3 weeks with taking any results, so we lost much time that lead to put more pressure on us to finish all work in one week. Also, he ask us to come more than four times in the week.
Dwaikat	During the experiment I was not clear till end what we are going to do. After submission of any report, no one mentioned that we need to calculate, also we speak irrelevant and get angry.
Faiz	He is helpful, gentle with his students and always try to let his students to learn and keeps monitoring them. If possible, I would love to take more courses with him in the future.
Faiz	Truly through the experiment cannot be predicted to learn on this topic.
Faiz	He is an excellent instructor, I ever met in this university. He was very much clear, about the subject experiment. He is very hard work and punctual. His way of teaching is very nice. He always concerned about his students understanding. He should be encouraged by university.
Faiz	Dr. Faiz is very nice open mind, always helping, and hard worker and disciplined.
Gondal	Very nice instructor, best in rest of all instructor with whom I did work. He is very much responsible in report seeing results evaluations and also has very good behavior towards questions. Kindly made to research with him.
Gondal	Professor Dr. Gondal is very nice and hard worker, disciplined, always helping.
Harrabi	I did not get much knowledge from him. He get angry when I asked him any questions. We want very quickly through the experiment.
Harrabi	This experiment was good for me, instructor was good explaining with the help of computer slides. Only the lacking work explanation was too fast.
Harrabi	The topic is too complicated to be explain and understand physically and methodically from such short time.
Naqvi	Professor Dr. Naqvi is very hard worker, disciplined, always helping students.
Ziq	He was helpful, gentle with his students and always try to let no learn and keeps motivates us. In the future, if possible, I would like to take more course with same instructor.
Ziq	He is a nice instructor with good understanding of the subject. Sometimes, he has too much work load so can give proper time to our graduate lab experiment. Overall he is very good instructor.

Grading policy

20%	Interactions with your advisor, experimental work, and following safety regulations.	Assigned by the current experiment advisor.
30%+	Report	Assigned by the current experiment advisor.
25%	Report	Assigned by two other advisors
25%	Presentation	Assigned by three other advisors

Experiments offered for phys503-142

code	Advisor	Experiment title
E101	Dr. Gondal	Laser induced breakdown spectroscopy
E102	Dr. Gondal	Nano materials by laser ablation in liquid
E205	Dr. Faiz	X-ray photoelectron spectroscopy
E206	Dr. Harrabi	Hot spots in superconductor strip
E207	Dr. Ziq	Giant magneto-resistance
E208	Dr. Ziq	Transport properties of superconductor
E301	Dr. Naqvi	Prompt gamma activation analysis
E302	Dr. Naqvi	Thermal neutron activation analysis
E303	Dr. Dwaikat	Gamma spectroscopy

Students' names and their grades

SN	ID	Name	Total	Grade
1	200991810	Mohamed Shemis	74.5	B
2	201304190	Sadig Al-Buradah	74.0	B
3	201402880	Amar Mohamedkhair	81.3	A
4	201403420	Ibsal Assi	72.2	B
5	201405000	Fatai Liadi	80.9	A
6	201405340	Muhammad Younas	79.4	B+
7	201407880	Mohsin Sarwar	83.1	A+
8	201408060	Lutfi Surachman	79.2	B+
9	201408460	Zamzam Ibnu Sina	79.8	B+
10	201409260	Idris Popoola	80.1	B+

King Fahd University of Petroleum and Minerals
Department of Physics
Physics 503 - Term 142

Memo

Date : 6 Feb. 2015
Subject: Experiment Assignments

Below are your assigned experiments. Please, contact your advisor to set suitable times for meetings. Your report is due on the last day of the assigned experiment. For example, the report for the first experiment is due on 8 Mar. A delay in submitting your report causes a deduction of 5% of your grade per day. Your presentation will be scheduled within a week after the due date of your report.

	ID	First name	Last Name	Exp #1 8 Feb - 8 Mar	Exp #2 8 Mar - 12 Apr	Exp #3 12 Apr - 10 May
1	200991810	Mohamed	Shemis	E102	E207	E302
2	201304190	Sadig	Al-Buradah	E205	E301	E207
3	201402880	Amar	Mohamedkhair	E303	E206	E102
4	201403420	Ibsal	Assi	E303	E205	E208
5	201405000	Fatai	Liadi	E302	E206	E101
6	201405340	Muhammad	Younas	E205	E208	E303
7	201407820	Mujahid	Sadaqat	E208	E303	E205
8	201407880	Mohsin	Sarwar	E101	E302	E206
9	201408060	Lutfi	Surachman	E301	E101	E205
10	201408460	Zamzam	Ibnu Sina	E206	E205	E301
11	201409260	Idris	Popoola	E207	E102	E206

code	Advisor	Experiment title
E101	Dr. Gondal	Laser induced breakdown spectroscopy
E102	Dr. Gondal	Nano materials by laser ablation in liquid
E205	Dr. Faiz	X-ray photoelectron spectroscopy
E206	Dr. Harrabi	Hot spots in superconductor strip
E207	Dr. Ziq	Giant magnetoresistance
E208	Dr. Ziq	Transport properties of superconductor
E301	Dr. Naqvi	Prompt gamma activation analysis
E302	Dr. Naqvi	Thermal neutron activation analysis
E303	Dr. Dwaikat	Gamma spectroscopy

King Fahd University of Petroleum and Minerals
Department of Physics
Physics 503 - Term 142

Memo

Date : 24 Feb. 2015
Subject: guidelines for report, presentation and advisor-student interaction

Report

- **Title page**
  - ✓ **Title of the experiment**
  - ✓ **Course name and term**
  - ✓ **Name of student and ID number**
  - ✓ **Name of supervisor**
  - ✓ **Date of submission**
- **Table of contents page**
- **Abstract page ——————————(maximum 1/2 page)———— 1/25**
  - ✓ Brief summary of the technique used and main findings.
- **Introduction————————————(maximum 2 pages)———— 5/25**
  - ✓ Background including, basic principle and theory, a brief review of literature.
  - ✓ Objectives
- **Experimental details——————(maximum 4 pages) ———— 6/25**
  - ✓ Description of equipment
  - ✓ Sample preparation
  - ✓ Description of methods used.
- **Results and Discussion—————(maximum 6 pages)———— 9 /25**
  - ✓ States the results of the research.
  - ✓ Data analysis
  - ✓ Discussion of results
- **Conclusion——————————————(maximum 1/2 page) ———— 1/25**
  - ✓ Summary of results and main findings.
- **References ————————————(maximum 1 pages) ———— 1/25**

Overall ———————————————————————————————— 2/25

Presentation

- **Project Title , student's name, supervisor's name**
- **Presentation Outline**———————————**(max 1 slide)**
    - ✓ Introduction
    - ✓ Theoretical Background
    - ✓ Experimental
    - ✓ Results and Discussion
    - ✓ Conclusion
- **Introduction**———————————————**(max 3 slides)**
    - ✓ Brief review of the work and literature.
- **Theoretical Background**——————————**(max 2 slides)**
    - ✓ Basic principle
- **Experimental procedure**——————————**(max 3 slides)**
    - ✓ Equipment used
    - ✓ Sample fabrication
    - ✓ Experimental measurement
- **Results and Discussion**———————————**(max 5 slides)**
    - ✓ Data Analysis and Interpretation
- **Conclusion**———————————————**(max 1 slide)**

	grades
Subject knowledge Correctness of the slides Question and answer Subject understanding	**10/25**
Clarity Graphics Logical sequence of presentation	**6/25**
Delivery Eye contact and Body language Language and Sound level	**3/25**
Time management Not exceeding the allocated time Balanced time distribution among topics	**3/25**
overall	**3/25**

Advisor-Student Interaction

- **Punctuality and Meeting deadlines**————————————**3/20**
- **Development of experimental skills**————————————**8/20**
  - ✓ Preparation for experiment - reading
  - ✓ Participation in doing the experiment
  - ✓ Checking validity of data
  - ✓ Keeping the experimental area clean and in order
  - ✓ Maintain experimental record
- **Interaction with Advisor**————————————**6/20**
  - ✓ Attitude and behavior
  - ✓ Answering questions
  - ✓ Discussing the experimental procedure and results
- **Ethical Responsibility**————————————**2/20**
  - ✓ Reporting his own data
- **Safety Concern**————————————**1/20**
  - ✓ Wearing proper safety gadgets
  - ✓ Handling equipment and chemicals properly

King Fahd University of Petroleum and Minerals
Department of Physics
Phys503 - Term 142

Presentations Schedules

Experiment #1

date	time	Room	Code	ID	Name	eval-1	eval-2	eval-3
10-Mar	0400-0435	6-209	E101	201407880	Sarwar	Fiaz	Naqvi	Ziq
10-Mar	0400-0435	6-211	E205	201304190	Al-Buradah	Dwiakat	Gondal	Harrabi
10-Mar	0445-0520	6-209	E102	200991810	Shemis	Fiaz	Naqvi	Ziq
10-Mar	0445-0520	6-211	E205	201405340	Younas	Dwiakat	Gondal	Harrabi
10-Mar	0600-0635	6-209	E303	201402880	Mohamedkhair	Fiaz	Naqvi	Ziq
10-Mar	0600-0635	6-211	E301	201408060	Surachman	Dwiakat	Gondal	Harrabi
12-Mar	0400-0435	6-209	E207	201409260	Popoola	Dwiakat	Gondal	Harrabi
12-Mar	0400-0435	6-211	E206	201408460	Ibnu Sina	Fiaz	Naqvi	Ziq
12-Mar	0445-0520	6-209	E208	201407820	Sadaqat	Dwiakat	Gondal	Harrabi
12-Mar	0445-0520	6-211	E303	201403420	Assi	Fiaz	Naqvi	Ziq
12-Mar	0600-0635	6-209	E302	201405000	Liadi	Dwiakat	Gondal	Harrabi

Experiment #2

date	time	Room		ID		eval-1	eval-2	eval-3
21-Apr	0400-0435	6-209	E101	201408060	Surachman	Fiaz	Naqvi	Ziq
21-Apr	0445-0520	6-209	E102	201409260	Popoola	Fiaz	Naqvi	Ziq
21-Apr	0400-0435	6-211	E208	201405340	Younas	Dwiakat	Gondal	Harrabi
21-Apr	0445-0520	6-211	E205	201408460	Ibnu Sina	Dwiakat	Gondal	Harrabi
21-Apr	0530-0605	6-211	E207	200991810	Shemis	Dwiakat	Gondal	Harrabi
23-Apr	0400-0435	6-209	E206	201402880	Mohamedkhair	Fiaz	Naqvi	Ziq
23-Apr	0445-0520	6-209	E206	201405000	Liadi	Fiaz	Naqvi	Ziq
23-Apr	0400-0435	6-211	E205	201403420	Assi	Dwiakat	Gondal	Harrabi
23-Apr	0445-0520	6-211	E301	201304190	Al-Buradah	Dwiakat	Gondal	Harrabi
23-Apr	0530-0605	6-211	E302	201407880	Sarwar	Dwiakat	Gondal	Harrabi

Experiment #3

date	time	Room		ID		eval-1	eval-2	eval-3
13-May	0400-0435	6-209	E101	201405000	Liadi	Fiaz	Naqvi	Ziq
13-May	0445-0520	6-209	E102	201402880	Mohamedkhair	Fiaz	Naqvi	Ziq
14-May	0400-0435	6-211	E205	201408060	Surachman	Dwiakat	Gondal	Harrabi
14-May	0400-0435	6-209	E206	201407880	Sarwar	Fiaz	Naqvi	Ziq
14-May	0445-0520	6-209	E206	201409260	Popoola	Fiaz	Naqvi	Ziq
13-May	0400-0435	6-211	E207	201304190	Al-Buradah	Dwiakat	Gondal	Harrabi
13-May	0445-0520	6-211	E208	201403420	Assi	Dwiakat	Gondal	Harrabi
13-May	0530-0605	6-211	E301	201408460	Ibnu Sina	Dwiakat	Gondal	Harrabi
14-May	0445-0520	6-211	E302	200991810	Shemis	Dwiakat	Gondal	Harrabi
14-May	0530-0605	6-209	E303	201405340	Younas	Fiaz	Naqvi	Ziq

Samples of graded student work

King Fahd University of Petroleum and Minerals
Department of Physics
Phys503 - Term 142

Experiment #1 Work

Student Name : Mohsin Sarwar

Student ID : 201407880

Code : E101

✓ Evaluator : Dr. Gondal

Advisor-Student Interaction

	grades	Out of
Punctuality and Meeting deadlines	3	3
Development of experimental skills	6	8
Interaction with Advisor	6	6
Ethical Responsibility	2	2
Safety Concern	1	1
Total	18	**20**

King Fahd University of Petroleum and Minerals
Department of Physics
Physics 503 - Term 142

Experiment #1 Talk

Student Name : Mohsin Sarwar

Student ID : 201407880

Code : E101

Evaluator : Dr. Faiz

	grades	Out of
Subject knowledge Correctness of the slides Question and answer Subject understanding	9	10
Clarity Graphics Logical sequence of presentation	4	6
Delivery Eye contact and Body language Language and Sound level	2	3
Time management Not exceeding the allocated time Balanced time distribution among topics	3	3
overall	2	3
Total	20	**25**

7- Apr- 2015

King Fahd University of Petroleum and Minerals
Department of Physics
Physics 503 - Term 142

Experiment #1 Talk

Student Name : Mohsin Sarwar

Student ID : 201407880

Code : E101

Evaluator : Dr. Ziq

	grades	Out of
Subject knowledge Correctness of the slides Question and answer Subject understanding	9	10
Clarity Graphics Logical sequence of presentation	4	6
Delivery Eye contact and Body language Language and Sound level	2	3
Time management Not exceeding the allocated time Balanced time distribution among topics	2	3
overall	2	3
Total	20	**25**

King Fahd University of Petroleum and Minerals
Department of Physics
Physics 503 - Term 142

Experiment #1 Talk

Student Name : Mohsin Sarwar

Student ID : 201407880

Code : E101

Evaluator : Dr. Naqvi

March 10, 2015

	grades	Out of
Subject knowledge Correctness of the slides Question and answer Subject understanding	8	10
Clarity Graphics Logical sequence of presentation	2	6
Delivery Eye contact and Body language Language and Sound level	2	3
Time management Not exceeding the allocated time Balanced time distribution among topics	2	3
overall	3	3
Total	19	**25**

19/25

King Fahd University of Petroleum and Minerals
Department of Physics
Physics 503 - Term 142

Experiment #1 Report

Student Name : Mohsin Sarwar

Student ID : 201407880

Code : E101

Evaluator : Dr. Gondal

	grades	Out of
Abstract	1	1
Introduction	5	5
Experimental details	5	6
Results and Discussion	7	9
Conclusion	1	1
References	1	1
Overall	2	2
Total	22	**25**

KING FAHD UNIVERSITY OF PETROLEUM AND MINERALS

DHAHRAN

DEPARTMENT OF PHYSICS

PHYS 503- GRADUATE LABORATORY

EXPERIMENTAL REPORT ON:

جامعة الملك فهد للبترول و المعادن
قسم الفيزياء
RECEIVED
09 Mar. 2015
وارد
King Fahd University of Petroleum & Minerals
PHYSICS DEPT

LASER INDUSED BREAKDOWN SPECTOCOPY (LIBS) AND ITS APPLICATION IN MATERIAL CHARACTERIZATION

PREPARED BY:

MOHSIN SARWAR

ID#: G201407880

SUPERVISED BY:

PROF. M.A. GONDAL

FEB-MAR: 2015

TABLE OF CONTENTS

Abstract

This report is regarding elemental analysis of different samples for learning about the application and physics of the laser induced breakdown spectroscopy (LIBS). LIBS is one of the most efficient tool for elemental analysis based on spectral analyses. The spectral lines of elements were recorded using solid samples by preparing them in the form of pallets containing the elements Ni, Cr, Co, Br, O and K, and by identification using standard NIST database. The calibration curve for detection of nickel was also drawn using standard samples of different concentrations containing Ni. The dependence of the LIBS signal intensity on the incident laser energy and time delay between the laser pulse and data acquisition system were also investigated.

1.0 Introduction

LIBS is one of the best technique that ~~can~~ provide s distinct spectral lines and characteristics of all the chemical species present d in a test sample. [1-5] A unique property of the LIBS is that samples do not need to be fluoresce, IR or Raman active. In this technique one can irradiate any sample with a laser beam and measure its optical spectrum. The laser beam initiates luminous plasma from the test sample and the plasma spectrum is the signature of the chemical species present in the sample.

In this report, the concept of the LIBS and how LIBS system works are discussed and the results obtained using LIBS technique to detect atomic emission lines of Ni, Cr, Co, Br, K and O are presented.

1.1 Laser Induced Breakdown Spectroscopy (LIBS)

LIBS is one of the technique of atomic emission spectroscopy (AES) which uses the laser to generate plasma by thermal vaporization, atomization and excitation of the sample. LIBS can analyze qualitatively any material irrespective of its physical state like solid, liquid and gas. The line wavelengths and intensities are ~~taken~~ recorded from laser produced plasma generated from the sample are identified using standard data base (NIST) qualitatively.

LIBS has the following advantages over the other techniques of atomic emission spectroscopy. [6-10]

- Very little sample is needed.
- All states of matter can be analyzed, as well as for both conductive and nonconductive samples.
- No waste is generated as very small amount of sample is ionized.
- Capability in harsh environment by remote analysis.
- Atomization and excitation are done in one step.
- Capable of multi elemental analysis.

1.2 Nd: YAG Laser

In LIBS Nd: YAG (neodymium doped Yttrium aluminums garnet Nd:$Y_3Al_5O_{12}$) solid state laser is used. Nd is lasing material which replaces 1% of yttrium ion from YAG. This laser has 1064nm wavelength which could be changed using nonlinear crystal to 1/4 (266 nm) of the actual wavelength. This change in the frequency is done by placing a nonlinear material in the path of laser, this material is polarized. Dipoles emit electromagnetic radiation of almost the double of the absorbing frequency due to their vibrations. Mainly there are two types of Nd: YAG laser one is the continuous wave laser (low energy) and the second is pulsed laser (high energy). In this experiment we are using pulse laser which is powerful as compared to other one.

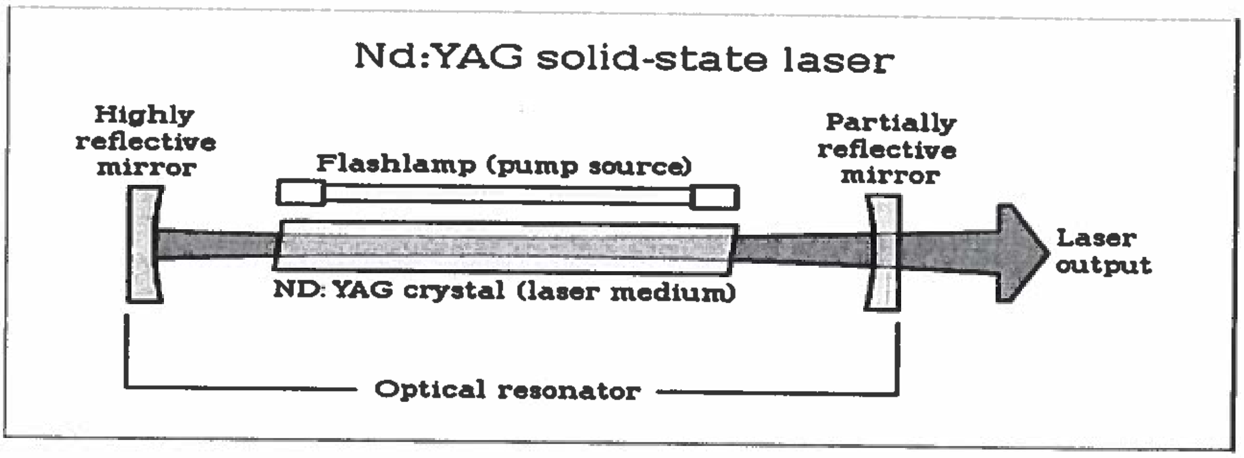

Figure 1: Schematic diagram of a ND: YAG laser.

1.2.1 Q switching

Principle to generate pulsed laser is the Q switching, it is a technique by which long pulsed laser can be changed into pulse laser to get more peak power of the laser beam. Laser of pulse width up to the order of nano seconds can be produced by using Q switching. An electrically active opaque material is used between the lasing medium and partially reflected mirror. This shutter is used to attain maximum energy inside the cavity as there is no stimulated emission during that time. When maximum population inversion occurs in the lasing medium, this opaque material is taken out to transmit photons, after transmission these photons reflect back and forth which are then responsible for stimulated emission. When metastable state becomes

english.

completely empty the opaque material again becomes active. In this way we can get a high power pulsed laser.

1.2.2 How to control energy of the Pulse

Laser pulse energy can be controlled by Q switch delay. There is specific time for which lasing material saturated, if we increase or decrease the time delay of the opening of shutter, saturation point cannot be achieved, so energy could be increased or decreased.

1.2.3 How to get the atomic signals from the plasma

In the beginning ionized state signals are in excess because of hot plasma state of elements in sample, with the passage of time plasma cools, signal of atomic transition can be recorded. So we adjust the delay in time in ICCD camera to collect the signals in the atomic transition regime of plasma to avoid the atomic transition.

1.3 Objectives

The objectives of this work are:

- To learn about the LIBS technique and its physical principles.
- To record atomic emission lines of different elements such as Ni, Cr, Co, Br, K and O from the sample containing of these elements.
- To draw the calibration curve of Ni by making pallets of different concentrations of Ni and corresponding LIBS signals.
- To carry out the parametric dependence of LIBS signal intensity on the incident laser energy and time delay.

2.0 Experimental details

Pallets of different concentrations containing Ni, Co, Cr, K, Br and O were prepared using hydraulic press. A pulsed laser emitting at 266 nm wavelength (fourth harmonic of high power Q Switch Nd: YAG laser) was applied for laser induced breakdown spectra generation. The UV convex lens of 30 nm was used to focus the laser on the sample. In order to avoid the crater, the sample was rotated by using X-Y rotatory tube. A miniature lens of focal length 10 mm was used to collect the spectra data from plasma spark; and it was fixed at the angle of 45^0 on the sample to collect the maximum LIBS signals. These signals were fed into 500 mm spectro-graph with grating groove density of 1200 lines/mm. The vertical output was connected with the time gated ICCD camera through a built in delay generator, which was synchronized with the Q switch of the Nd: YAG laser. The spectrograph was interfaced with the computer to generate the spectra.

Laser energy was measured using an energy meter (Ophir model300) to study the LIBS signal dependence on the laser energy.

The LIBS signal intensity was optimized by changing the gate delay and the incident laser energy.

In the end pure samples of Ni of known concentration in ppm were prepared. Different LIBS signals intensity corresponding to the different concentration were recorded, and then after knowing the LIBS signal intensity of the sample in the unknown sample a calibration curve was drawn to find the concentration of Ni in our unknown concentration sample.

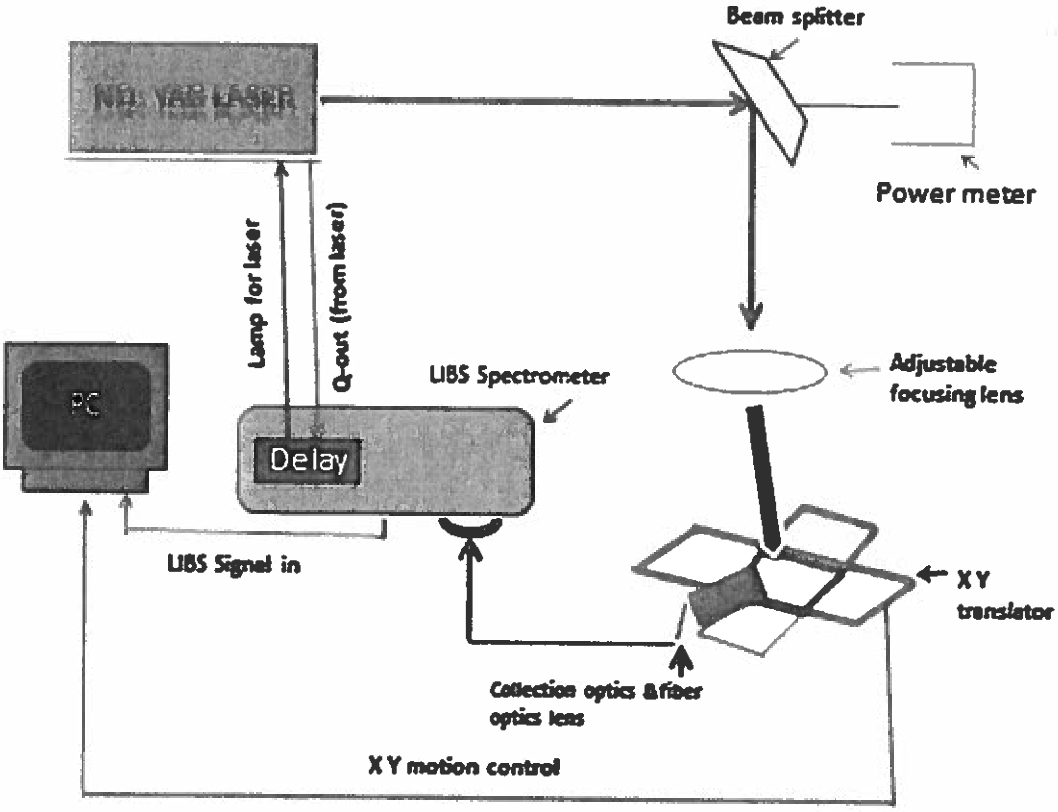

Figure 2: Schematic diagram of the experimental set up of pulsed LIBS system at laser research laboratory, KFUPM

3.0 Results and discussions

The main parameters of the LIBS are followings which were studied in this experiment.

- The concentration of the element in the sample
- The incident laser energy.
- Time delay.

3.1 Detection of atomic emission spectral lines from mixture of elements in a sample

Table 1: Atomic emission transition lines of the elements in the sample ~~range~~ in of 300-400 nm range ~~regions~~.

Element	Signal Intensity	Wavelength	Transition	
			Lower Level	Upper Level
Cr II	6062	319.5	$^{2}P_{3/2}$	$^{2}P_{312}$
Cu I	8276	327.39	$^{2}S_{1/2}$	$^{2}P_{1/2}$
Ni II	7771	335.8	$^{5}D_{1}$	$^{3}P_{2}$
Ni I	9601	339.1	$^{3}F_{4}$	$^{3}F_{4}$
Co I	8211	341.7	$^{4}F_{9/2}$	5/2
Cr I	9646	343.6	$^{5}G_{4}$	$^{5}G_{5}$
Ni I	8050	346.1	$^{3}D_{3}$	$^{5}F_{4}$
Ni I	8657	348.3	$^{3}F_{2}$	$^{3}D_{1}$
Co I	8394	349.5	$^{4}F_{3/2}$	$^{4}G_{5/2}$
Ni I	10333	351.0	$^{3}D_{1}$	$^{3}P_{0}$
Ni I	8729	356.6	$^{1}D_{2}$	$^{1}D_{2}$
Co I	7984	358.7	$^{2}F_{5/2}$	$^{2}F_{5/2}$
Ni I	6980	359.7	$^{3}D_{1}$	$^{3}P_{1}$
Ni I	9841	361.9	$^{1}D_{2}$	$^{1}F_{3}$
Cr I	10385	364.8	$^{5}G_{2}$	$^{5}F_{2}$
Cr I	8464	375.7	$^{5}F_{1}$	$^{5}D_{0}$

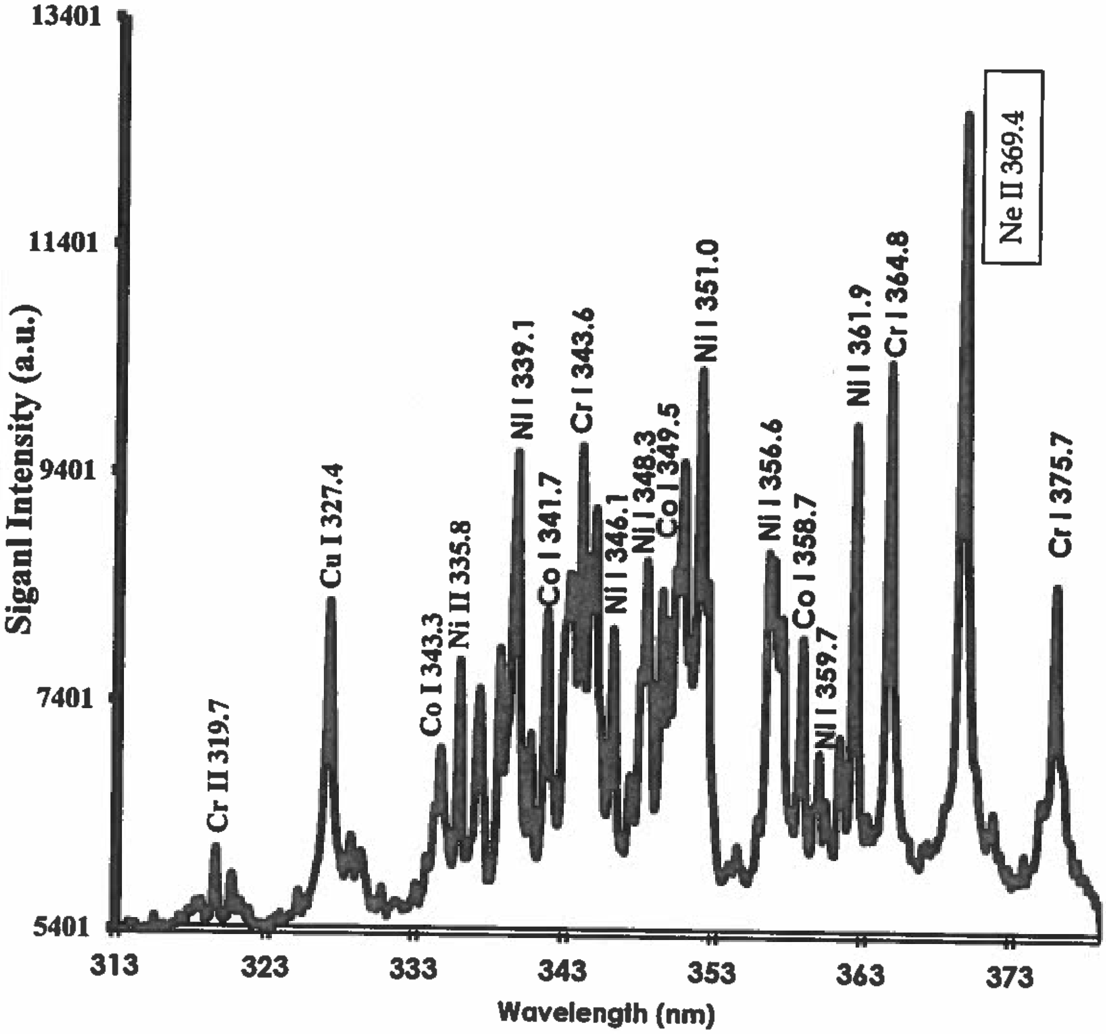

Figure 3: Typical LIBS spectrum of mostly Ni, Cr and Co in the range of 300-400 nm regions for the time delay of 100 μs

Table 2: Atomic Emission Transition lines of the elements in the sample ~~range of~~ 780 nm to 900 nm range.

Element	LIBS Signal (a.u)	Wavelength (nm)	Transition	
			Lower level	Higher level
K I	5867	807.9	$^2D_{3/2}$	$^2F_{5/2}$
K I	6213	807.8	$^2D_{3/2}$	$^2F_{5/2}$
Br I	7484	815.3	———	———
Br I	9021	815.4	———	———
K I	5207	841.7	$^2D_{5/2}$	$^2P_{3/2}$
O I	5269	844.6	$^3S_1$	$^3P_0$
K I	5167	850.5	$^2D_{3/2}$	$^2F_{5/2}$

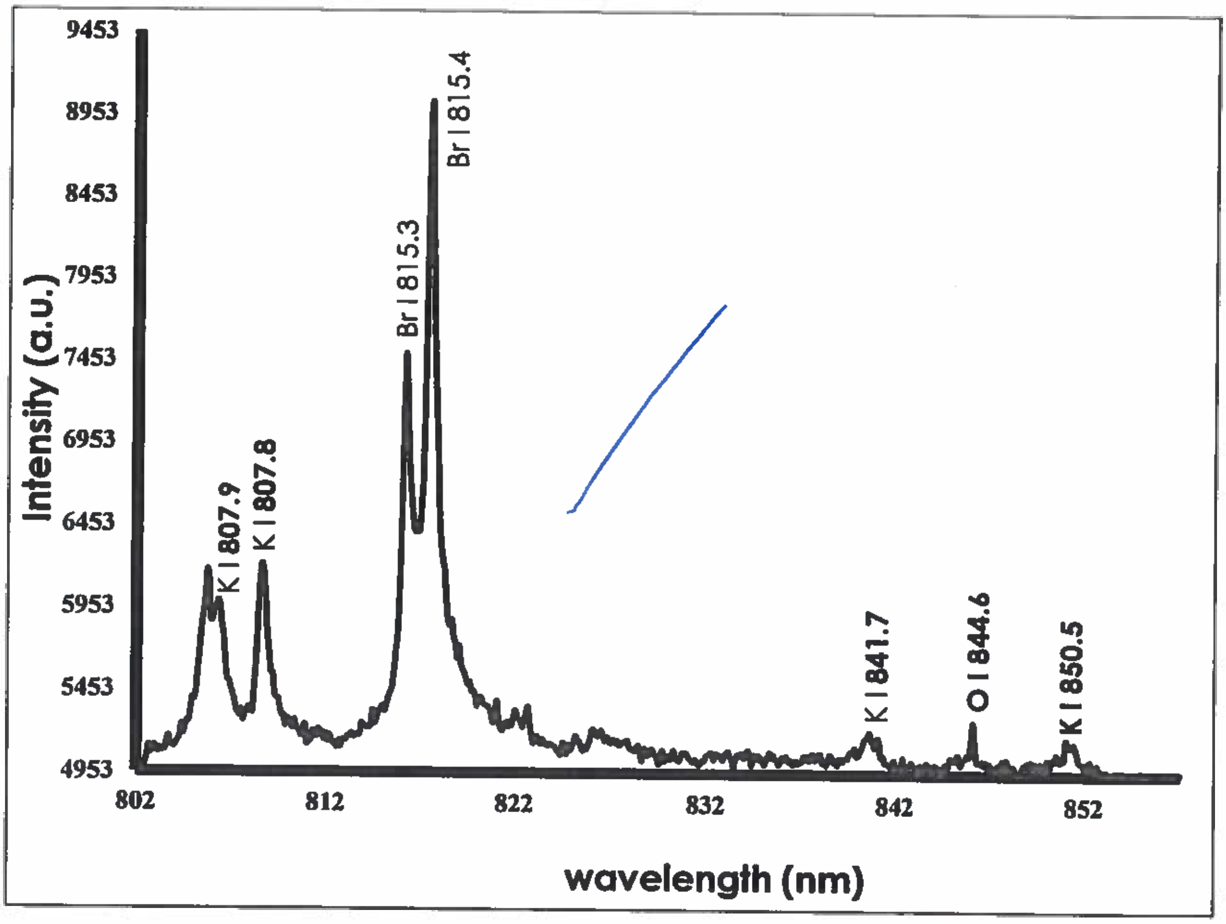

Figure 4: Typical LIBS spectrum of K, O and Br in the region of 780-900 nm wavelengths for the gate delay of 100 μs

3.2 Calibration curve of Nickel

The calibration curve was drawn by plotting the LIBS signal intensity versus concentration of nickel for the wavelength of 341.4 nm atomic transition line as shown in figure 5. LIBS signal intensity is directly proportional to the concentration of the element as is revealed in the fiq.5. The calibration curve can be used to determine the concentration of nickel from any unknown sample by recording the LIBS signal intensity.

Table 3: LIBS signal intensities at different concentration of Nickel.

Signal Intensity (a.u)	Concentration (ppm)
12812	25000
13345	50000
13945	75000
14316	100000
15061	150000

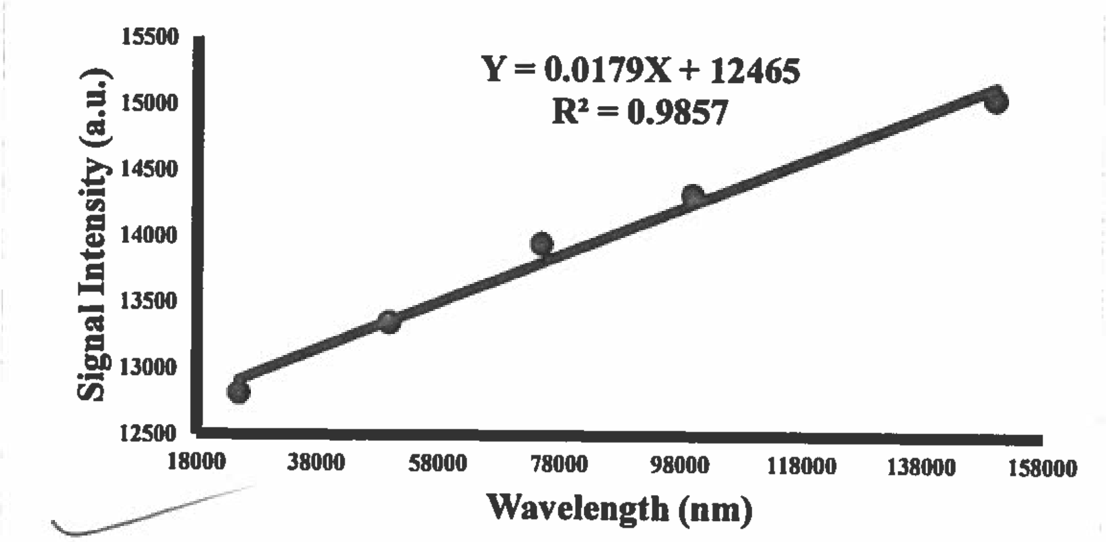

Figure 5: Calibration curve for the LIBS measurement of Nickel at different concentrations

3.3 Dependence of the LIBS signal intensity on the time delay

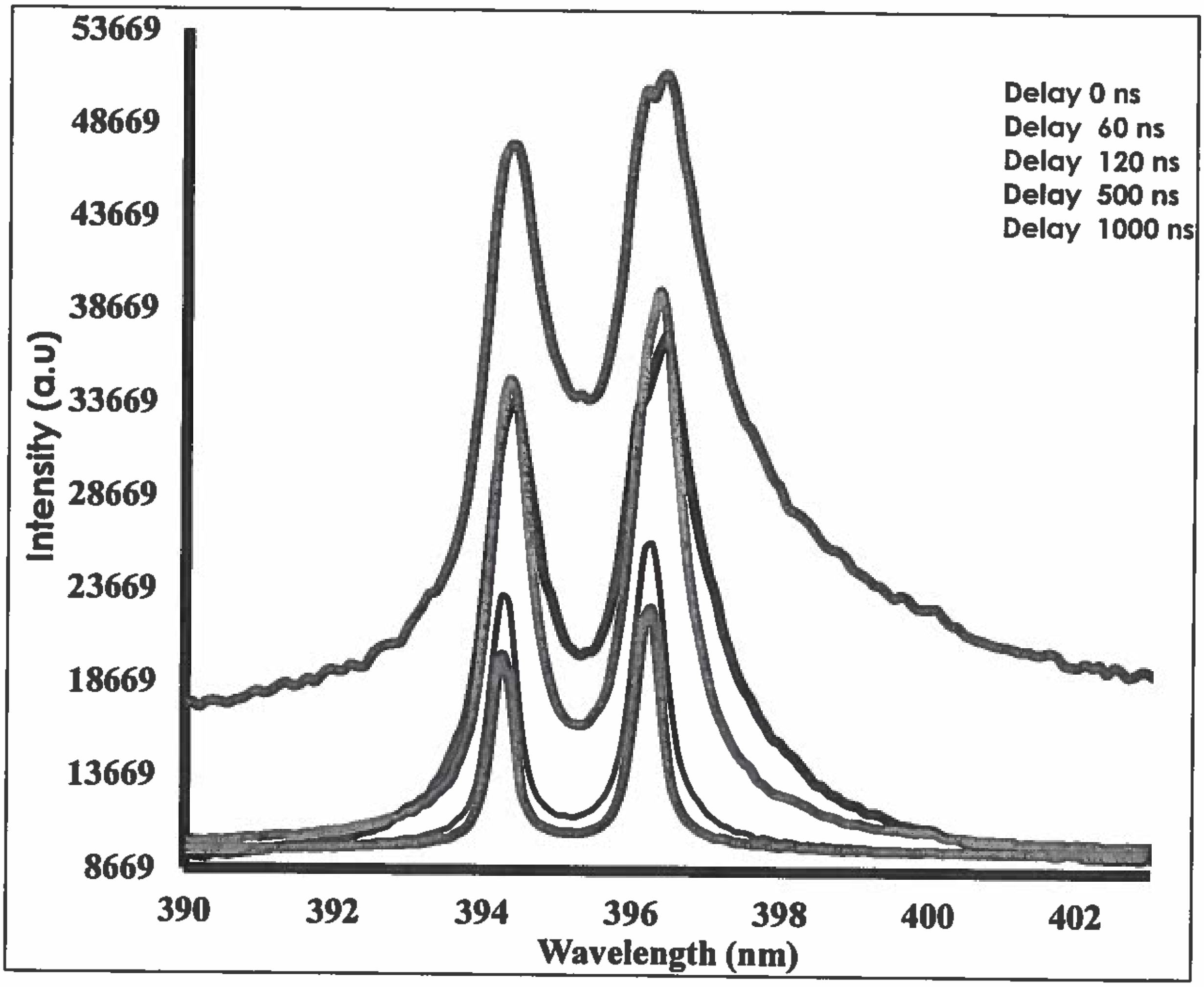

Figure 6: Dependence of the LIBS signal intensity on the time delay for the element Al in the ~~range of~~ wavelength of 370-420 nm wavelength range

It is evident from our experiment as shown in the figure 6 that the best time delay was of 500 ns. At 0 seconds spectrum was so vide because at that moment plasma was very hot and in the ionized state, but when the time goes on plasma becomes cool and now in this duration, the LIBS signals lie in the range cold plasma state and emit the atomic transitions. Similarly when we move too away at the time of 4000 ns LIBS signals become too weak which also non desirable as excited states have certain fixed life time.

3.4 Laser Energy dependence

The LIBS signal on incident laser energy dependence was also carried out for Al at finger print on its wavelength of 396.9 nm. The pulsed laser energy was varied in the range of 50mJ to 140 mJ and for each value of laser energy, the LIBS signal intensity was recorded as shown below. The energy dependence of LIBS signal intensity for Al 396.9 nm line is shown in the figure 7. It can be noticed that the LIBS signal intensity increases with the increase in the incident laser energy.

Table 3: LIBS signal intensity at different laser energies

Energy (mJ)	Intensity (a.u)
50	10282
80	24552
100	42300
140	72080

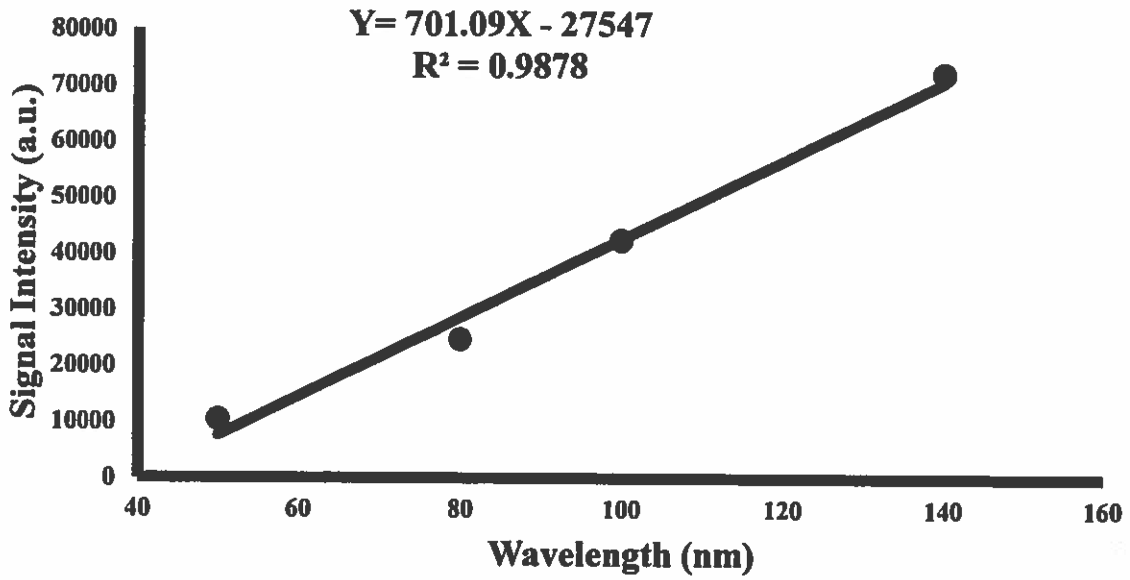

Figure 9: Energy dependence of LIBS signal intensity for Al 396.9 nm

4.0 Conclusion

In this experiment the LIBS technique was used to detect atomic spectra from the mixture of Ni, Co, Cr, Br, K and O. Three basic parameters of LIBS have been studied also, which are the concentration, energy and gate time delay. It was noticed that the best LIBS signal intensity was found at the delay of 500 ns, the LIBS signal intensity increases with the increase of the concentration of Ni and LIBS signal intensity increases linearly with the rise in the incident laser energy.

5.0 Acknowledgements

This work was very much important to boost my experimental communication, writing skills and to learn new technology for elemental analysis. I would like to thanks to Almighty ALLAH whose blessing made this work easy for me. I also like to thank my teacher Dr. M. A. Gondal who helped me to learn about this experiment in details. Thanks are also due to Dr. Abdul-Aziz Al-Jalal for assigning me this experiment.

References

1. M. A. Gondal, Y. W. Maganda, M.A. Dastageer, F. F. Al Adel, A. A. Naqvi , T. F. Qahtan, Optimization of Plasma Parameters and Detection of Fluoride in Toothpaste using Laser Induced Breakdown Spectroscopy, Optics & Laser Technology 57 (2014) 32–38. (2014)
2. M. A. Gondal, Y. W. Maganda, M.A. Dastageer, F. F. Al Adel, A. A. Naqvi , T. F. Qahatan Detection of Carcinogenic Chromium in Synthetic Hair Dyes using Laser Induced Breakdown Spectroscopy, Applied Optics, Vol. 53, 1636-1643 (2014).
3. A.I. Khalil, M. A. Gondal, M. A. Dastageer, Detection of Trace Elements in Non-Degradable Organic Spent Clay Waste Using Optimized Dual-Pulsed Laser Induced Breakdown Spectrometer, Applied Optics, Vol. 53, 1709-1717 (2014).
4. M. A. Gondal , A. Khalil, Effect of Ambient Conditions on Laser-Induced Breakdown Spectroscopy Performance, Laser Physics Vol. 22, No. 12, pp. 1771–1779 (2012).
5. M. A. Gondal, Z. S. Seddigi, M. M. Nasr, Spectroscopic Detection of Health Hazardous Contaminants in Lipstick using Laser Induced Breakdown Spectroscopy, J. Hazardous Materials 175, 726-732(2010)
6. M. Nasr, M. A. Gondal, Z. Seddighi Detection of Hazardous Pollutants in Chrome Tanned Leather Using Locally Developed Lased Induced Breakdown Spectrometer, Environmental Monitoring and Assesment Volume 175, Issue 1-4, April 2011, 387-395(2011).
7. M. A. Gondal, T. Hussain, Z. H.Yamani and M.A. Baig , Monitoring of Remediation Process of Chromium Contaminated Soil using Laser Induced Breakdown Spectroscopy, J. Hazardous Materials, 163,1261-1271 (2009)
8. M. N. Siddiqui, M. A. Gondal ,M. Nasr Determination of Trace Metals Using Laser Induced Breakdown Spectroscopy in Insoluble Organic Materials Obtained from Pyrolysis of Plastics Waste, Bulletin of Environmental Contamination & Toxicology, Vol. 83 Page 141-145(2009).
9. M. A. Gondal ,T. Hussain, Z. H. Yamani and O.S.B. Al-Amoudi Spectral Determination of Chloride Content in Different Types of Cement Using LIBS, Spectroscopy Letters, 42, 171-177 (2009).
10. T. Hussain, M. A. Gondal and Z. H.Yamani (2007), Measurement of Nutrients in Green House Soil with Laser Induced Breakdown Spectroscopy, Environmental Monitoring and Assessment, 124, 131-139 (2007).
11. NIST Atomic spectra databasehttp://www.nist.gov/physlab/data/asd.cfm

King Fahd University of Petroleum and Minerals
Department of Physics
Physics 503 - Term 142

Experiment #3 Report

Student Name : Amar Mohamedkhair

Student ID : 201402880

Code : E102

Evaluator : Dr. Ziq

	grades	Out of
Abstract	1	1
Introduction	4	5
Experimental details	4	6
Results and Discussion	7	9
Conclusion	1	1
References	1	1
Overall	2	2
Total	20	**25**

جامعة الملك فهد للبترول والمعادن
King Fahd University of Petroleum & Minerals

Department of Physics

Physics 503
Graduate Laboratory
Term 142

جامعة الملك فهد للبترول و المعادن
قسم الفيزياء
RECEIVED
10 MAY 2015
وارد
King Fahd University of Petroleum & Minerals
PHYSICS DEPT

20/25

Synthesis of SiO_2 nanoparticles by pulsed laser ablation (PLA) in liquids

Prepared by: *Amar Kamal Mohamedkhair*
Student ID : *G201402880*

Supervisor : *Prof. M. A. Gondal*

10/05/2015

CONTENTS

CONTENTS

ABSTRACT

The pulsed laser ablation in liquid technique was applied to synthesis SiO_2 nano-size from SiO_2 micro-size powder dispersed in deionized water (DW). The synthesized material was characterized using X-Ray diffraction technique (XRD) for crystalline structure, and Field Emission Scanning Electron microscope (FESEM) to investigate its surface morphology and particle size. The absorption coefficient of the synthesized SiO_2 nanoparticles was investigated in the UV-Visible region. The band gap energy of the synthesized SiO_2 nanoparticles was also evaluated from the Tauc plot which 0.72eV and it agrees with the reported value in often literature.

1. INTRODUCTION

1.1 Pulsed laser ablation in liquids (PLA)

The beginning of pulsed laser ablation at the liquid-solid medium was first done by Patil and co-workers in 1987, they used a pulsed laser to ablate a iron target in water to form iron oxides with metastable phases .This techniques is known as Liquid Phase Pulsed Laser Ablation (PLAL), here the solid target is kept under the surface of water and a high energy laser beam is focused onto the target surface through the liquid. After this work, Ogale protracted the prospect of PLAL for the surface modulation of metals like nitriding, ccarbiding and metallic oxidation. This pioneering work started new routes for materials processing depend on the PLAL. Since that time, the PLAL technique has been used to produce several kind of new materials, such as metal oxides, nanodiamond , related nanocrystals, nanocrystal alloys metallic nanocrystals.

These studies shows that the PLAL has become a successful method for fabrication of thin films with different kinds by changing the target and the liquid environment in which the target immerged. This technique has many advantages compared to the classical physical techniques (including vapor phase transport [8], chemical vapor deposition [9], and pulsed laser ablation in vacuum [10]), also chemical techniques (such as hydrothermal techniques [11], soft-template [12] and use different type of surfactants [13,14]), These advantages include (1) a chemically 'clean and simple' synthesis, the synthesized product is usually obtained without byproducts and no need for more purification; (2) cheap instruments and easily controlled parameters; (3) the extreme confined conditions and induced high pressure region which is favors the formation of unusual metastable phases ,and high temperature.

These advantages provide an opportunity for the designer to merge selected liquids and solid to synthesize nanostructures with certain functions.

1.2 The principle of pulsed laser ablation in liquids PLAL

In PLAL a high power laser beam is focused on the surface of the solid target immersed under the surface of the liquid. When the laser beam hits the surface of the target the target surface starts to evaporate at the point where the laser beam hits, as the temperature is too high due to the inter action, this evaporation is in the form of an ablation plume, which include species such as ions, atoms, and clusters, travelling with high kinetic energy. The high energy species in the plume start colliding with the surrounding liquid molecules and react with them producing a new compound including atoms from the liquid and the solid target. Due the nanosecond scale and the high intensity, the pressures and the instantaneous temperatures within the volume of the reaction can be extremely light. Such high pressure, high temperature, and high density conditions provide a 'brute force' method of synthesizing new materials that have hitherto been inaccessible using milder, more classical method.

Figure:1 represents the PLAL process. From the figure it one can notice that the setup consists of a high energy short pulsed laser source e.g. Nd:YAG , and a lens is used to focus the laser beam in a small spot on the target. The solid target is placed under the surface of the liquid by few millimeters. The liquid and the target are placed in a container that may have a wide opening or a small window to avoid the splash resulting from the interaction of the laser beam with the target surface. The laser source is then turned on firing laser pulses toward the on to with a certain energy and pulse duration causing the ablation [16].

The laser ablation process take place in several steps [17]:

1. The laser beam interacts on the surface of the target make it evaporating with some of the liquid in the surrounding environment.
2. A chemical reaction take place between the evaporated particles as they are highly excited energetically and electronically.
3. The result from this reaction is nanoparticles composed of atoms from both the target and the liquid. These nanoparticles are in the form of a suspension in the liquid.
4. The formed nanoparticles are accumulated together forming collides which may considered as a secondary target for the laser beam if the laser beam are kept running for too long, which will cause the change in the composition, size, or morphology of the formed nanoparticles[18].

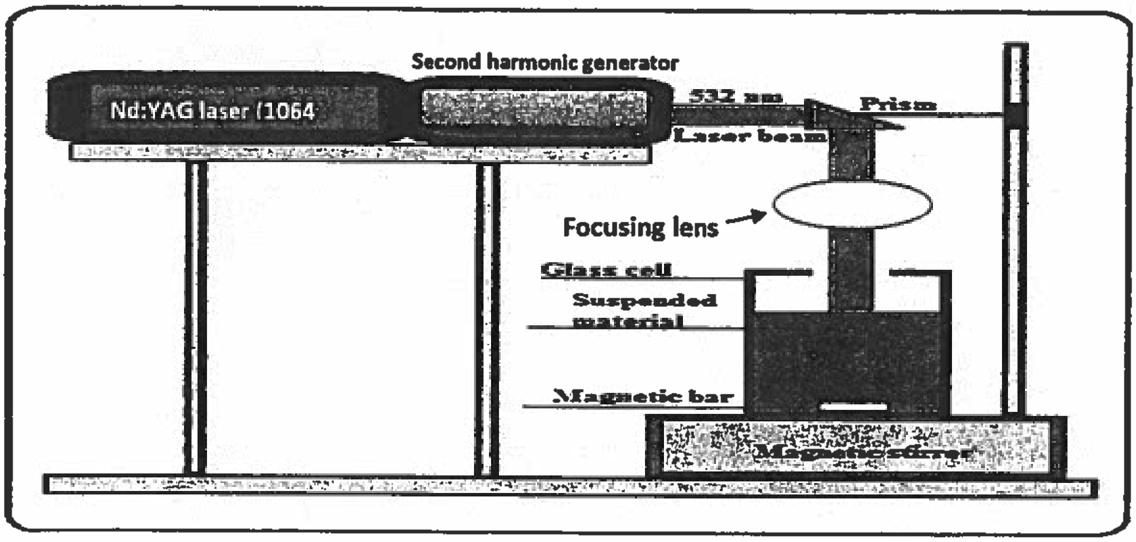

Figure 1: Schematic diagram of a typical PLAL setup

Formation of nanoparticles using PLAL has the same idea as the laser ablation of solids in gas or in vacuum. As in laser ablation in vacuum or gas we can prepare different materials with different oxidation state and different material ratios we can do the same in PLAL by changing the laser wave length, pulse duration, laser flounce, and target material [19]. The difference between the laser ablation in liquids and in gas or vacuum is in the plasma expansion process. In gas or vacuum the plasma can expand freely but in case of liquids the plasma expansion is confined with the surrounding liquid layers. This liquid layer confinement of the plasma makes the plasma pressure increase due to the formation of more particles from the target and by increasing the temperature due to the laser interaction with the target surface novel materials can be prepared. Also the presence of the liquid around the target during the laser ablation allow some liquid particles (those surrounding the target) to evaporate as well as the target material so they will be excited as well and as they all confined by the same volume created by the liquid layers the chemical reaction can take place easily. Preparing the nanoparticles by PLAL technique is alternative to the well-known chemical vapor deposition (CVD) method, as it is relative simplicity and the low cost of the experimental setup. Moreover, the produced nanoparticles are free of any counter-ions or surface-active substances [7].

1.3 Nd:YAG lasers

Nd:YAG laser is considered as one of the most commonly used types of laser and it has many applications. It uses a flash light or a diode laser as an optical pump. It emits light at different wave lengths, the main one is in the infrared region (UV) with a wave length of 1064 nm. Nd:YAG lasers operate in two modes:

Continues mode

In the contentious mode the atoms are stimulated by the optical pump and as they release their energy the laser is emitted, but this one is not as powerful as the pulsed one.

Pulsed mode (Q-switching mode)

In this mode, an optical switch (Q-switch) is placed in the laser cavity of the Nd:YAG lasers. This switch only opens when the population inversion is maximum in the neodymium ions. When it opens it allows the light to flow in the cavity depopulating the excited laser-medium at maximum population inversion. In this Q-switched mode, output powers of 250 megawatts and pulse durations of 10 to 25 nanoseconds have been achieved [21].

No wa

The high-intensity pulses may be efficiently frequency doubled to generate laser light at 532 nm, or higher harmonics at 355 and 266 nm.

Very large ??

Nd:YAG absorbs mostly in the bands between 730–760 nm and 790–820 nm [20]. So in order to select a good optical pump, the wave length of the emitted light should be taken into consideration. At low current densities krypton flash lamps have output between 760 and 810 nm, so it works fine more than the ordinary Xenon lamps for pumping Nd:YAG lasers.

The amount of the neodymium dopant in the material varies according to its use. For continuous wave output, the doping is significantly lower than for pulsed lasers. The lightly doped continues wave rods can be optically distinguished by being less colored, almost white, while higher-doped rods are pink-purplish.

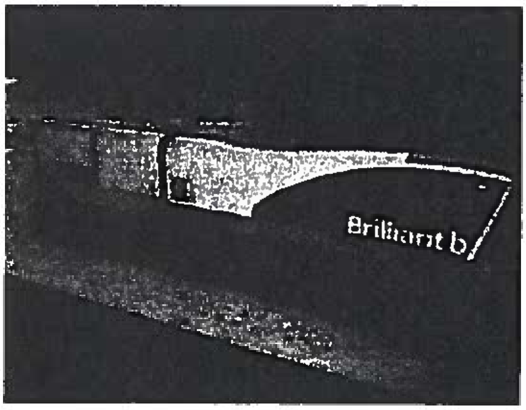

Not clear.

Figure 2: Nd-YAG Laser

2. EXPERIMENTAL SETUP DETAILS

A high power laser beam from Q switched Nd:YAG laser at 532nm using second harmonic, was used as a ablation source. The maximum energy of Laser pulse was 450 mJ and power is 2W with pulse width of 6 ns at repetition rate of 10 Hz. A prism and lens with suitable adjustment was used to focus the laser beam at the center of target. A magnetic rotator is used to rotate the target. The rotation protects the surface of target against any crater due to high intensity of laser beam. The target was placed in a glass vessel and height of water was 2mm above the powder target (50 ml liquid (hydrogen per oxide). High speed of magnetic stirrer was used in order to prepare a homogenous solution. Fig. 1 shows the focusing arrangement used in this experiment, and figure 3 shows the practical view of the experiment.

Figure 3. Experimental setup in the Laser

3. SAMPLE ANALYSIS AND CHARACTERIZATION

To study the optical properties of nano structured synthesized particles for SiO_2, UV-Vis Spectrophotometer was used to investigate the UV absorption spectrum. The structural composition and surface morphology is studied by X-ray Diffraction (XRD) and Field Emission Scanning Electron Microscopy (FESEM) analysis.

3.1 UV-Visible Spectrophotometer for band gap measurement

UV-Vis absorption spectrum was obtained with Spectrophotometer (JASCO-670).H_2O_2 was used as base fluid to make the reference point for the instrument. The sensitivity of UV-Vis spectrometer in the region of 200 nm to 8000 nm with 601 data points. The data was plotted to calculate the band gap energy of synthesized material.

3.2 Field Emission Scanning Electron Microscopy (FESEM)

Surface morphology was studied by using Field Emission Scanning Electron Microscope (FESEM, TESCAN Ultra-High resolution) operating at 20kV and equipped with an X-ray energy dispersive spectroscope detector (EDS).

3.3 X-ray Diffraction Analysis (XRD)

The X-ray diffraction analysis was performed on X-ray diffractometer (Model D-8, Bruker-axs). Analysis used the Cu-Kα radiation and was operated at 30 KV. The intensity of the diffracted rays from the powder sample was recorded versus the angle between the detector and the X-ray, $2\theta^0$. The X-ray used was the strongest line emitted from Cu-Kα at 1.5406A°.

3.4 Sample Preparation

0.1g of high purity silicon oxide(SiO_2) micro-size powder was dispersed in deionized water (DW) of about 20ml in order to synthesize SiO_2 nanoparticles. SiO_2 powder solution was ablated by 532nm laser for 40 minutes while it was being stirred by a magnetic stirrer.

4. RESULTS AND DISCUSSION

4.1 UV-V Spectrophotometer analysis

From the UV-Vis spectrophotometer, we obtained a graph between absorption intensity and the wave length.

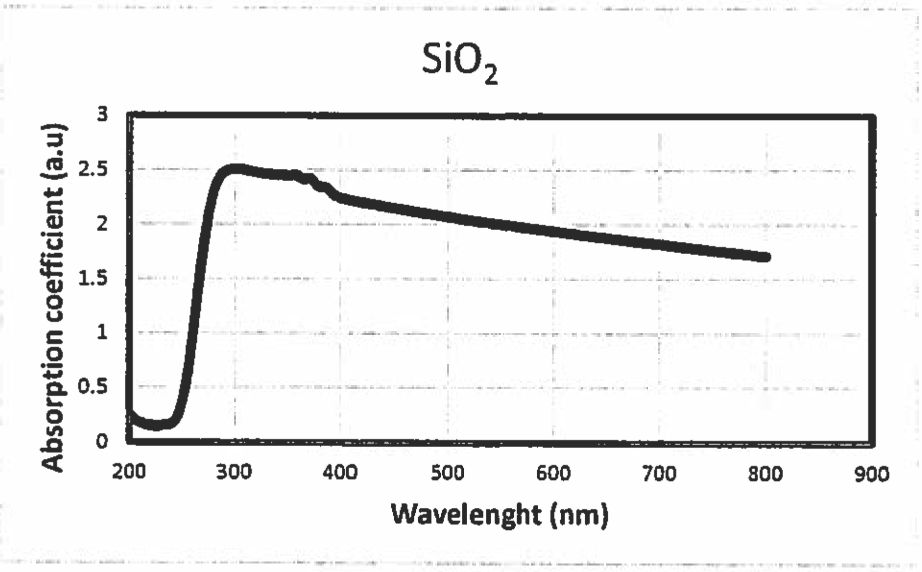

Figure 4: *the UV-V spectrum of SiO_2 nano-size*

The energy band gap of the SiO_2 nanoparticles was estimate by Tauc plot. The Tauc equation is given as $(\alpha E)^n= A\ (E - Eg)$ where A is a constant, α is absorption coefficient, n is equal to 2 for materials with direct band gap and equals ½ for materials with indirect band gap, E is the energy of the incident photon and E_g is the energy band gap. The silicon has a direct band gap.

Figure 5: shows the plot of $(\alpha E)^2$ as a function of E of the light. The band gap energy was evaluated from the linear part of the curve to the energy axis. The band-gap energy of the SiO_2 nanoparticles was found to be 0.72 eV.

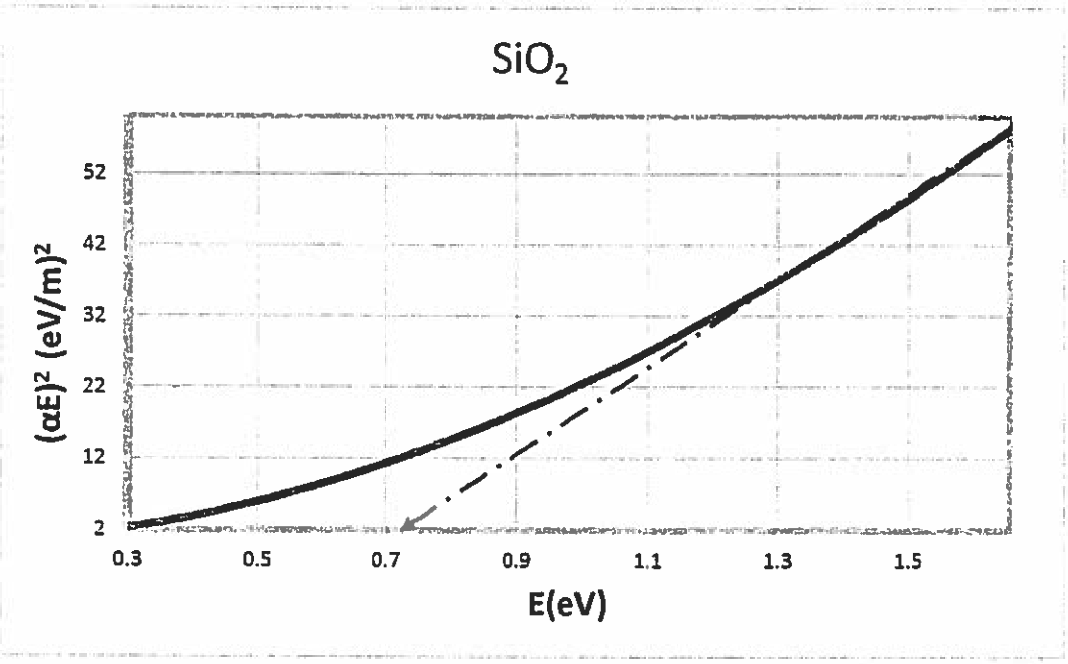

Figure 5: Tauc plot of the synthesized SiO_2 nanoparticle in deionized H_2O

4.2 The X-ray Diffraction analysis

To insure the formation of the SiO_2, an x-ray diffraction analysis was calculated. The figure (6) and (7) show x-ray diffraction pattern of the sample before and after the ablation.

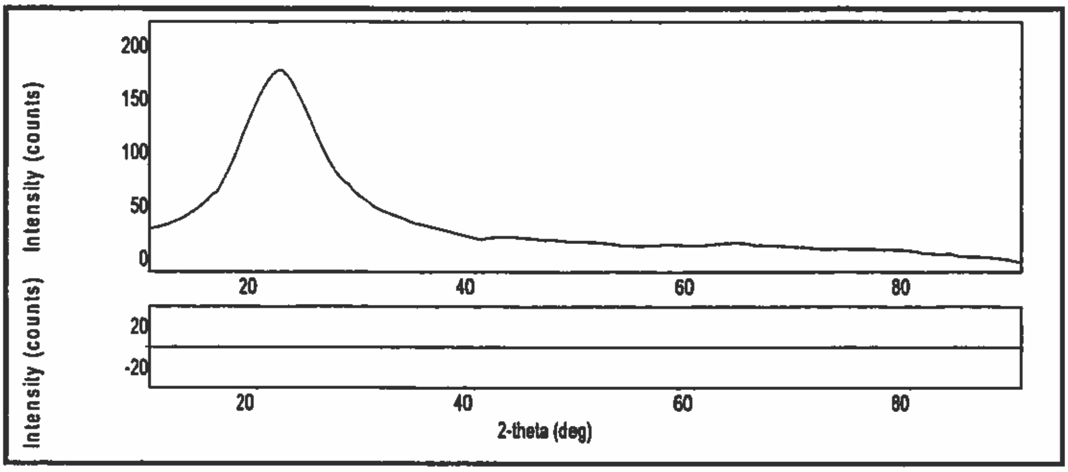

Figure 6: XRD pattern for SiO_2 micro-size (before ablation).

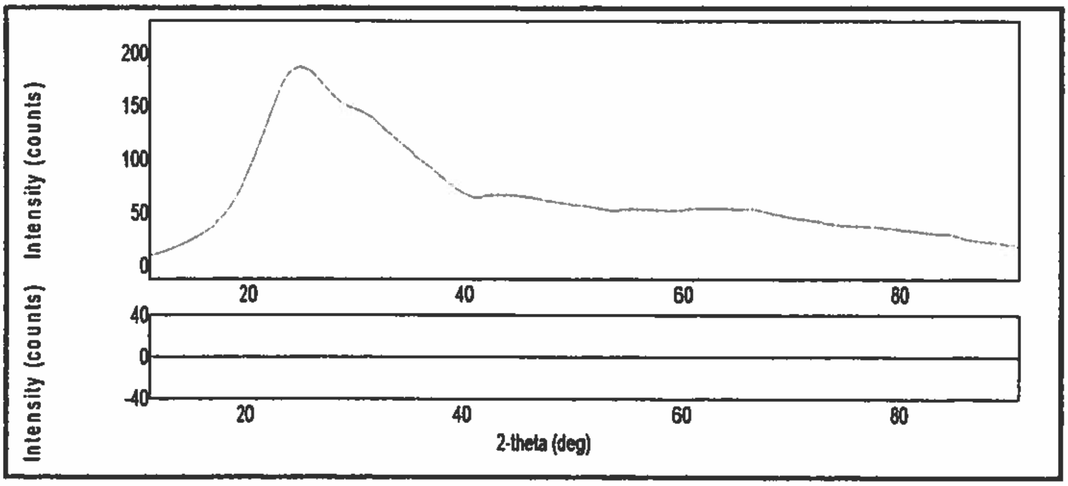

Figure 7: XRD pattern for SiO_2 nano-size (after ablation)

The broad peak in the XRD pattern for SiO_2 confirms the amorphous nature for the silicon. By comparing between figures (6) & (7), we can observe that the peak for SiO_2 in micro-size is ranging from 15° to 25° in 2θ angle while the peak is ranging from 15° to 40° in 2θ SiO_2 nano-size. So we can conclude that the full width at half maximum (FWHM) for SiO2 peak in the final state (nano-size) is wider than the SiO2 peak in the initial state (micro-size).

4.3 Energy Dispersive Spectrum (EDS)

The EDS analysis of the synthesized SiO_2 nanoparticle is shown in figure (8). The presence of silicon and oxygen in the EDS spectrum confirms synthesis of SiO2.

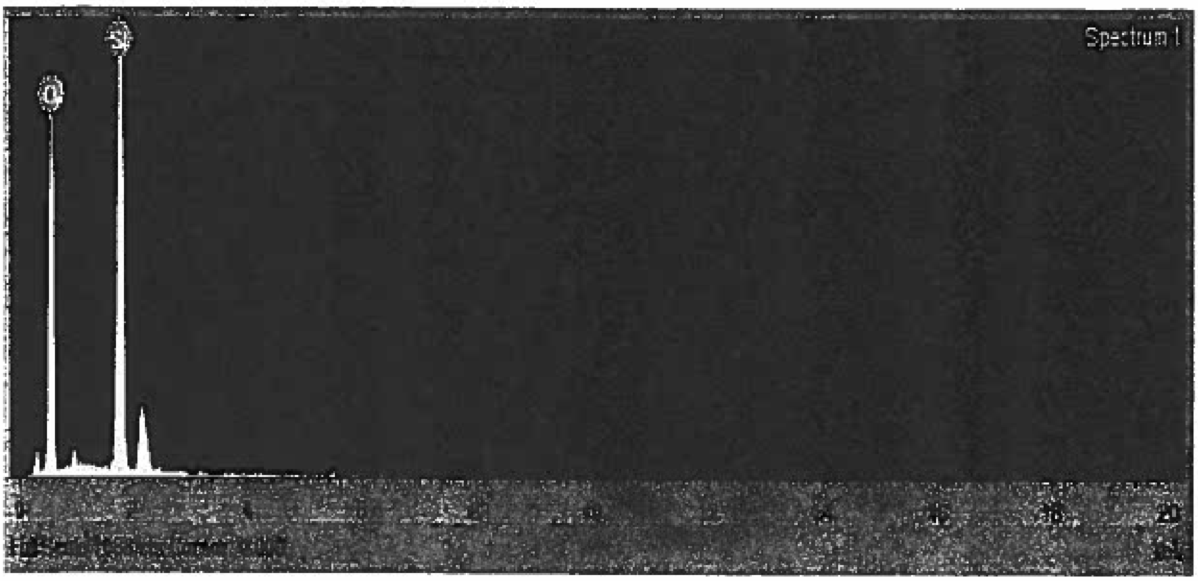

Figure 8: The EDS analysis of the synthesized SiO_2 nanoparticle

4.4 Morphological studies using (FESEM)

In order to study the morphology of the synthesized nanoparticles of SiO_2 and determined the particle size we studied the synthesized material using the Field Emission Scanning Electron Microscope (FESEM). The obtained images from the FESEM presented here in figure (9) which is present the morphology of the SiO_2 micro-size and figure (10) for the SiO_2 nano-size which is found around 30 nm.

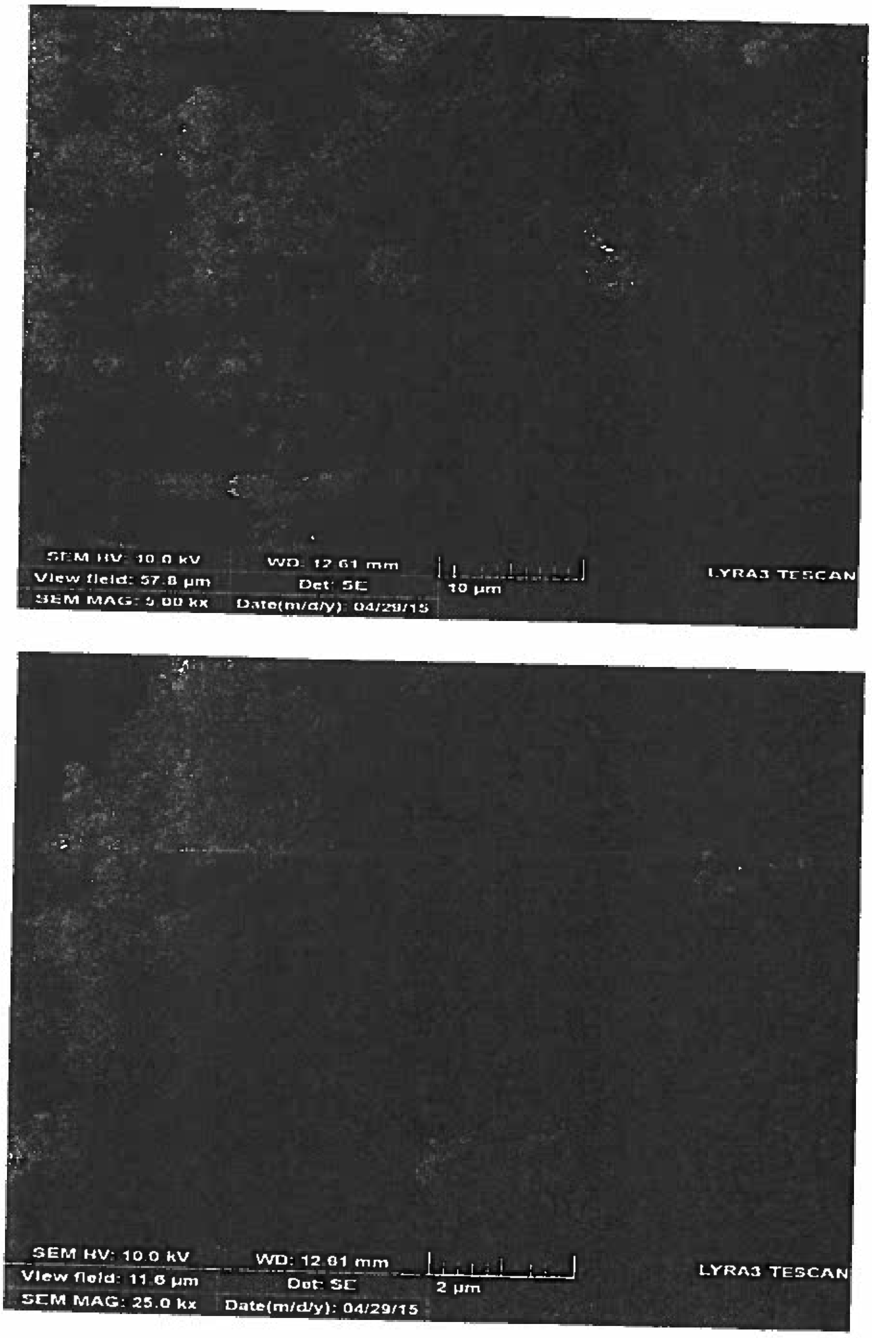

Figures 9: the morphology of the SiO_2 micro-size recorded by FESEM.

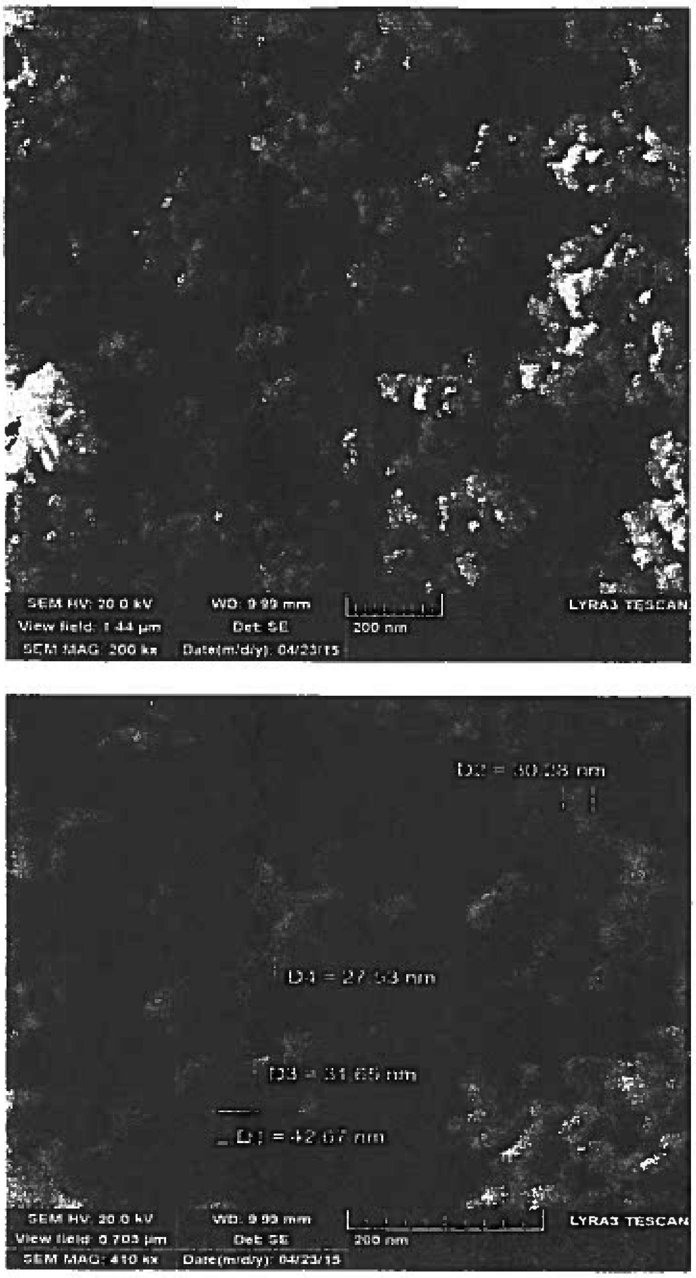

Figures 10: the morphology of the SiO_2 micro-size recorded by FESEM.

5. CONCLUSION

Pulsed Laser ablation technique was applied to synthesize the nanoparticles of silicon Oxide from pure silicon oxide powder of micrometer size using 532 nm wavelength of Nd:YAG Laser with 6 ns pulse width and 250 mJ Laser beam energy in 3% hydrogen peroxide mixture in water as oxidant. XRD analysis concluded the formation of amorphous nanoscale SiO_2 material. FESEM images showed the geometry of new particles. UV-Vis absorption spectrum was used to determine the band gap energy which resulted as 0.72 eV.

6. REFERENCES

1. M.A. Gondal, Tawfik A. Saleh, Q.A. Drmosh, Synthesis of nickel oxide nanoparticles using pulsed laser ablation in liquids and their optical characterization Applied Surface Science 258 (2012) 6982–6986.
2. Patil P P, Kulkarni S A, Phase D M, Kulkarni S K, Bhide V G, Kanetkar S M Ghaisas S V, Ogale S B, Phys. Rev. Lett., 1987, 58, 238.
3. Thin Solid Films, 1988, 163, 215, Ogale S B.
4. Kimball B, Kempa K, Rybczynski J, Wu P F, Steeves D Huang Z P, , Sennett M, Giersig M, Rao D V G L N, Li W Z, Carnahan D L, Lao J Y, Ren Z F, Nano Lett., 2003, 3, 13.
5. Lieber C M , Duan X F, Adv. Mater., 2000, 12, 298.
6. Zhang C Y, Wang J B, Zhong X L, Yang G W, Chem. Phys. Lett., 2002, 361, 86.
7. J. Phys. Chem. B, 2004, 108, 3492,Yang H G, Zeng H C.
8. Sun Y, Fuge G M, Ashfold M N R, Riley D J, Adv. Mater., 2005, 17 2477.
9. Mayers B, Sun Y G, Xia Y N, Gates B, Nano lett., 2002, 2, 165.
10. Letsinger R L, Mirkin C A, Mucic R C, Storhoff J J, Nature, 1996, 382, 607.
11. Zhou B C, Li Y D, Li X L, Fan S S, Deng Z X, Zhou B C, Sun X M, Angew Fan S S, Wang J W, Sun X M, Angew. Chem. Int. Ed., 2002, 41, 333.
12. Dong Q Z, Chen J W, Yang J, Song Z L, Guo Z X, Lian J S, Mater. Lett., 2004, 58, 337.
13. Schiffers W P, Shaw S J, Emmony D C, Gentry T P, J. Phys. D, 1999, 32, 1612.
14. Voronov V V, Simakin A V, Voronov V V, Shafeev G A, Kirichenko N A, Appl. Phys. A, 2004, 79, 1127.
15. Quantum Electronics (3rd ed.), Yariv, Amnon (1989). Wiley. pp. 208–211.
16. Solid-state laser engineering, Walter Koechner (1965) , Springer-Verlag, p. 507

King Fahd University of Petroleum and Minerals
Department of Physics
Physics 503 - Term 142

Experiment #1 Report

revised on 14/04/2015

Student Name : Muhammad Younas

Student ID : 201405340

Code : E205

Evaluator : Dr. Harrabi

	grades	Out of
Abstract	0.5	1
Introduction	4	5
Experimental details	3	6
Results and Discussion	4	9
Conclusion	0	1
References	1	1
Overall	0.5	2
Total	13	**25**

جامعة الملك فهد للبترول و المعادن
قسم الفيزياء
RECEIVED 08 MAR 2015 وارد
King Fahd University of Petroleum & Minerals
PHYSICS DEPT

KING FAHD UNIVERSITY OF PETROLEUM AND MINERALS

DHAHRAN 31261

DEPARTMENT OF PHYSICS

PHY 503 (GRADUATE LABORATORY)

Term-142

EXPERIMENT ONE (E205)

X-RAY PHOTOELECTRON SPECTROSCOPY

BY

Muhammad Younas

(ID: g201405340)

Supervised by

Dr. Mohammed Faiz

8 MARCH 2015

Table of contents

1.0 ABSTRACT

NO

In this experiment, I learned the X-ray photoelectron spectroscopy (XPS) ~~technique, how to analyze a sample in the~~ XPS; data analysis, and data interpretation. The investigated sample is Gadolinium doped polymer in a pellet form; the results showed the presence of Si as impurity in the sample and the other elements in the sample are Carbon, Nitrogen, Oxygen and Gadolinium. Hydrogen cannot be detected due to limitations of XPS. We also observed that an element in different electronic environments can be detected quite accurately in XPS.

2.0 INTRODUCTION TO XPS

The idea of X-ray photoelectron spectroscopy (XPS) is based on famous photoelectric effect which was explained by Albert Einstein in 1905, for which he got a Nobel Prize in 1921. Einstein suggested that light is composed of tiny particles called photons, and each photon has energy. According to the photo electric effect, when light shines on a metal, it takes one photon to eject one electron from a metal if the energy of the photon is more than the work function of the electron in the metal. But when the energy of the photon is less than the work function then no electron is emitted. It does not depend upon the intensity of the light. The extra energy of photon above the work function shows up as the kinetic energy of the emitted electron.

Mean free path of an electron is the average distance an electron can travel before in-elastically scattered by another particle. In solids it is about 3 Å. It is the key parameter that makes the XPS technique surface sensitive. Since 1950s, X-ray photoelectron spectroscopy has been developed as a very useful surface characterization technique [1] [2]. In 1960s, Kai Seighbahn and his research group in Uppsala (Sweden) developed several significant improvements in XPS. Siegbahn received the Nobel Prize for Physics in 1981, to acknowledge his extensive efforts to develop XPS into a useful analytical tool [3]. It is usually used to measure the elemental composition of a surface, empirical formula of pure materials, elements that contaminate a surface, oxidation state of each element within the surface, uniformity of elemental composition across the surface and uniformity of elemental composition across the depth (i.e. depth profiling). Practically XPS detects all elements with atomic number (Z=3) and above, but usually difficult to detects hydrogen (Z=1) and helium (Z=2). This is due the following reasons.

1) In a high vacuum system, it is very unlikely that any H or He would be present in the sample.

2) Very small photo ionization cross-section of H and He due to which we cannot observe them in the XPS spectrum [4].

XPS is mostly used to study inorganic compounds, metals alloys, semiconductors, polymers, glasses, ceramics, paints and many others; however non-dry, out gassing, radioactive or highly magnetic materials can pose serious challenges [5]. XPS uses soft x-rays with photon energy of 50-2000 eV to examine core-levels as oppose to Ultraviolet Photoelectron Spectroscopy (UPS) that uses UV radiation to examine valence levels.

2.1 Theory of XPS

According to Einstein relation, the energy of a photon is given as:

$$E = h\,v$$

Where, h= Planck's constant and v = radiation frequency

The process associated with photo ionization can be explained by the following equation:

$$A + hv \rightarrow A^{+} + e^{-}$$

Where A is an atom in the sample's surface. According to the law of conservation of

$$E(A) + hv = E(A^{+}) + E(e^{-})$$

Where A^{+} shows the atom is ionized after photoelectron emission. Since we have the energy of the electron to be made up of kinetic energy (KE) alone, the equation above can be rearranged to give the kinetic energy (KE) of the photoelectron:

$$KE = hv - \{E(A^{+}) - E(A)\}$$

The content within the bracket represent the change between the energy of the ionized atom and the neutral atom, which is commonly known as the *binding energy (BE)* of the electron. Therefore,

$$KE = hv - BE$$

This equation is valid only for the photoelectrons that have not lost energy (elastic electrons) when leaving the sample. A normal XPS spectrum is a plot of photoelectron current intensity (Counts/second) versus binding energy (eV). Each element yields a unique set of XPS peaks at characteristic binding energies that undeviatingly pinpoint each element that exist on the surface of the material being analysed. Only the elastic electrons contribute to the XPS peaks. The inelastic electrons (the electrons that have lost energy due to collisions in the sample) contribute to the background of the XPS spectrum. Moreover, the intensity of the characteristic peaks is related to the concentration of the element within the surface portion [6].

?

2.2 Objectives

Our goal is to show the power of XPS technique to determine the elemental composition in the sample (Gadolinium doped polymer) as well as to determine; if ~~there is~~ any impurity present or not. Also we want to demonstrate the capability of XPS in distinguishing different electronic environments of an element in the sample.

not well written

3.0 EXPERIMENTAL SETUP

The experimental setup consist of a source of fixed energy radiation, an electron energy analyser, a ultra-high vacuum chamber, a low-energy electron (flood) gun, and a sputter ion gun, as shown in Figure 1. The XPS Spectrometer used in this work is of model number ESCALAB 250xi and is shown in Figure 2.

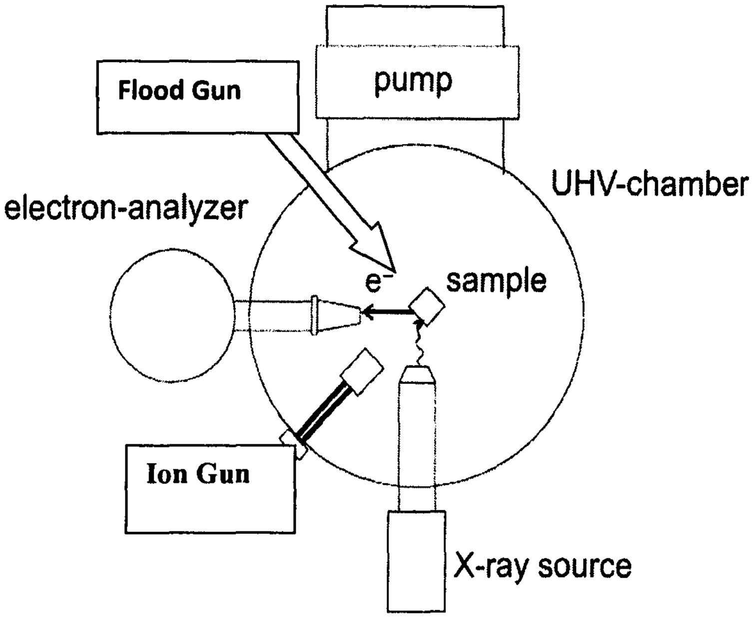

Figure 1: A schematic diagram of UHV chamber with other XPS components.

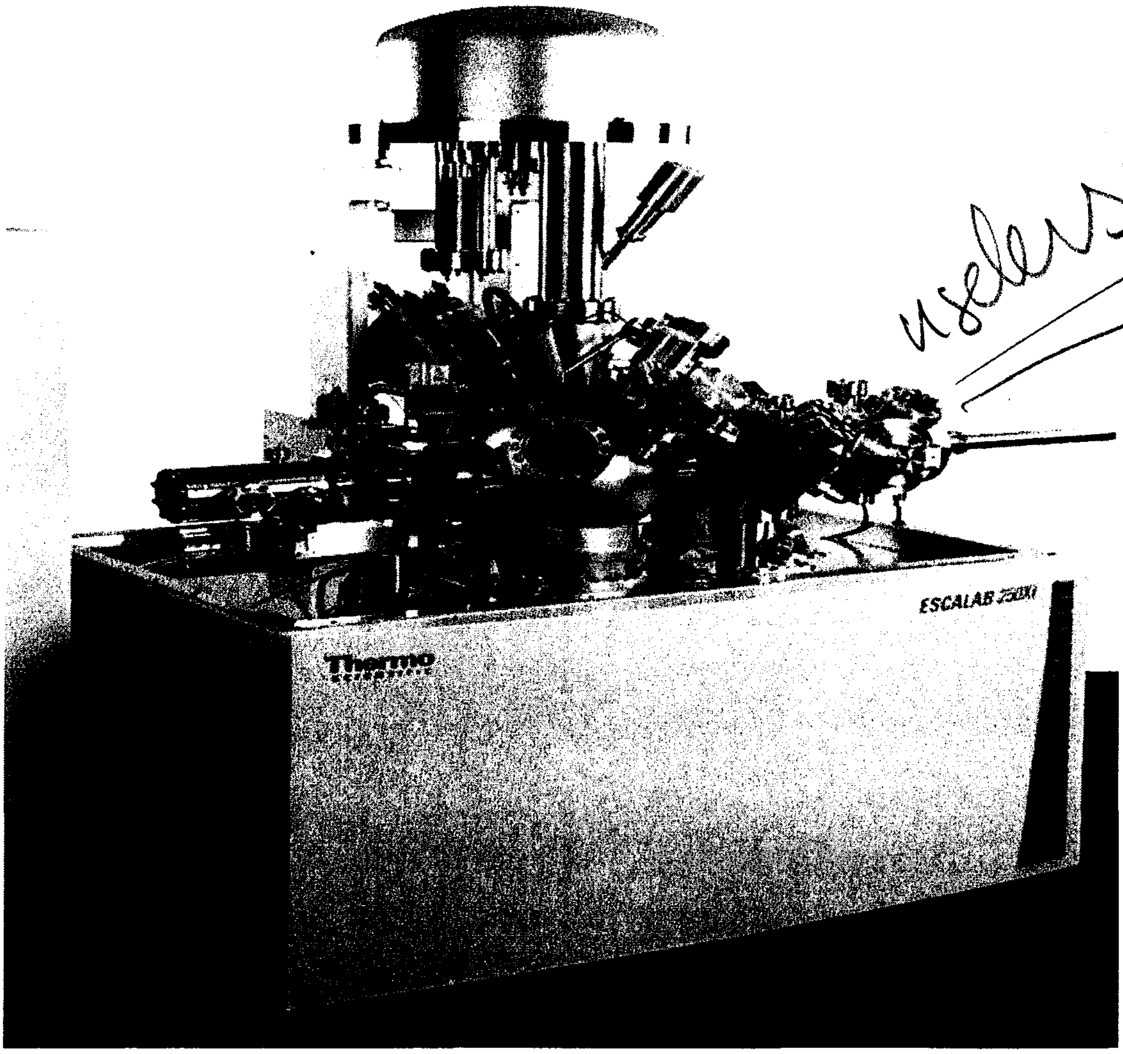

useless

Figure 2: X-ray Photoelectron Spectroscopy Equipment (Model ESCALAB 250xi)

3.1 Vacuum System

Most spectrometers these days are built to operate in the ultra high vacuum (UHV) range of 10^{-9} to 10^{-10} mbar, this pressure range is also recommended for XPS for the following reasons.

1. At high pressure, the photoelectron has very high tendency to be scattered by residual gas molecule, which in turn affect the actual spectrum display and in the noise within the spectrum [7].
2. Gas molecules have a high tendency to stick to sample surface at a pressure of 10^{-6} mbar and thus contaminate the sample surface.

3. The distance between sample and detector is almost of 1 m. To avoid the photo electron from collision (hence loosing energy) with the gas molecules for this long distance, we need UHV.
4. The mean free path is normally in the range of 3A°. If there is a contamination on the sample then it will be difficult for the photoelectrons to come out in sufficient amount for the XPS spectra.

3.2 X-ray Source

X-rays can be generated by using a high energy electron to bombard an anode (Cr, Fe, Co, CU, Mo & Ag) material. The energy of X-ray generated is a function of the type of anode material used. The most generally used x-ray sources are Mg $K\alpha$ radiation: $h\nu$=1253.6ev and Al $K\alpha$ radiation: $h\nu$=1486.6ev. In our case, we are using Al $K\alpha$.

Space

3.3 Electron Energy Analyser

What electron energy analyser does is to measure the kinetic energy (KE) distribution of emitted photoelectrons from the sample. There are two types of analyser that are in common usage; namely the cylindrical mirror analyser (CMA) and the concentric hemispherical analyser (CHA). The latter is the most commonly used for high performance XPS instruments. Since the cornerstone of XPS is spectral resolution, it led to the development of CHA with sufficient good resolution as oppose to CMA. We are using CHA in our experiment.

3.4 Sputter Ion Gun

This is used for etching (cleaning) of the sample surface which is achieved by use of argon ion beam. The ion beam is usually produced by leaking the Argon in the ion gun source chamber and ionized by electron bombardment. The produced Ar^+ ions are collected from the source, focused and accelerated onto the sample surface by arrangement of a set of electrostatic lenses. In our case we are unable to do etching due to the nature of sample (polymer).

3.5 Flood Fun

This is an XPS component that uses low energy electrons (i.e. 0–10 ev) to neutralize positively charged Insulator or semiconductor sample surfaces. When X-rays strike the surface of an insulator excess positive charges are left on the surface after emission of photoelectrons, so there is always need for neutralization. In the case of conducting sample the ground connection to the sample provides neutralizing electrons.

3.6 The Sample Structure

Following is structure of the Gadolinium doped polymer.

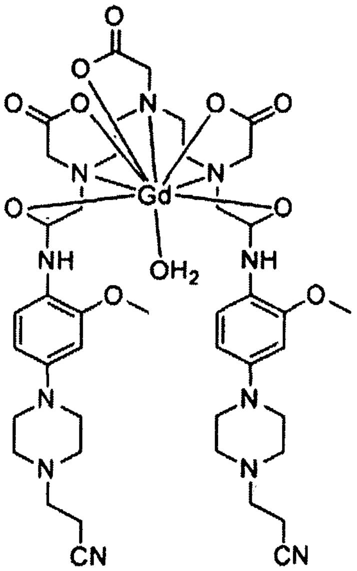

Chemical Formula: C42H58GdN11O11
Molecular Weight: 1050.23

Atoms in the Gadolinium doped polymer unit cell

C-C	21
C=C	6
C=O	3
C-O	7
C-N	24

Unfortunately, the XPS machine is out of the service due to some technical problems. Therefore, we could not perform the experiment and were given raw data to analyze as per the agreement with the course coordinator.

4.0 RESULTS AND DISCUSSION

4.1 Charge Shift Correction

A thin layer of carbonaceous material is usually found on the surface of most air exposed samples, carbon in this layer is generally known as adventitious carbon [8]. Adventitious carbon is generally comprised of carbon-carbon bonds [9].

In our case the charge shift in adventitious C 1s binding energy is 1.9eV, because the actual binding energy for carbon is 284.8 eV [8], and the spectrum value was 282.9 eV. As a result we added 1.9eV into the spectrum value to make it 284.8 eV. This charge shift in carbon was used to correct the binding energy of the entire elements in Gadolinium doped polymer sample before fitting the spectrum.

4.2 Survey Spectra

The purpose of the survey spectra is to give overall information about the elements present in the sample and their relative abundance. A wide scan of the sample was carried out to have snap shot of what elements are present in the sample; the survey spectrum obtained is shown below (Figure 3).

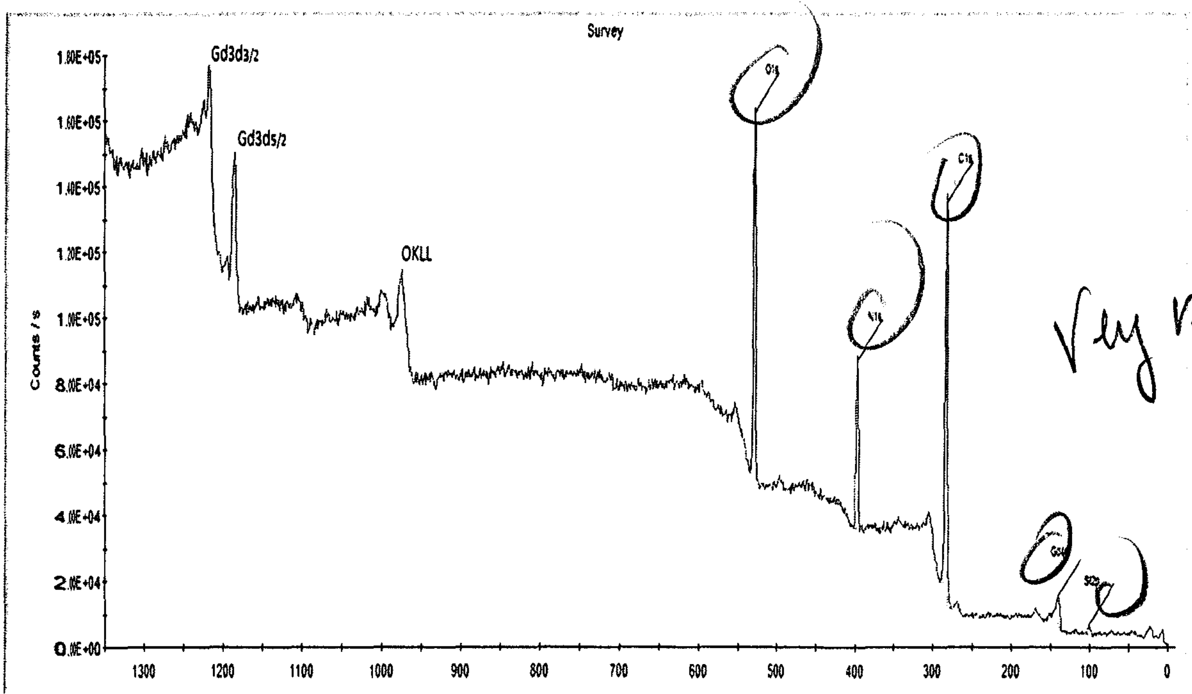

Very Bad

not clear

Figure 3: Survey spectrum of the sample (Gadolinium doped polymer)

From the Survey spectrum we can see that the elements present in the sample are O, C, N, Gd and Si as impurity, while the C 1s is adventitious carbon, due to the exposure of the sample to moist air and UHV environment.

4.3 Elemental Spectra

From the survey spectra, one determines what elements are present in the sample. Now we will see all the present elements in the sample one by one in details. The first element is carbon. The spectra of carbon and its fitted curves are shown in the following figure 4.

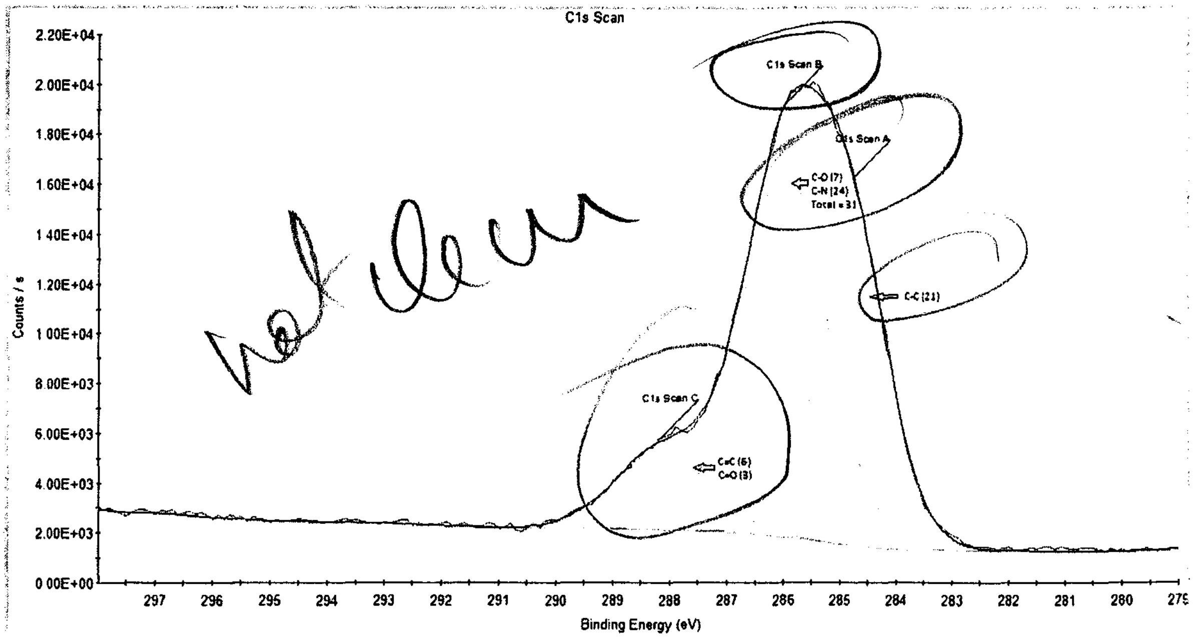

not clear

Figure 4: Fitted spectra for carbon

The three fitted peaks shown in the figure 4 shows the three different electronic environments of carbon. These includes C-C, C-N & C-O and C=C & C=O peaks from lower to higher binding energies respectively as mentioned in the figure. We can observe that the intensities of the three peaks are different. This is in accordance with the given data [9]. The peak intensities show the ratios between peaks approximately as 1:3:2.

The second element in the survey spectra is Nitrogen. The fitted spectrum for nitrogen is given in the figure 5.

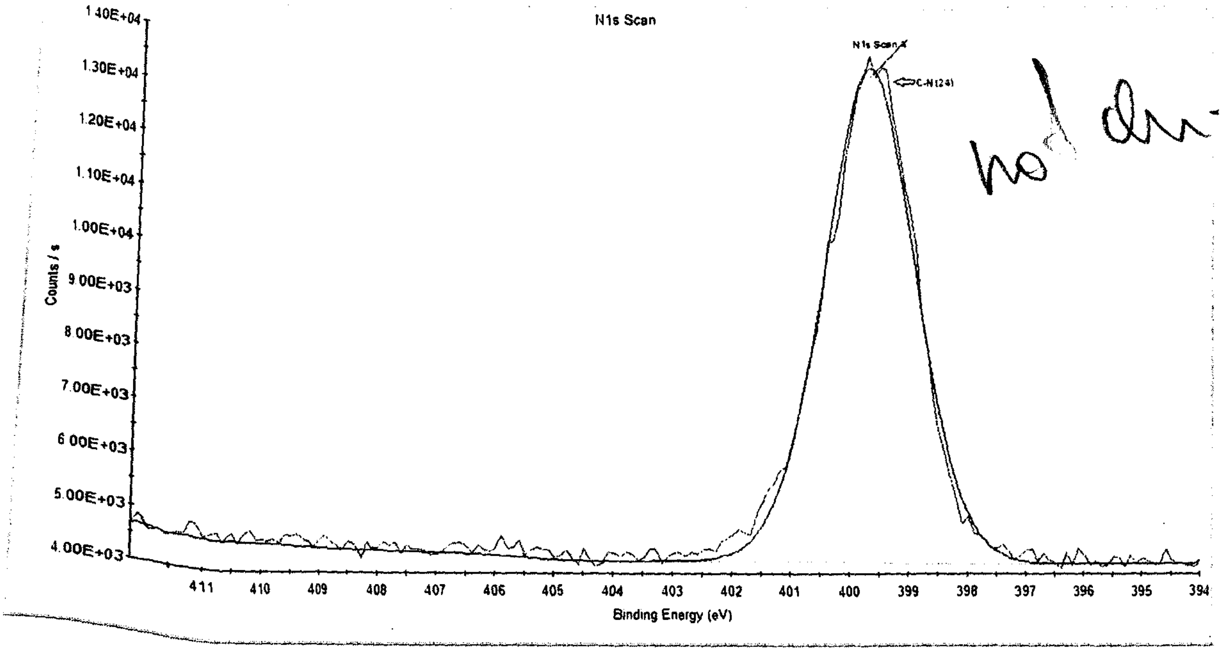

no! dw

Figure 5: Fitted spectra for nitrogen

The nitrogen has only one fitted peak which shows that nitrogen has only one electronic environment with carbon. The peak intensity shows the C-N bonds.

The third element in the survey spectra is oxygen. The fitted Spectrum for oxygen is given in the figure 6.

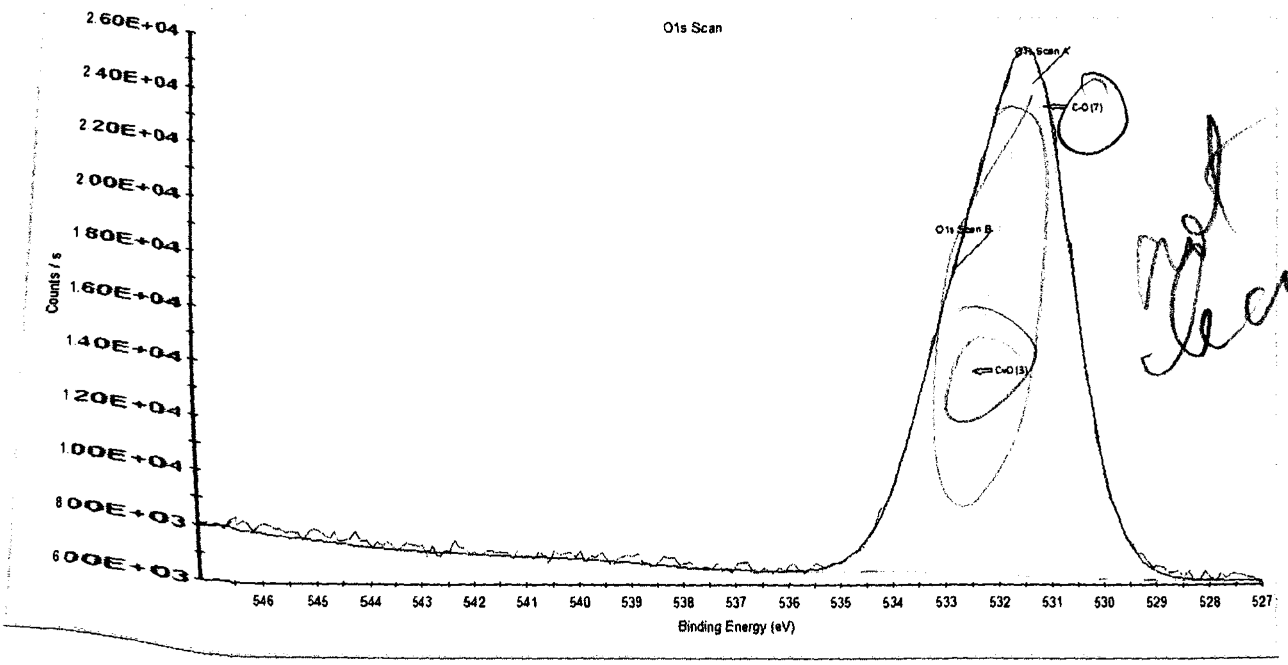

not clear

Figure 6: Fitted spectra for Oxygen

The spectrum in the figure 6 shows that oxygen has two different electronic environments which are C-O and C=O. The peak intensities show the ratio approximately 1:2.

The spectrum of Gd4d is shown in the figure 7.

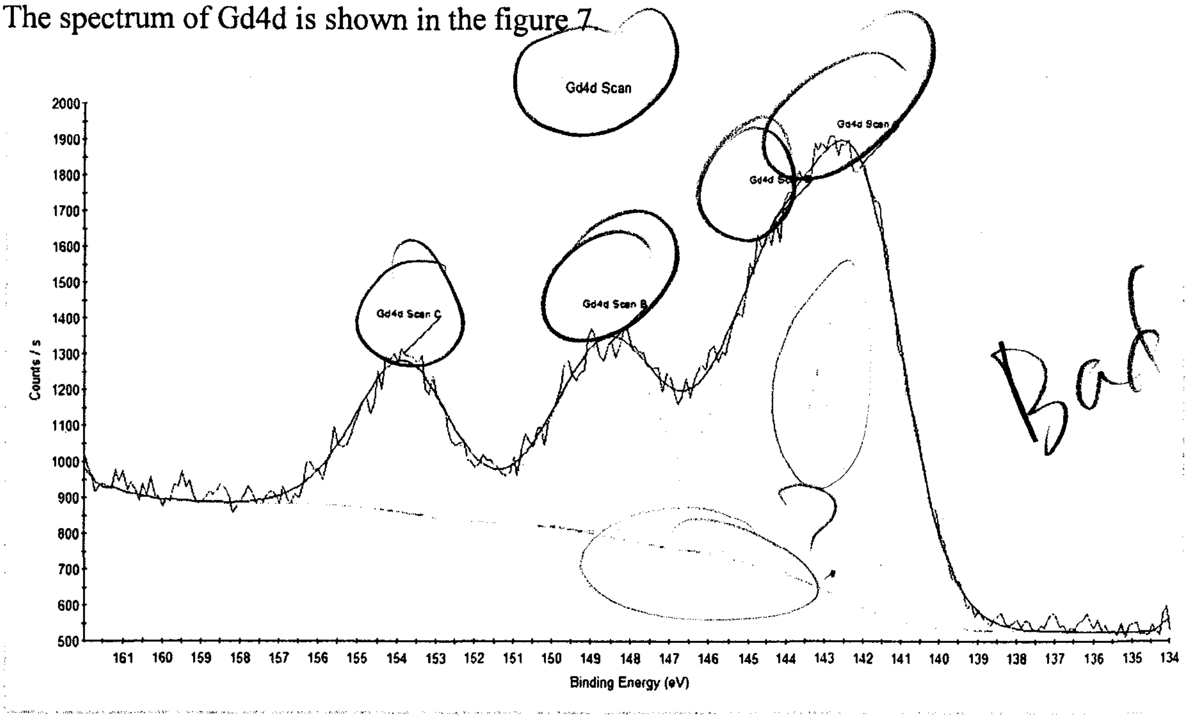

Bad

Figure 7: Fitted spectra for Gadolinium

We can observe that there are four fitted peaks in the spectra. But if we see the sample structure then we can found that Gd has only two different electronic environments. So, where these peaks are coming from? These peaks are called multiplet peaks. These peaks are special property of the some elements like transition metals and lanthanide rare earth elements. Since Gadolinium belongs to lanthanide rare-earth elements which has ground state configuration [Xe] $4f^7 5d^1 6s^2$.This shows the f-sub shell is half filled and have unpaired electron. When an electron from the core electrons left the atom as a result of photoelectric effect then coupling between these unpaired electron gives these multiplet peaks[10] [11].

Figure 8 shows the fitted spectra of the all the elements present in Gadolinium doped polymer sample:

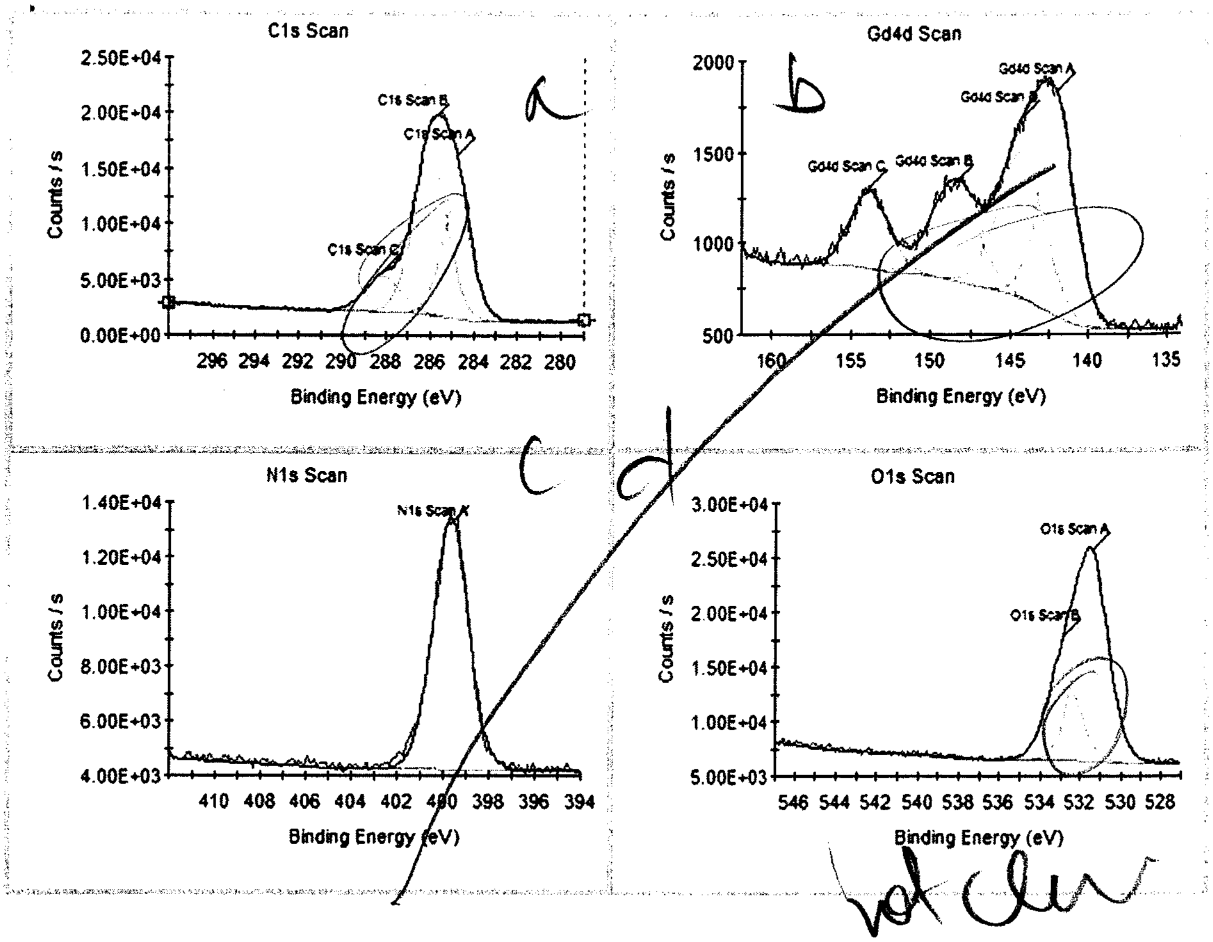

not clear

Figure 8: Fitted spectra for the entire element present in Gd doped polymer sample

not explained

The spectra of all the elements are explained individually above. Figure 8 shows the overall comparison of all elements present in the sample in which we fitted the peaks in all elements to know the area under the peaks. This area is required in order to quantify the elements. Table 1 below show the fitted data obtained from the Gd doped polymer sample.

Name	Peak BE	FWHM eV	Area (P) CPS.eV	Atomic %
C1s Scan A	284.8	1.58	18413.77	22.04
C1s Scan B	286.0	1.77	28814.23	34.49
C1s Scan C	288.1	1.93	6648.85	7.96
Gd4d Scan A	142.0	2.78	3000.09	0.34
Gd4d Scan **B**	148.5	3.37	1977.31	0.22
Gd4d Scan C	153.8	2.81	1290.19	0.15
Gd4d Scan D	144.3	3.37	2924.14	0.33
N1s Scan A	399.7	1.78	17809.89	12.07
O1s Scan A	531.4	1.87	356816.83	15.33
O1s Scan B	532.9	1.92	16511.73	7.07

Table 1: XPS fitted data for Gadolinium doped polymer

From the Table 1, there are three (3) different c1s peaks with different binding energies, which implies that they are in different electronic environment. Also we can observe the atomic percentages of the three C1s peaks are different which are according to the given values of sample. In the case of nitrogen only one peak has been observed which shows its electronic bond with carbon. The area under the curve shows its quantification. Oxygen has two different peaks at two slightly different binding energies which show its two different electronic environments with carbon single bond carbon and carbon double bond carbon. Gadolinium has four fitted peaks. These peaks are due to multiplet splitting phenomenon which has been explained in the preceding paragraph. The data shows that Gadolinium has very small amount of atomic percentage in the sample which matches the given data. From these quantification results we can observe the power of XPS.

You didn't analyze

5.0 CONCLUSION

In summary, we analyzed Gadolinium doped polymer sample using XPS technique. In the results, we have found that silicon is present in the sample as an impurity. Also we have calculated the elemental composition through peak intensities by calculating the area under the peaks. Most importantly we observe that the same elements with different electronic environments can be detected through XPS quite accurately. These all observations show the power of XPS technique for elemental analysis.

6.0 REFERENCES

1. Briggs, D., "*Surface Analysis of Polymers by XPS and Static SIMS*",Cambridge, UK: Cambridge University Press. 198 (1998).
2. Siegbahn, K.; Edvarson, K. I. Al "*β-Ray spectroscopy in the precision range of 1 : 1e6*". Nuclear Physics 1 (8): 137–159 (1956).
3. Electron Spectroscopy for Atoms, Molecules and Condensed Matter, Nobel Lecture, December 8, (1981).
4. Nenad Stojilovic, "*Why can't we see Hydrogen in X-Ray Photoelectron Spectroscopy*", J. Chem. Educ., , 89 (10), pp 1331–1332 (2012).
5. http://en.wikipedia.org/wiki/X-ray_photoelectron_spectroscopy
6. Natalia Maximova., "*Application of the X-ray photoelectron spectroscopy for Development of the Nobium chemical Mechanical process, photo modification of silicon for the field release mass spectrometer, and analysis of the multifunctional oxide hetero-structures*", (2008).
7. John F. Watts and John wolstenholme., *"An Introdution to SURFACE ANLYSIS by XPS and AES"*, University of surrey, uk (2003).
8. M.C Biesinger,*"X-ray photo electron spectroscopy (XPS) reference pages."*,(2013). Available from: http://www.xpsfitting.com/2011/01/what-is-adventitious-carbon.html
9. http://xpssimplified.com/
10. J.A. Gupta and Co. "*Interfacial layer formation in Gd2O3 films deposited directly on Si (0 0 1)*", Applied Surface Science 173 318-326 (2001).
11. http://www.xpsfitting.com/2008/09/multiplet-splitting.html

Too much from internet

King Fahd University of Petroleum and Minerals
Department of Physics
Physics 503 - Term 142

Experiment #2 Report

Student Name : Fatai Liadi

Student ID : 201405000

Code : E206

Evaluator : Dr. Harrabi

	grades	Out of
Abstract	0.5	1
Introduction	4	5
Experimental details	5.5	6
Results and Discussion	7	9
Conclusion	1	1
References	0.5	1
Overall	1.5	2
Total	20	**25**

Ok

جامعة الملك فهد للبترول و المعادن
قسم الفيزياء
RECEIVED
12 APR 2015
وارد
King Fahd University of Petroleum & Minerals
PHYSICS DEPT

KING FAHD UNIVERSITY OF PETROLEUM AND MINERALS

DHAHRAN

DEPARTMENT OF PHYSICS

PHYS-503: GRADUATE LABORATORY (TERM 142)

HOTSPOT IN SUPERCONDUCTOR NbTiN STRIP

Student Name: Liadi Fatai Ayofe

Student ID: g201405000

Instructor:
Dr. Khalil Harrabi

April 12, 2015

Contents

Abstract

The current pulse technique has been used to study the destruction of **NbTiN** superconductivity with a step bias current in the nanoseconds of range. The increment in bias current above the critical current I_c creates a spot in the superconductivity filament called phase- slip center (**PSC**) or hotspot (**HS**). The appearance of the voltage caused due to this increment of current in **NbTiN** strip at 4.0K was measured. The delay time t_d of the nucleation spot decrease as the current increases was measured. The aforementioned delay time t_d values were plotted against applied current to critical current ratio $\frac{I}{I_c}$ and ~~deduce~~ the heat escape time. was deduced

1.0 Introduction

Superconductivity is an absolute remarkable phenomenon discovered in 1911 by a Dutch physicist Heike Kamerlingh Onnes with his student in the Leiden laboratory. He found that the resistance of mercury metal disappeared suddenly below a transition temperature. He also discovered relatively that small magnetic fields destroy superconductivity and the critical magnetic field is a function of temperature [1]. In few years after discovery of superconductivity, an important property of superconductor known as Meissner effect: below the critical temperature, the magnetic field is expelled from the interior of the superconductor (as shown in the ***figure 1*** below). This effect will occur only if the magnetic field is very small. Then, if the magnetic fields become higher, it penetrates the interiors of the material and loses its superconductivity [2].

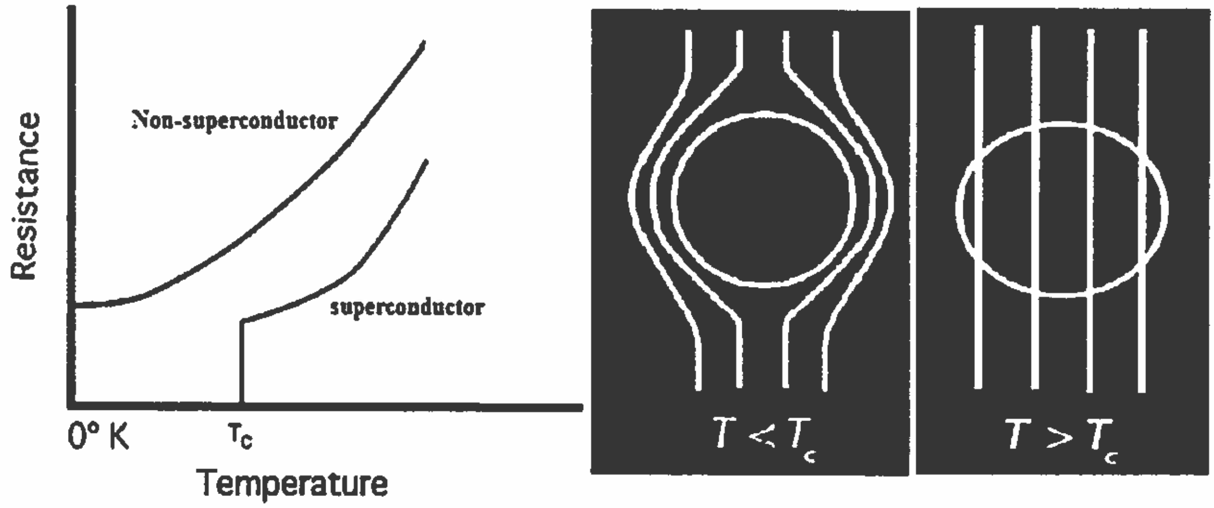

Figure 1: shows the relationship between resistance and temperature for non-superconductor and superconductor, meissner effect

Superconductors are classified into type I and type II with regards to their magnetic properties. Type I superconductor exhibits meissner effect, if the magnetic field produces is higher than critical magnetic field, the superconductivity destroy and the material become normal. Critical magnetic field is the minimum field applied when material loses its superconductivity. Example of type I superconductors are tin, aluminum and lead. While type II superconductors are generally alloys and they are characterized by a lower critical magnetic field B_{C1} and upper critical magnetic field B_{C2}. The magnetic flux start entering superconductor at B_{C1} and at B_{C2} superconductivity disappeared. Examples of type II superconductor are Niobium titanium, Niobium tin.

not enough

1.1 Applications

Superconductor has numerous applications such as technological application, civilian and military application [1]. Among the technological application: superconducting nanowire single-photon detector (**SNSPD**). This is based on cooling superconducting wire below critical temperature and biased with direct current that is close but less than critical current. Critical current is the minimum current needed to destroy locally superconductivity. When photon incident on this material which is made typical from approximate 5 nm thick niobium nitride films, it breaks electron cooper pairs and critical current fall below the bias current. This lead to formation of a resistive region called Hotspot (**HS**) across the width of nanowire. This resistive region then leads to detectable voltage pulse of about 1 nanosecond. Resistance heating caused by direct current aids the growth of resistive region along the axis of the nanowire until the current flow is blocked before the resistive region subside and the wire becomes fully superconducting again [3,4]. This figure below depicts basic operation of superconducting nanowire single-photon detector (**SNSPD**).

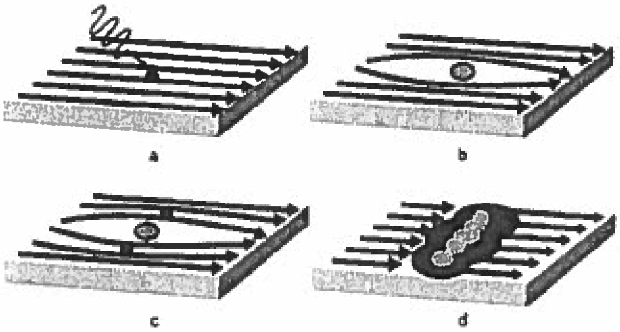

Figure 2: Shows Superconducting Nanowire Single Photon Detector operations

Niobium-titanium is often chosen because of its superior mechanical properties. It has a critical magnetic field of 15 Tesla and a critical temperature of 10 K. Among the many applications: Magnetic Resonance Imaging, Lazer surgery, Mine detonator, Nuclear electric power plants in remote areas. Also, High temperature superconductor materials can be superconducting at liquid nitrogen temperatures making possible long distance transmission of electric power at higher temperatures [1].

1.2 Objective of Experiment

The objective of this experiment is to study the formation of Phase-slip center (**PSC**) or Hotspot (**HS**) in NbTiN superconducting strip.

2.0 Experimental Details

Our NbTiN film, 20 nm thick and 5 μm wide, was deposited at room temperature on sapphire by DC magnetron sputtering in an argon-nitrogen plasma (STAR-Cryoelectronics. NM, USA). The final pattern, including two lateral probes, 1 mm apart from one another, plus four contact pads was obtained by using standard photo-litographic process and ion milling. The measurements were performed at 4 K on one sample width 3 nm. The critical temperature T_c = 8.5 K. The *figure 3* below shows the schematic representation of the experiment setup.

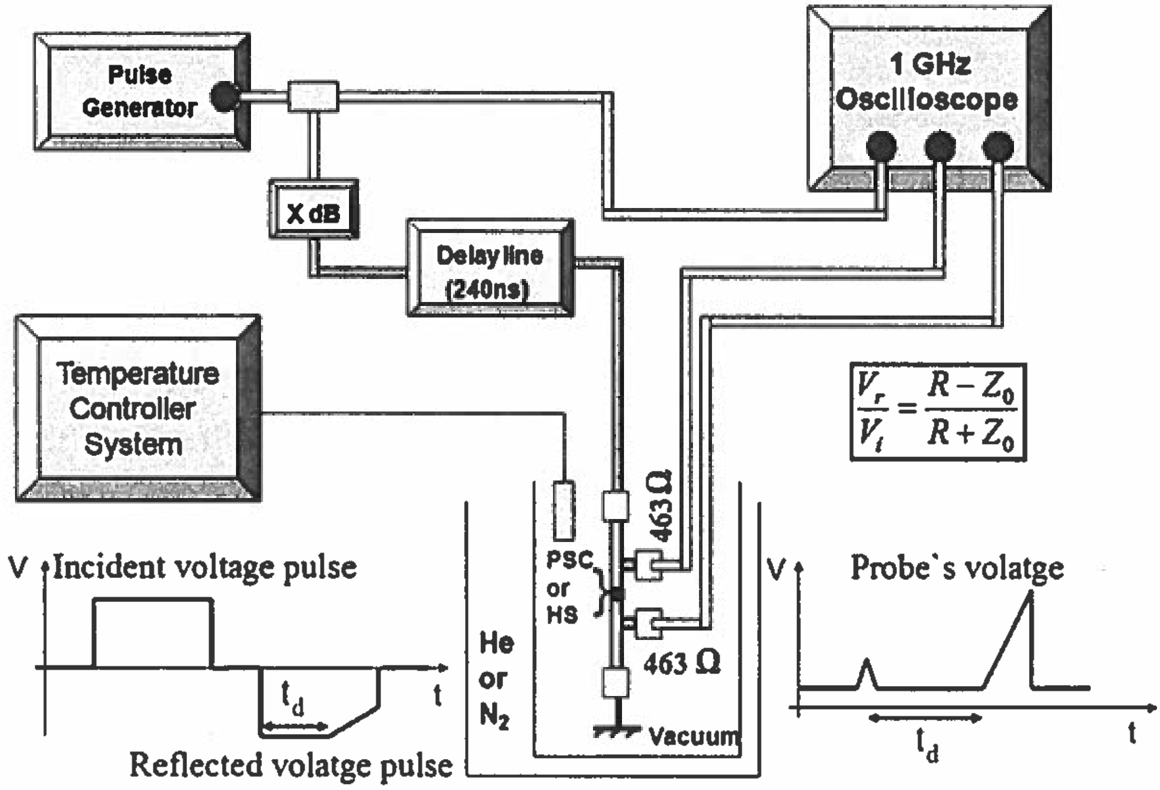

Figure 3: ***Shows the experimental setup used for pulse measurements. It consists of a pulse generator used to send a pulse, delay line is required to separate the incident pulse (Vi) from the reflected pulse (Vr), and an oscilloscope is used to measure the voltage and the delay time td. R represents the appeared resistance of the PSC or HS. The temperature controller is used to change the substrate temperature***

The sample was mounted in the helium cryostat (a device used to maintain low temperature of samples under investigation) to keep the temperature below critical temperature of the sample which is 8.5 K. A pulse generator was used to send electrical pulse with pulse duration of 450 ns at 10 kHz into the sample through a coaxial cable of impedance $Z_o = 50\Omega$ and measuring the

X dB - what is the role.

voltage response using lateral probes. A delay line was used to separate incident voltage from reflected one by 240 ns. These incident and reflected voltage response and delay time **t_d** were measured by fast oscilloscope. The current *I* passing through the sample is given by

$$I = \frac{Vi - Vr}{Z_o}$$

3.0 Results and Discussion

The sample was cooled to 4 K which is lower than the critical temperature of the sample (8.5 K). The electrical current pulse was send to the sample through pulse generator. When the current applied is greater than the critical current, the voltage response start coming up which is the sign of the formation of Phase-slip center **PSC** or Hotspot **HS** on the sample. This voltage response was taken with fast oscilloscope. Different dissipative mode appeared based on the changes in current amplitude using attenuator. The delay time **t_d** which is the time required to destroy superconductivity of the sample was recorded and the values of this delay time **t_d** was reducing as the applied current ***I*** increases. The voltage responses which marks the destruction of the superconductivity of the sample occur after a delay time **t_d** for the current amplitude greater than the critical current ***I_c*** are shown in the ***figure 4*** below. The critical current ***I_c*** was calculated to be 28.25 mA at 4 K.

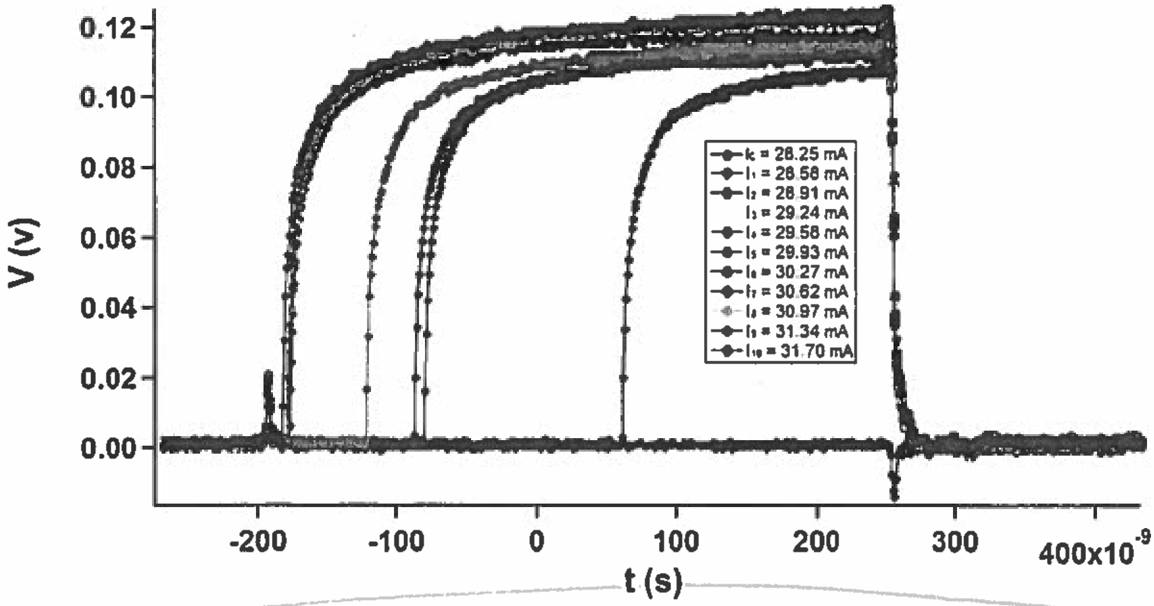

Figure 4: Shows Voltage response versus time of sample NbTiN for $I > I_c$ at T =4 K

very short more explanation is required

The saturation voltage response as a function of time as shown in the figure above has been reported to be characteristic of nucleation of a Phase-slip center **PSC** [8]. The plot of time delay t_d against reduced current I/I_c is shown in the *figure 5* below.

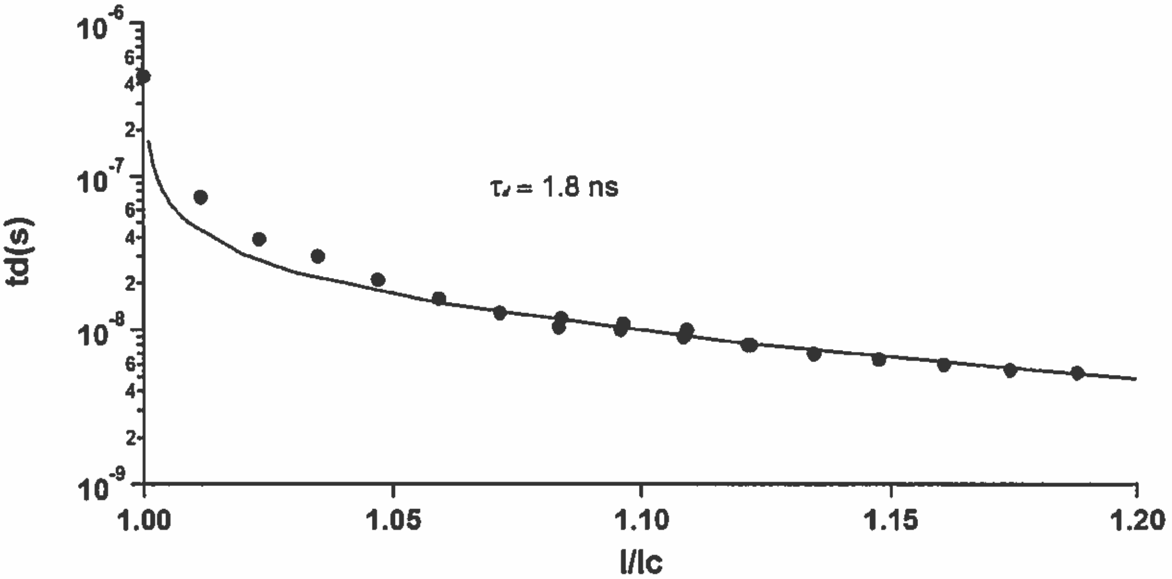

Figure 5: Schematic diagram of delay time t_d against reduced current I/I_c

The discernment of the phase-slip center from the vortex flow mode by delay time t_d is described by time dependent Ginzburg-Landau (TDGL) equation and it's simplified to zero dimension. The time dependent Ginzburg-Landau (TDGL) equation is given by [5, 9, 10]:

$$t_d\left(\frac{I}{I_c}\right) = \tau_d \int_0^1 \frac{2f^4 df}{\frac{4}{27}\left(\frac{I}{I_c}\right)^2 - f^4 + f^6}$$

Where τ_d is pre-factor of the integral and it was interpreted as the gap of relaxation time. It is referred to as an adjustable parameter to fit experimental delay time, was found experimentally to be proportional to the film thickness, and actually to coincide with the cooling time of the film [5, 9, 10, 11, 12].

ok

4.0 Conclusion

The electrical current pulse technique has been used to study the voltage response as a function of delay time of **NbTiN** strip sample due to applied current exceeding critical current I_c of 28.25 mA. Consequently, further increase in applied current led to transformation of phase-slip center **PSC** to hotspot **HS** which marks complete transition to normal state and voltage saturation.

Acknowledgements

My sincere gratitude goes to my supervisor Dr. Khalil Harrabi for dedicating his time to put me through the whole process and also for his guidance and sublime encouragement. I would like extend my gratitude to the physics department for the opportunity given to broaden my practical experience.

References

1. J. Bardeen, L.N. Cooper, J.R. Schrieffer, 1957. *Theory of superconductivity.* Department of Physics, University of Illinois, urbana, Illinois.
2. K.H. Bennemann, J.B.Ketterson, *History of Superconductivity: Conventional, High Transition Temperature and Novel Superconductors* Dept. of Physics and Astronomy,Northwestern University, Evanston,USA.
3. C. M Natarajan, M. G Tanner, R. H Hadfield, *Supercond. Sci. Technol.* **25** 063001 (16pp) (2012)
4. S. N. Dorenbos, P. Forn-Díaz, T. Fuse, A. H. Verbruggen, T. Zijlstra, T. M. Klapwijk, V. Zwiller. *Low gap superconducting single photon detectors for infrared sensitivity,* Applied Physics Letters **98**, 251102 (2011)
5. K. Harrabi, *Hotspot Temperatures Reached in Current-Driven Superconducting Niobium Filaments.* J Supercond Nov Magn **26**:1865–1868, (2013)
6. K. Harrabi, Resistive states created in superconducting NbTiN filaments by an electrical current pulse, AIP ADVANCES **5**, 037102 (2015)
7. F. R. Ladan K. Harrabi · M. Rosticher, P. Mathieu, J. P. Maneval, C. Villard, *J Low Temp Phys* 153: 103–122 (2008)
8. K. Harrabi, *Temperature Elevation of Current-Driven Phase-Slip Centers in* $YBa_2Cu_3O_7$ *Strips.* J Supercond Nov Magn **28**:573–577 (2015)
9. Pals, J.A., Wolter, J.: Phys. Lett. A **70**, 150 (1979)
10. Tinkham, M.: In: Gray, K.E. (ed.) Non-Equilibrium Superconductivity, Phonons and Kapitza Boundaries, Chap. 8, NATO Conference. Plenum, New York (1981)
11. K, Harrabi, Ladan, F.R., Dinh Lam, V.u., Maneval, J.-P., Hamet, J.-F., Vill'egier, J.-P., Bland, R.W.: J. Low Temp. Phys. 157, 36 (2009)
12. K, Harrabi,: J. Supercond. Nov. Magn. 26, 1865 (2013)

King Fahd University of Petroleum and Minerals
Department of Physics
Physics 503 - Term 142

Experiment #2 Report

Student Name : Fatai Liadi

Student ID : 201405000

Code : E206

Evaluator : Dr. Naqvi

	grades	Out of
Abstract	1	1
Introduction	4	5
Experimental details	5	6
Results and Discussion	7	9
Conclusion	1	1
References	1	1
Overall	2	2
Total	21	**25**

$\frac{21}{25}$

جامعة الملك فهد للبترول و المعادن
قسم الفيزياء
RECEIVED
12 APR 2015
وارد
King Fahd University of Petroleum & Minerals
PHYSICS DEPT

KING FAHD UNIVERSITY OF PETROLEUM AND MINERALS

DHAHRAN

DEPARTMENT OF PHYSICS

PHYS-503: GRADUATE LABORATORY (TERM 142)

HOTSPOT IN SUPERCONDUCTOR NbTiN STRIP

Student Name: Liadi Fatai Ayofe

Student ID: g201405000

Instructor:
Dr. Khalil Harrabi

April 12, 2015

Contents

Abstract

The current pulse technique has been used to study the destruction of **NbTiN** superconductivity with a step bias current in the nanoseconds of range. The increment in bias current above the critical current I_c creates a spot in the superconductivity filament called phase- slip center **(PSC)** or hotspot **(HS)**. The appearance of the voltage caused due to this increment of current in **NbTiN** strip at 4.0K was measured. The delay time t_d of the nucleation spot decrease as the current increases was measured. The aforementioned delay time t_d values were plotted against applied current to critical current ratio $\frac{I}{I_c}$ and deduce the heat escape time.

1.0 Introduction

Superconductivity is an absolute remarkable phenomenon discovered in 1911 by a Dutch physicist Heike Kamerlingh Onnes with his student in the Leiden laboratory. He found that the resistance of mercury metal disappeared suddenly below a transition temperature. He also discovered relatively that small magnetic fields destroy superconductivity and the critical magnetic field is a function of temperature [1]. In few years after discovery of superconductivity, an important property of superconductor known as Meissner effect: below the critical temperature, the magnetic field is expelled from the interior of the superconductor (as shown in the *figure 1* below). This effect will occur only if the magnetic field is very small. Then, if the magnetic fields become higher, it penetrates the interiors of the material and loses its superconductivity [2].

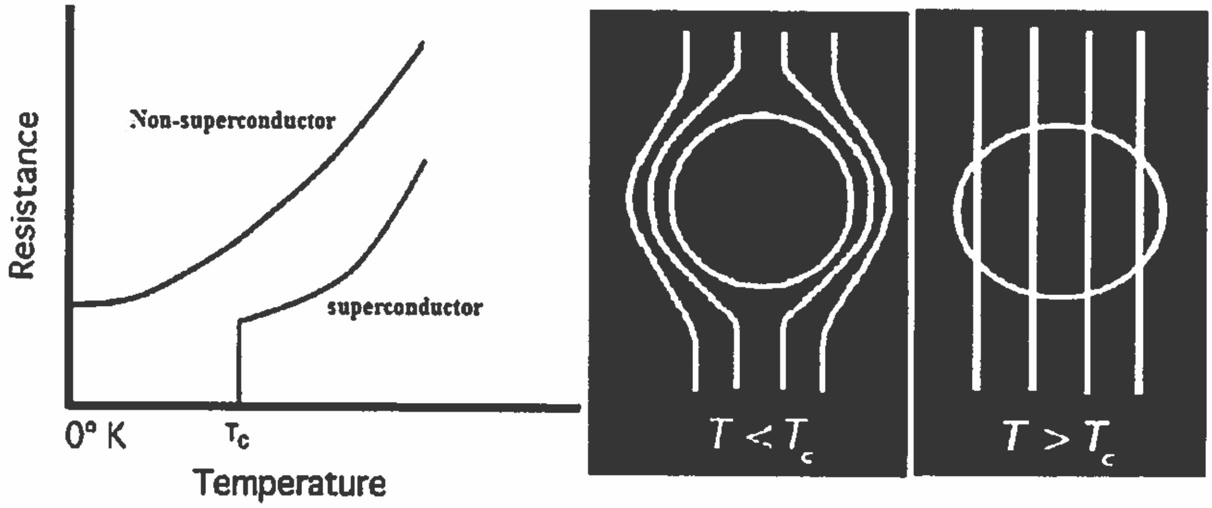

Figure 1: shows the relationship between resistance and temperature for non-superconductor and superconductor, meissner effect

Superconductors are classified into type I and type II with regards to their magnetic properties. Type I superconductor exhibits meissner effect, if the magnetic field produces is higher than critical magnetic field, the superconductivity destroy and the material become normal. Critical magnetic field is the minimum field applied when material loses its superconductivity. Example of type I superconductors are tin, aluminum and lead. While type II superconductors are generally alloys and they are characterized by a lower critical magnetic field B_{C1} and upper critical magnetic field B_{C2}. The magnetic flux start entering superconductor at B_{C1} and at B_{C2} superconductivity disappeared. Examples of type II superconductor are Niobium titanium, Niobium tin.

1.1 Applications

Superconductor has numerous applications such as technological application, civilian and military application [1]. Among the technological application: superconducting nanowire single-photon detector **(SNSPD)**. This is based on cooling superconducting wire below critical temperature and biased with direct current that is close but less than critical current. Critical current is the minimum current needed to destroy locally superconductivity. When photon incident on this material which is made typical from approximate 5 nm thick niobium nitride films, it breaks electron cooper pairs and critical current fall below the bias current. This lead to formation of a resistive region called Hotspot **(HS)** across the width of nanowire. This resistive region then leads to detectable voltage pulse of about 1 nanosecond. Resistance heating caused by direct current aids the growth of resistive region along the axis of the nanowire until the current flow is blocked before the resistive region subside and the wire becomes fully superconducting again [3,4]. This figure below depicts basic operation of superconducting nanowire single-photon detector **(SNSPD)**.

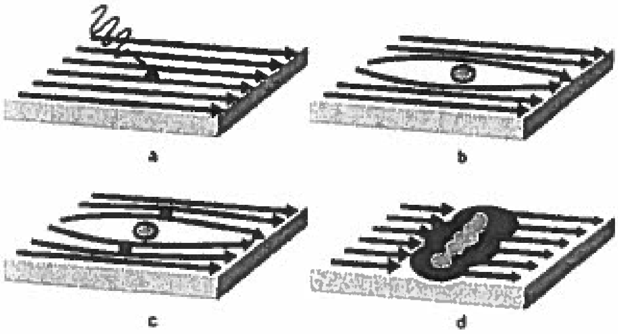

Figure 2: Shows Superconducting Nanowire Single Photon Detector operations

Niobium-titanium is often chosen because of its superior mechanical properties. It has a critical magnetic field of 15 Tesla and a critical temperature of 10 K. Among the many applications: Magnetic Resonance Imaging, Lazer surgery, Mine detonator, Nuclear electric power plants in remote areas. Also, High temperature superconductor materials can be superconducting at liquid nitrogen temperatures making possible long distance transmission of electric power at higher temperatures [1].

1.2 Objective of Experiment

The objective of this experiment is to study the formation of Phase-slip center **(PSC)** or Hotspot **(HS)** in NbTiN superconducting strip.

2.0 Experimental Details

Our NbTiN film, 20 nm thick and 5 μm wide, was deposited at room temperature on sapphire by DC magnetron sputtering in an argon-nitrogen plasma (STAR-Cryoelectronics. NM, USA). The final pattern, including two lateral probes, 1 mm apart from one another, plus four contact pads was obtained by using standard photo-litographic process and ion milling. The measurements were performed at 4 K on one sample width 3 nm. The critical temperature T_C = 8.5 K. The *figure 3* below shows the schematic representation of the experiment setup.

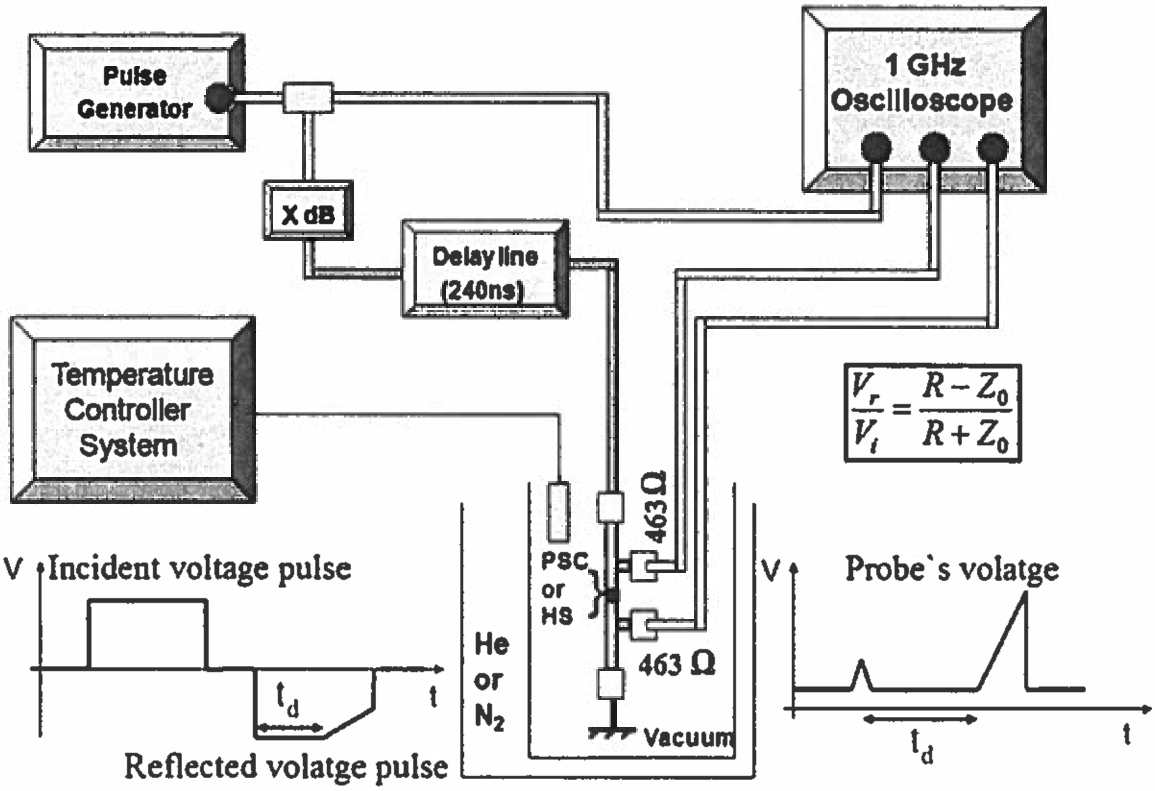

Figure 3: ***Shows the experimental setup used for pulse measurements. It consists of a pulse generator used to send a pulse, delay line is required to separate the incident pulse (Vi) from the reflected pulse (Vr), and an oscilloscope is used to measure the voltage and the delay time td. R represents the appeared resistance of the PSC or HS. The temperature controller is used to change the substrate temperature***

The sample was mounted in the helium cryostat (a device used to maintain low temperature of samples under investigation) to keep the temperature below critical temperature of the sample which is 8.5 K. A pulse generator was used to send electrical pulse with pulse duration of 450 ns at 10 kHz into the sample through a coaxial cable of impedance $Z_o = 50\Omega$ and measuring the voltage response using lateral probes. A delay line was used to separate incident voltage from reflected one by 240 ns. These incident and reflected voltage response and delay time t_d were measured by fast oscilloscope. The current I passing through the sample is given by

$$I = \frac{Vi - Vr}{Z_o}$$

3.0 Results and Discussion

The sample was cooled to 4 K which is lower than the critical temperature of the sample (8.5 K). The electrical current pulse was send to the sample through pulse generator. When the current applied is greater than the critical current, the voltage response start coming up which is the sign of the formation of Phase-slip center **PSC** or Hotspot **HS** on the sample. This voltage response was taken with fast oscilloscope. Different dissipative mode appeared based on the changes in current amplitude using attenuator. The delay time t_d which is the time required to destroy superconductivity of the sample was recorded and the values of this delay time t_d was reducing as the applied current I increases. The voltage responses which marks the destruction of the superconductivity of the sample occur after a delay time t_d for the current amplitude greater than the critical current I_c are shown in the ***figure 4*** below. The critical current I_c was calculated to be 28.25 mA at 4 K.

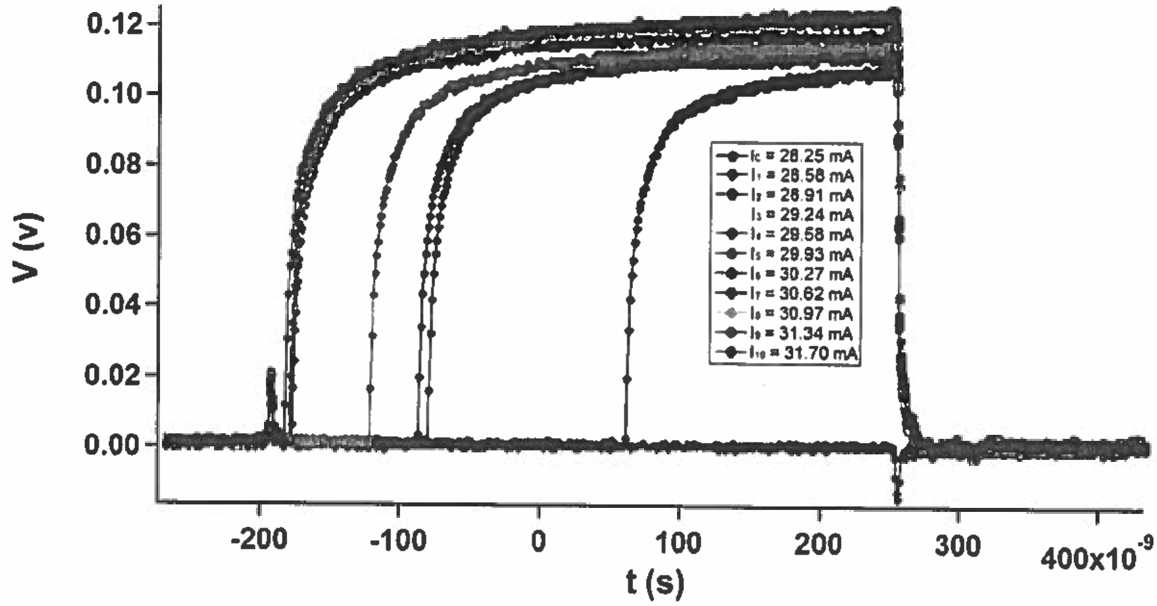

Figure 4: Shows Voltage response versus time of sample NbTiN for $I > I_c$ at $T = 4$ K

The saturation voltage response as a function of time as shown in the figure above has been reported to be characteristic of nucleation of a Phase-slip center **PSC** [8]. The plot of time delay t_d against reduced current I/I_c is shown in the *figure 5* below.

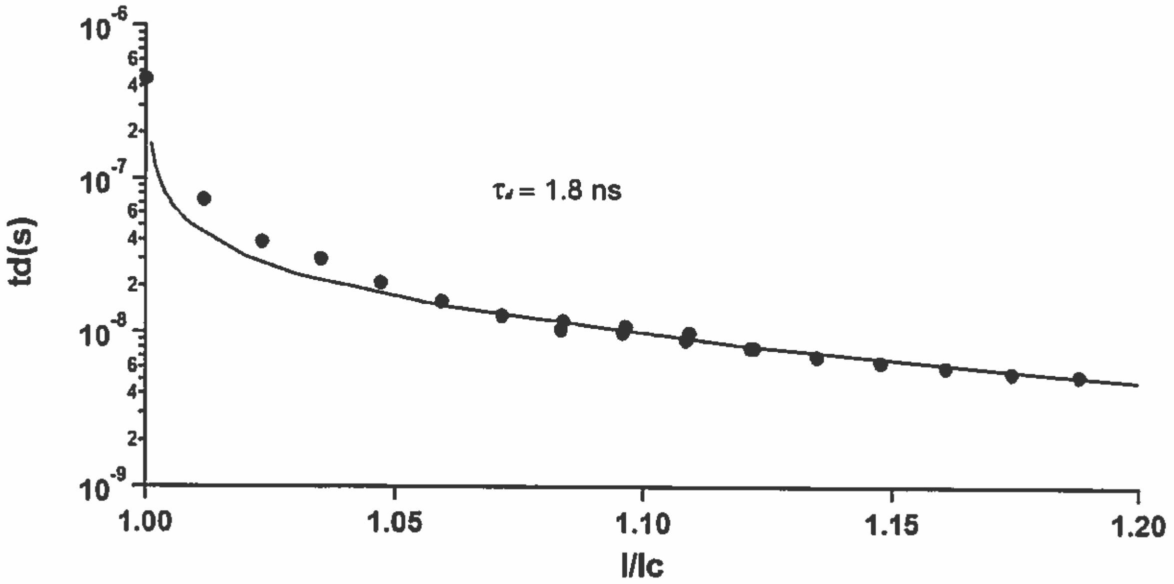

Figure 5: Schematic diagram of delay time t_d against reduced current I/I_c

The discernment of the phase-slip center from the vortex flow mode by delay time t_d is described by time dependent Ginzburg-Landau (TDGL) equation and it's simplified to zero dimension. The time dependent Ginzburg-Landau (TDGL) equation is given by [5, 9, 10]:

$$t_d\left(\frac{I}{I_c}\right) = \tau_d \int_0^1 \frac{2f^4 df}{\frac{4}{27}\left(\frac{I}{I_c}\right)^2 - f^4 + f^6}$$

Where τ_d is pre-factor of the integral and it was interpreted as the gap of relaxation time. It is referred to as an adjustable parameter to fit experimental delay time, was found experimentally to be proportional to the film thickness, and actually to coincide with the cooling time of the film [5, 9, 10, 11, 12].

4.0 Conclusion

The electrical current pulse technique has been used to study the voltage response as a function of delay time of **NbTiN** strip sample due to applied current exceeding critical current I_c of 28.25 mA. Consequently, further increase in applied current led to transformation of phase-slip center **PSC** to hotspot **HS** which marks complete transition to normal state and voltage saturation.

Acknowledgements

My sincere gratitude goes to my supervisor Dr. Khalil Harrabi for dedicating his time to put me through the whole process and also for his guidance and sublime encouragement. I would like extend my gratitude to the physics department for the opportunity given to broaden my practical experience.

References

1. J. Bardeen, L.N. Cooper, J.R. Schrieffer, 1957. *Theory of superconductivity.* Department of Physics, University of Illinois, urbana, Illinois.
2. K.H. Bennemann, J.B.Ketterson, *History of Superconductivity: Conventional, High Transition Temperature and Novel Superconductors* Dept. of Physics and Astronomy,Northwestern University, Evanston,USA.
3. C. M Natarajan, M. G Tanner, R. H Hadfield, *Supercond. Sci. Technol.* **25** 063001 (16pp) (2012)
4. S. N. Dorenbos, P. Forn-Díaz, T. Fuse, A. H. Verbruggen, T. Zijlstra, T. M. Klapwijk, V. Zwiller. *Low gap superconducting single photon detectors for infrared sensitivity,* Applied Physics Letters **98**, 251102 (2011)
5. K. Harrabi, *Hotspot Temperatures Reached in Current-Driven Superconducting Niobium Filaments.* J Supercond Nov Magn **26**:1865–1868, (2013)
6. K. Harrabi, Resistive states created in superconducting NbTiN filaments by an electrical current pulse, AIP ADVANCES **5**, 037102 (2015)
7. F. R. Ladan K. Harrabi · M. Rosticher, P. Mathieu, J. P. Maneval, C. Villard, *J Low Temp Phys* 153: 103–122 (2008)
8. K. Harrabi, *Temperature Elevation of Current-Driven Phase-Slip Centers in $YBa_2Cu_3O_7$ Strips.* J Supercond Nov Magn **28**:573–577 (2015)
9. Pals, J.A., Wolter, J.: Phys. Lett. A **70**, 150 (1979)
10. Tinkham, M.: In: Gray, K.E. (ed.) Non-Equilibrium Superconductivity, Phonons and Kapitza Boundaries, Chap. 8, NATO Conference. Plenum, New York (1981)
11. K, Harrabi, Ladan, F.R., Dinh Lam, V.u., Maneval, J.-P., Hamet, J.-F., Vill'egier, J.-P., Bland, R.W.: J. Low Temp. Phys. 157, 36 (2009)
12. K, Harrabi,: J. Supercond. Nov. Magn. 26, 1865 (2013)

King Fahd University of Petroleum and Minerals
Department of Physics
Physics 503 - Term 142

Experiment #1 Report

Student Name : Idris Popoola

Student ID : 201409260

Code : E207

Evaluator : Dr. Gondal

	grades	Out of
Abstract	1	1
Introduction	4	5
Experimental details	3	6
Results and Discussion	6	9
Conclusion	1	1
References	1	1
Overall	2	2
Total	18	**25**

KING FAHD UNIVERSITY OF PETROLEUM & MINERALS

جامعة الملك فهد للبترول و المعادن
قسم الفيزياء
RECEIVED 08 MAR 2015 وارد
King Fahd University of Petroleum & Minerals
PHYSICS DEPT

PHYSICS DEPARTMENT

EFFECT OF DOPING ON THE VARIATION OF RESISTIVITY WITH TEMPERATURE OF $N_{1-x}S_xMNO_3$ SAMPLES

GRADUATE LABORATORY (PHYS 503)

TERM 142 (FALL 2015)

BY:

POPOOLA, IDRIS KAYODE (g201409260)

SUPERVISOR:

Dr. KHALIL ALI ZIQ

SUBMITTED: MARCH 8, 2015

TABLE OF CONTENT

ABSTRACT

In this experiment I studied the effect of doping on the variation of resistivity with temperature of $N_{1-x}Sr_xMnO_3$ samples for two values of x (x = 0.33 and 0.62). The study was carried out by the four-point probe technique in a closed cycle cryostat. I found that variation in doping proportion greatly has effect on the behaviour of NSMO. The sample x = 0.33 which is moderately doped exhibit different phases such P-F, I-M, MIT transitions phase at suitable temperature. Whereas, the over-doped sample x = 0.62 largely behaves as an insulator material. Consequently, it can be said that doping proportion is key determinant of the behaviour of the perovskites structure NSMO samples. ?

Please define NSMO in line (2)

1. INTRODUCTION

Scientists have shown great interest in investigating hole-doped mixed manganites which have manifested rich physics phenomena and their role in important technological applications [1] Among the exotic physics properties manifested by these complex materials are: colossal magnetoresistance (CMR) and giant magnetoresistance (GMR), paramagnet-insulator to ferromagnetic-metal phase transitions with decreasing temperature [1]. The interplay between charge, spin and lattice degrees of freedom are largely responsible for these important properties [2]. Manganite has been deployed in technologies such as data storage devices, biodetection, sensor technology and magnetic refrigeration. Manganite compounds are generally $R_{1-x}A_xMnO_3$, where R stands for rare-earth elements and A is a divalent alkaline earth metal [1]. Manganite undergoes a paramagnetic-insulator to ferromagnetic/antiferromagnetic transition when cooled below the transition temperature. This transition depends on the doping level x [1]. The doping level x has been found by various researches to be responsible for the determination of the different phases that can coexist or dominate the structure (e.g., ferromagnet versus antiferromagnet, metal versus insulator). The room temperature paramagnetic to low temperature ferromagnetic transition temperature T_c and electrical resistivity $\rho(\Omega cm)$ are observed to depend on the processing conditions. $\rho(\Omega cm)$ exhibits a shoulder at T_c. Mansour et al had performed transport and magnetotransport measurements on $Nd_{0.67}Sr_{0.33}MnO_3$ samples in which they introduced disorder by ultrafast quenching from 1200°C down to liquid nitrogen temperature in a fraction of second under ambient pressure. Their transport measurements showed that the peak temperature of the quenched sample is 299 K while that of the as grown is 256K recording a shift of 27K to lower temperature. They remarked that this is an indication that the quenching treatment has forced the sample to have a MIT temperature similar to a doping of x = 0.30, corresponding to a shift to lower doping level in the phase diagram of $Nd_{1-x}\,Sr_x\,MnO_3$. Magnetic ordering paramagnetic–ferromagnetic (PM–FM) transition is said to induce a structural distortion which in turn changes the electronic band structure leading to an insulator-to-metal (I–M) transition and decreased scattering of the charge carriers by the spins during the ordering process resulting in a resistivity anomaly across the PM to FM transition [4]. Review of literature in this specific composition range revealed that the effects due to both the transitions [PM–FM, I–M) overlap [4]. Large magnetoresistance have been reported in the studies of hole-doped manganese oxide with perovskite structure, $R_{1-x}A_xMnO_3$. It is reported that the deviation of the e_g band filling (n=1-x) from n = 1, or the so called hole doping, causes an insulator-metal transistion [5].

Reference

X

what

In this experimental work I studied the characteristic variations of resistivity of NSMO x=0.33 and NSMO x=0.62 with temperature. The data that are got from the two samples were compared to understand effects of difference in hole doping proportions.

English ??

2. EXPERIMENTAL DETAILS

2.1 Description of equipment

Weighing balance: this was used to measure the constituents samples in the given proportions for sample preparation.

Mortar and pestle: these were used to pulverize the reactants of the samples in order to have a fine powdery substance for effective solid reaction.

Hydraulic press: this was used to achieve a pelleted sample after thorough mixing of the reactants samples in the given proportion by exerting pressure on the mixed pulverized samples.

Evacuation Chamber: the evacuation chamber was used to remove air and moisture from the quartz tube to prevent possible oxidation of the sample in the tube. Non-reactive argon was also flushed into the quartz tube at interval to ascertain that the samples remain pure as prepared.

Furnace: the furnace operating at 1200°C was used to sintered the sample.

Vacuum pump: air in the cryostat was evacuated with the aid of the vacuum pump. This is very important in order to isolate the cryostat from external temperature as a result of possible heat transfer by convection. The vacuum tube was also used to achieve a very low pressure in the cryostat.

Cryostat: a cryostat is a device used to maintain low temperatures of samples under investigation. Low temperatures of the sample are maintained within a cryostat by using different kinds of refrigeration methods, like fluid bath, such as liquid helium or nitrogen. There are different types of cryostats such as closed cycle cryostat, continuous flow cryostat, bath cryostat, multistage cryostat, etc. Closed cycle cryostat was used in this experiment. The close cycle cryostat consists of a chamber through which cold helium vapour is pumped into the system. It has an external mechanical refrigerator which extracts the warmer helium exhaust vapour with the aid of vacuum pump. The extracted helium vapour is cooled and recycled. Closed-cycle cryostats needs not be refilled with helium and can run continuously for an indefinite period. Closed cycle cryostat is capable of operating from above room temperature down to approximately 4K.

Refrigerator: this was used to achieve near helium liquid temperature of about 4K in the cryostat.

Resistance meter: this measure the resistance of the samples at a set interval of temperature.

Temperature meter: this display the operating temperature of the cryostat at which the corresponding resistance is being measured.

not needed in this form!
Better write paragraph to describe their use in experiment

Desktop computer: result of the experiment was display on a Labview programme installed on the desktop computer.

Figures 1, 2, 3, 4 Ind 5 below are some of the photographs of equipment used for the experiment

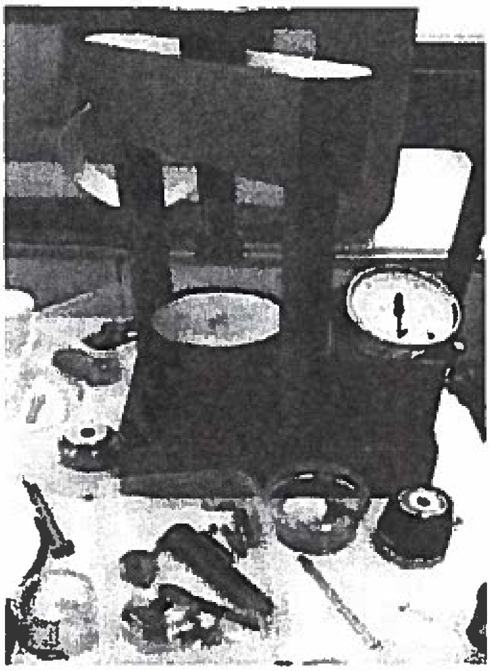

Fig 1: Hydraulic Press

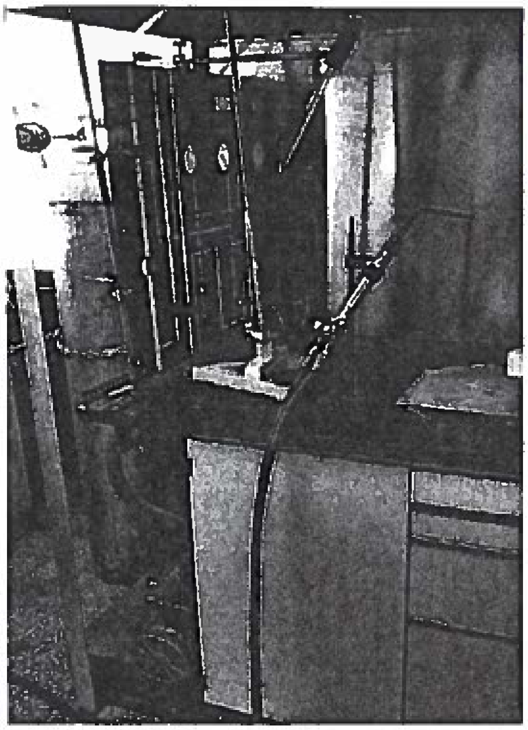

Fig 2: Evacuation Chamber

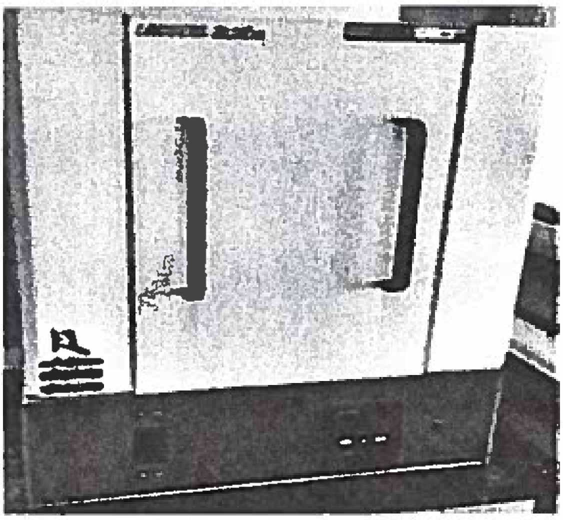

Fig 3: Furnace

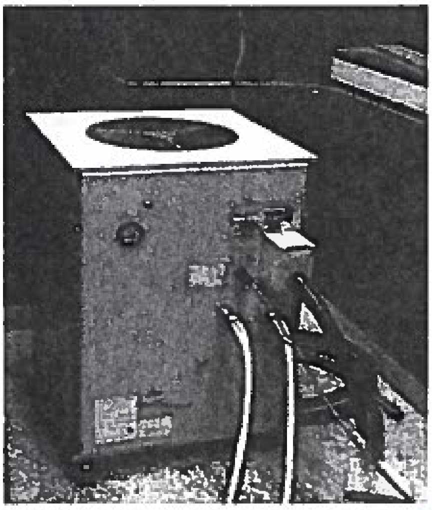

Fig 4: Refrigerator

Fig 3 what is message
conveying !
Fig 4 Refi – Same?

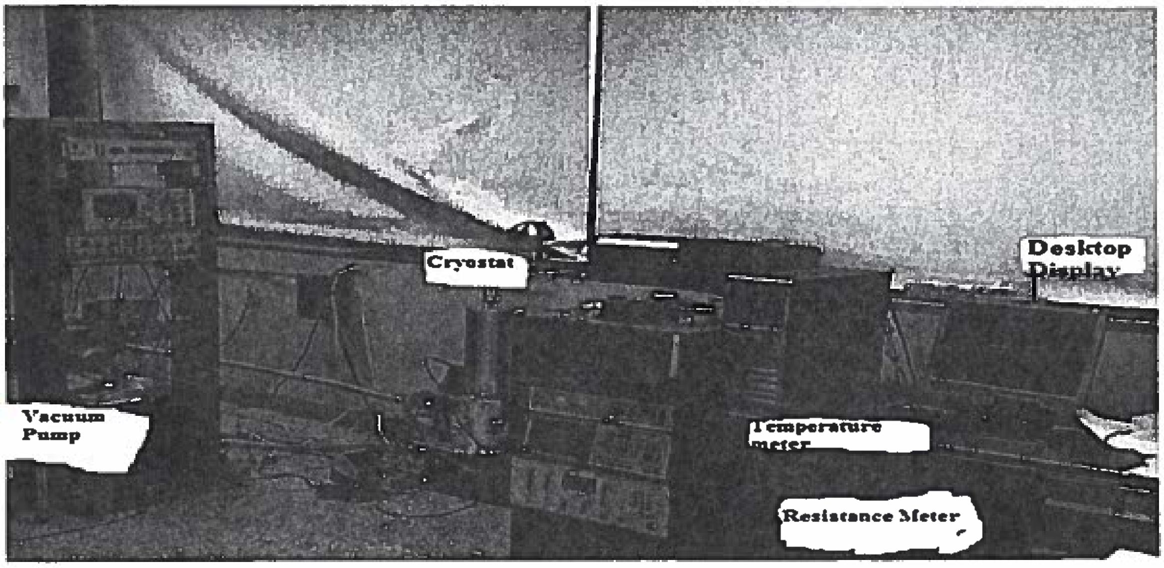

Fig 5: Setup of Equipment for measurement

Schematic diagram would have been better to show set up and to explain

2.2 Sample Preparation

The standard solid-state reaction method was used in the preparation of the $Nd_{1-x}Sr_xMnO_3$ (where x = 0.33 and 0.62) polycrystalline samples investigated in this study. Stoichiometric proportions of high purity powder of the ~~oxides~~ Nd_2O_3, $SrCO_3$, and MnO_2 were mixed, pressed into a pellet and calcinated at 1200 °C several times with intermediate grinding and mixing in order to obtain a single phase. The stoichiometric combination of the compounds was performed by grinding the reactants together in a mortal and carefully transferred into labeled plastic containers. The uniformly mixed samples were hydrostatically pressed to form pelleted substances. The small pellets were carefully transferred into a clean quartz tube and sealed after evacuation. The evacuation was carried out by creating a neck a few centimeters above the samples and then connects it to vacuum pump, and the tube was flushed with argon at intervals a few times to remove components of air (like oxygen, moisture, nitrogen, etc.). The tube was finally sealed, with non-reactive argon, and ready for annealing process. The annealing process was performed by subjecting the samples, in the evacuated quartz tube, to very high temperature of 1200°C. The samples were finally sintered at 1200 °C and then cooled slowly. The characterization of the samples has been reported by Monsour and Ziq [1]. The samples were gently extracted from the furnace and put in labeled plastic tubes for further characterization.

What means here several times (heating at 120 C or dlt

Did you prepare the sample or used just as prepared prior by some one else!

2.3 The Four-Probe Technique

Four-point probe method was used to determine the resistivity of the sample at different temperatures. The basic principle involve in this technique is the fact that; potential difference across two ends of a conductor is proportional to current flowing through a conductor ~~under~~ unchanged physical conditions like temperature and mechanical stress (Ohm's law i.e V = IR, the constant of proportionality, R, is the resistance). At a constant temperature it is also known that, the resistance, R, of a conductor is proportional to its length and inversely proportional to its cross-sectional area (R ά L and R ά 1/A), the constant of proportionality is the resistivity of the material). The resistivity which is an intrinsic property of the materials is used in the characterisation of materials. The Four-point probe consist of four equally spaced thin metallic conductors with finite dimension. The tips of each thin conductors is made to contact the sample surface with the aid of silver paste to ensure firm contact (see Figure 6). A high impedance current source is used to supply current through the two outer probes, the voltmeter is connected across the two inner probes.

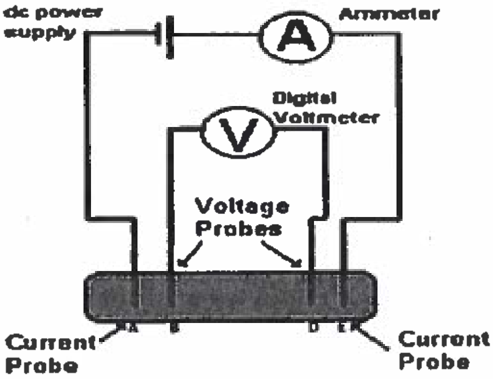

Fig 6: Schematic Diagram of Four-probe Technique

The inner probes draw no current because of the high input impedance of the voltmeter in the circuit and there was no voltage drop at points B and D. The sample was then arranged in a closed cycle Helium-cryostat, as shown in Figure 4, using vertical orientation. The four-probed sample $Nd_{1-x}Sr_xMnO_3$ was carefully mounted on the blank sample holder of the closed cycle cryostat, and each probe was soldered to the appropriate terminals with vertical orientation. The mechanical pump was opened to evacuate air content from the cryostat and the diffusion pump was started as well as the compressor after the evacuation pump.The measurements was carried out with the aid of computer program (Labview). I measured the resistance of the sample $Nd_{1-x}Sr_xMnO_3$ for the temperature range 285 K to 4K in 200 steps with 0T applied magnetic fields. The tolerance temperature was set at 0.04K.

3. RESULT AND DISCUSSION

The dimensions of the samples were measured with the aid of digital vernier caliper and tabulated as shown in table 1 and 2. The length interval between the voltage probes is labelled Lv. The cross-sectional areas were calculated and the resistance values from the experiments were converted to resistivities (Ωcm) by the formula RA/L_v (where R is resistance, A is cross-sectional area). The obtained results were plotted against temperature with the aid of Matlab.

Table 1: x=0.33

						Average
L_v (mm)	3.10					(0.31cm)
Breadth (mm)	0.88	0.96	1.04	0.89	1.11	0.97 (0.097cm)
Length (mm)	3.10	2.80	2.10	1.40	0.40	1.96 (0.196cm)

Table 2: x=0.62

						Average
L_v (mm)	3.12					(0.31cm)
Breadth (mm)	1.37	1.31	1.35	1.31	1.33	1.33 (0.13cm)
Length (mm)	2.56	2.59	2.54	2.51	2.50	2.54 (0.25cm)

The variations of resistivity as a function of temperature are shown in Figures 7 and 8 for the doping samples of x = 0.33 and x = 0.62 respectively.

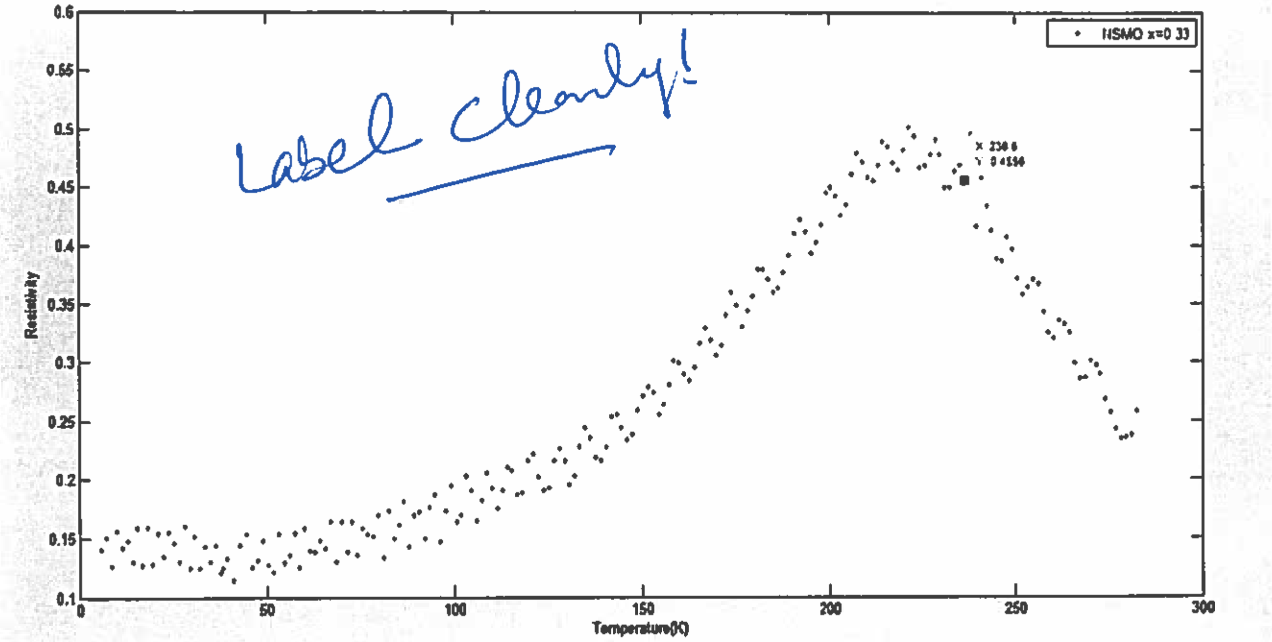

Label clearly!

Fig 7 Fig Caption?

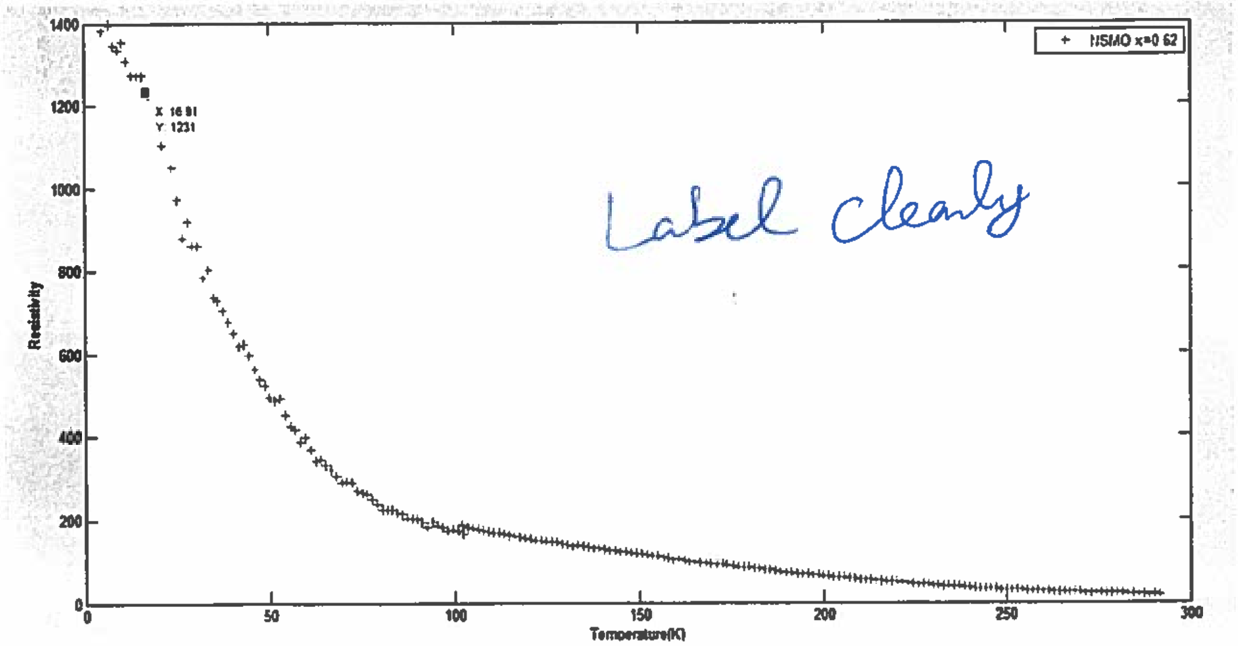

Label clearly

Fig 8 Fig. Caption

The x = 0.33 sample exhibits metal-insulator-transition (MIT) at a temperature of 229.7 K with a maximum resistivity of 0.5017Ωcm. Similar result was reported by [6]. The x = 0.62 sample, on the other hand, shows no distinct metal-insulator transition and has a maximum resistivity of 1397Ωcm at a temperature of 6.78K. Apparently the large doping value favors the formation of the insulating phase over the metallic one, resulting in more significant competition between the metallic and insulating phases and shifting the metal-insulator transition to lower temperatures. Hence, the doping variation caused enormous variation in resistivity as a function of temperature. For a doping of x = 0.33 the sample exhibits a paramagnetic–ferromagnetic transition at about 200K; whereas no ferromagnetic transition was observed for the sample x=0.62. Sample x = 0.33 shows ferromagnetic features at a much lower temperature in the metallic region. Ferromagnetism arises from the alignment of electron spins throughout the solid [7]. The x = 0.33 sample manifests semiconductor properties at temperature of 236K and above while the over-doped sample x = 0.62 behaves majorly as an insulator with slight transition noticed at temperature of 17K. Important fact to be noticed is that the electronic and magnetic properties critically depend on x in the hole-doped Mn oxide [5] It is well known that for magnetic perovskites, the doping may significantly change the groundstate of the system [6].

→ very brief discussion
→ limited results ? (only Two graphs)

4. CONCLUSION

of

7 Variation in doping proportion greatly has effect on the behaviour NSMO. The sample x = 0.33 which is moderately doped exhibit different phases such P-F, I-M, MIT transistions phase at suitable temperature. Whereas, the over-doped sample x = 0.62 largely behaves as an insulator material. Consequently, it can be said that doping proportion is key determinant of the behaviour of the perovskites structure NSMO samples.

References

1. A.I. Mansour · K.H. Ziq · A.F. Salem · R. Hamam, J Supercond Nov Magn (2014) 27:183–186

2. Tokura, Y., Nagaosa, N.: Science 462, 288 (2000)

3. Pawan Kumar, Ravikant Prasad, Avanish Kumar Srivastava, Hari Krishna Singh, Rakesh Kumar Dwivedi, Mangala Prasad Singh, Journal of the Korean Physical Society, Vol. 59, No. 4, October 2011, pp. 27922796

4. M. Pattabiraman, Narayani Senthilkumaran, P. Murugaraj, and G. Rangarajan JOURNAL OF APPLIED PHYSICS VOLUME 85, NUMBER 8

5. A. Urushibara, Y. Moritomo, T. Arima, A.Asamitsu, G. Kido, Y. Tokura, Physical Review B Volume 51, Number 20, 15 May 1995.

6. J. Wosik,a) L.-M. Xie, M. Strikovski, P. Przyslupski,b) M. Kamel, V. V. Srinivasu, and S. A. Long JOURNAL OF APPLIED PHYSICS VOLUME 91, NUMBER 8 15 APRIL 2002

7. S.O Pillai Chapter 9, Solid State Physics, revised sixth edition, New Age International publisher.

King Fahd University of Petroleum and Minerals
Department of Physics
Physics 503 - Term 142

Experiment #3 Report

Student Name : Ibsal Assi

Student ID : 201403420

Code : E208

Evaluator : Dr. Gondal

	grades	Out of
Abstract	1	1
Introduction	4	5
Experimental details	5	6
Results and Discussion	8	9
Conclusion	1	1
References	1	1
Overall	2	2
Total	22	**25**

جامعة الملك فهد للبترول و المعادن
قسم الفيزياء
RECEIVED
11 MAY 2015
وارد
King Fahd University of Petroleum & Minerals
PHYSICS DEPT

بسم الله الرحمن الرحيم

Department of Physics

PHYS 503: Graduate Laboratory

Exp No. 3: Transport Properties of $FeSe_{1-x}As_x$ Superconductor

Student Name:

Ibsal Adel Assi

Supervisor:

Prof. Khalil Ziq

Date of Submission:

10th of May, 2015.

22/25

Contents

Abstract

The superconductivity of $FeSe_{1-x}As_x$ has been studied for different arsenic concentrations and structures. Three samples used in this study, two of them were single crystals with different arsenic concentration and the last was poly-crystal. The arsenic concentration does affect the superconductivity behavior.

Introduction

Superconductivity is a state in which some materials behave at low temperature, below the critical temperature, to have zero electrical resistance. It has been first discovered by Heike Onnes in 1911 in Lieden. Those materials, superconductors, are characterized by Meissner effect which means the complete ejection of the magnetic field lines away from the material.

Superconductors are classified into two main categories according to their response to the applied magnetic field. The first is called type I supper conductors at which the superconductivity state breaks down totally when the applied magnetic increases above the critical value H_c. The second class is called type II superconductors, in this type the material has two critical field values H_{c1} and H_{c2} when the field exceeds the first value the material will become partially superconducting with magnetic vortices distributed in the material. When the field strength passes H_{c2} the superconducting state will be totally destroyed. Figure 1 summarizes the two classes clearly. {Reference} ?

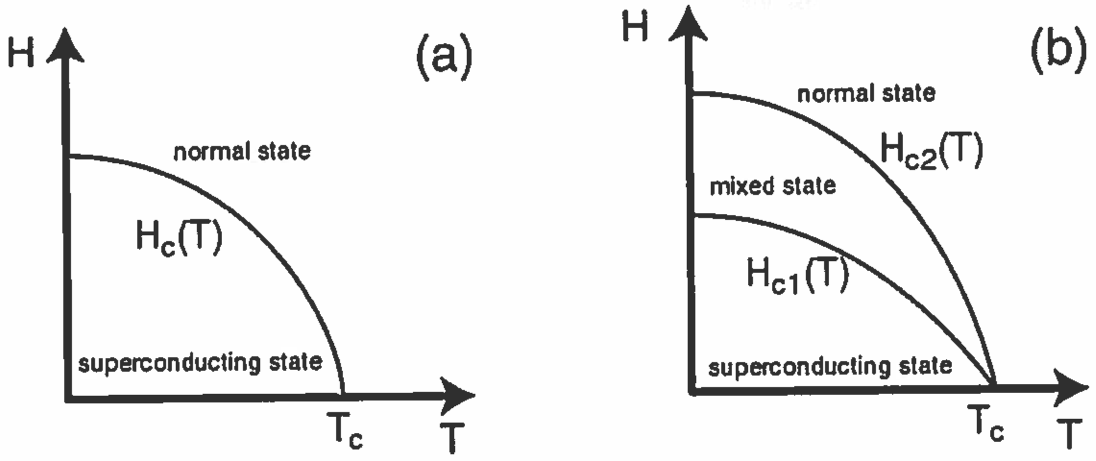

Figure 1:(a) Type I H -T behavior. (b) Type II H -T behavior

To measure the resistance behavior at low temperature 4 *probe method* is ~~one~~ the appropriate way. Two wires are connected to pass current through the material and the other two lies in the middle used to measure the voltage difference across the two points. Using Ohms law we can determine the resistance of the superconducting piece.

$V = IR$ ………… (1) Where V is the voltage, I is the current and R is the resistance.

Figure 2 below shows 4 probe method connections.

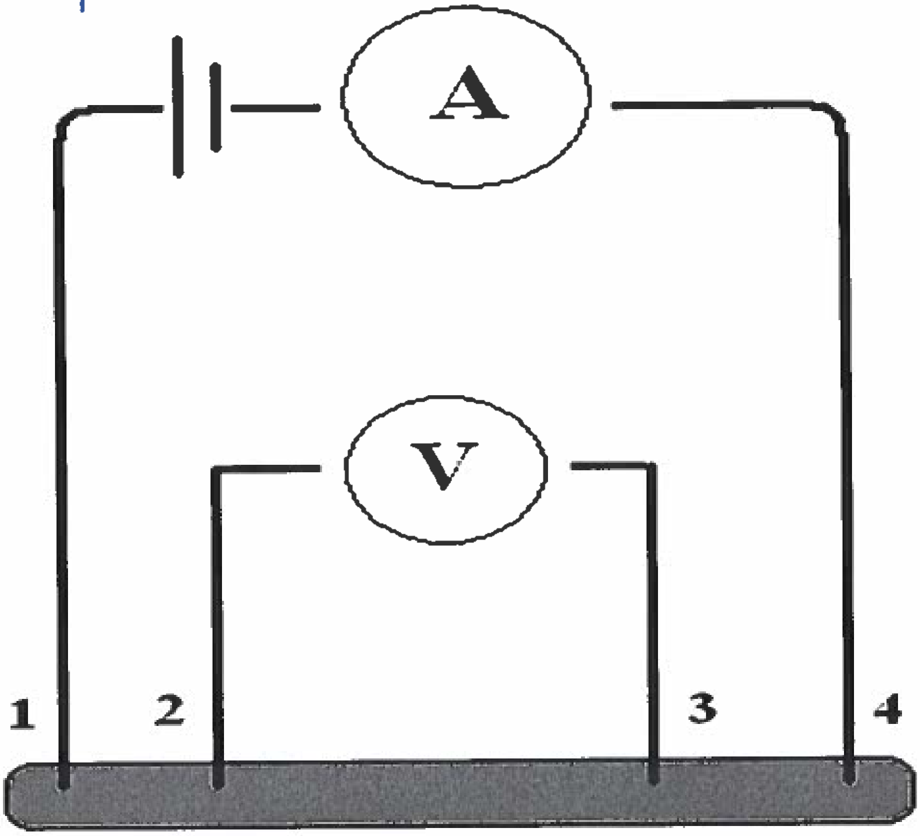

Figure 2: 4 Probe connection. 2 & 3 are voltage probes. 1& 4 are current probes

Set up

Experimental Details

~~Setup~~

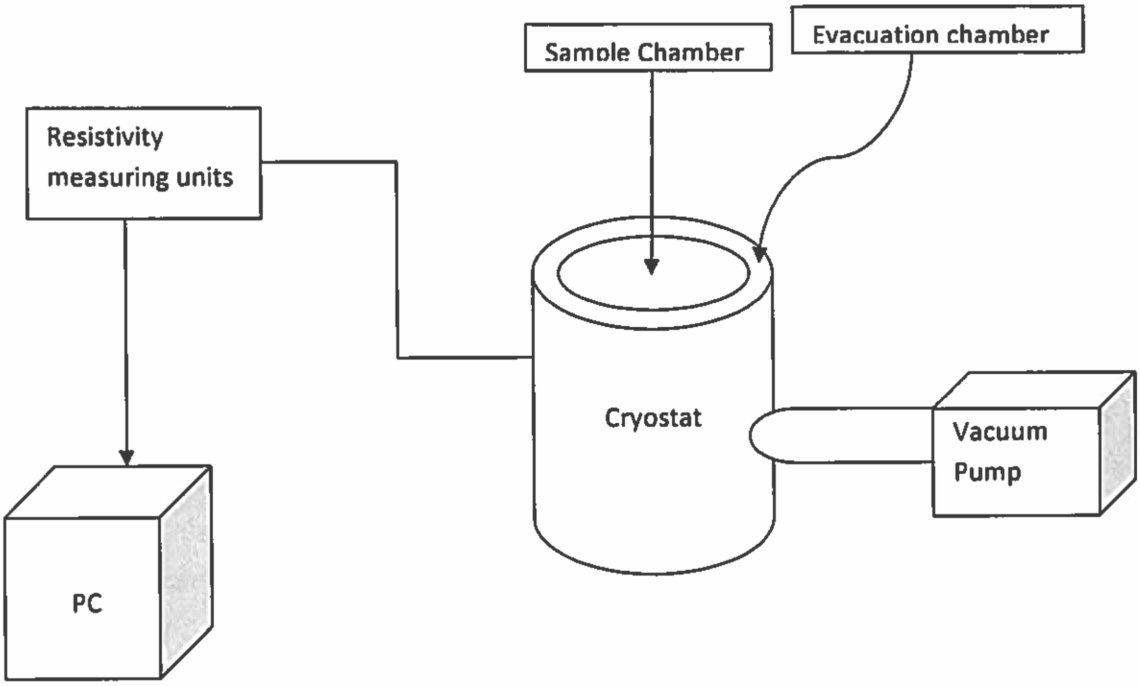

Figure 3: Experimental Setup for resistivity measurements

The sample can be connected inside the sample chamber as shown in figure 3, then the system closed and vacuum pump starts pumping up to 10^{-7} mbar to ensure that no vacuum between the two chambers to avoid temperature transfer from the surrounding. After reaching this vacuum, the refrigerator cycle operated to cool the system down up to 4 K and resistivity measurement takes place from room temperature up to 4K.

Sample Preparation

Our samples were Iron-based superconductor materials which have the general form $FeSe_{1-x}As_x$. Two samples have been single crystals with arsenic concentration of 0.01 and 0.04% and the other sample is poly crystal with As concentration 0.01%.

For each sample, at room temperature, the powders of different concentrations have been grinned mixed together using mortar and pestle, pressed into pellets and sealed in quartz tubes under partial pressure of argon (20-25%).

All samples were annealed in programmable furnace which was programmed to raise the temperature from room temperature up to 200 ^{0}C at rate 60 ^{0}C/ hour at stops at 200 ^{0}C for 24 hours then heats again at same rate to reach 500 ^{0}C and then stops for 24 hours and then after it raised again up to 700 ^{0}C at the same rate. Finally, the sample cooled down to room temperature and pressed into pellets after mixed together. The following table shows the concentrations of each sample used.

Sample	**x**	**1-x**	**Fe (grams)**	**Se (grams)**	**As (grams)**	**$FeSe_{1-x}As_x$ (grams)**
1	0.01	0.99	0.4144	0.0056	0.5798	0.9997
2	0.04	0.96	0.4148	0.0223	0.5627	0.9997
3 (poly)	0.01	0.99	0.4144	0.0056	0.5798	0.9997

Table 1: Three samples and their elemental concentrations.

Experimental Procedure

The samples have been cleaned using sandpaper to ensure that there's a connection with the probes. For each sample, we connected the wires (4 probes) with the sample and then we transferred the sample inside the cryostat and then the sample wires connected from the other side in the chamber. The cryostat then closed and the pump switched on to evacuate the spacing between the inner chamber and the surrounding to prevent heat transfer while cooling up to pressure around 10^{-7}mbar (took an hour and a half). Then the refrigerator switched on to cool down the sample. Temperature controller and software been adjusted to take measurements along the cooling process from 300 K to 4K (took almost 3 hours). The resistance-temperature behavior is then appears on the PC screen.

As an extra work, we studied the heating process of 2 samples and compare the behavior of R-T curve in both cases. Figure 4 summarizes the experimental procedure.

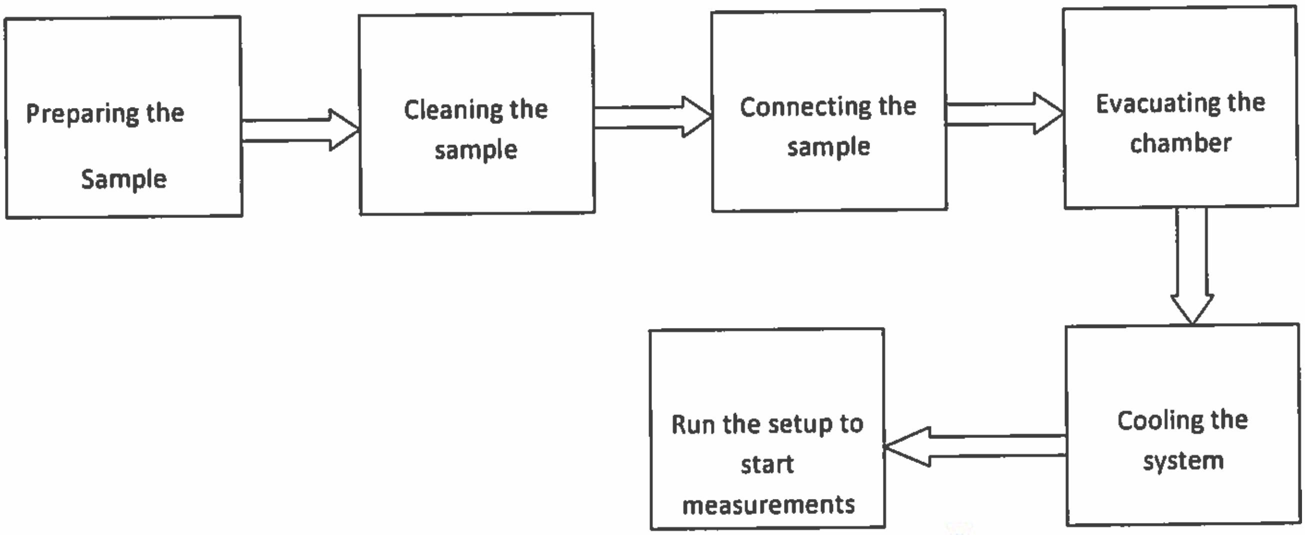

Figure 4: Experimental Procedure

for what ??

Results and Discussion

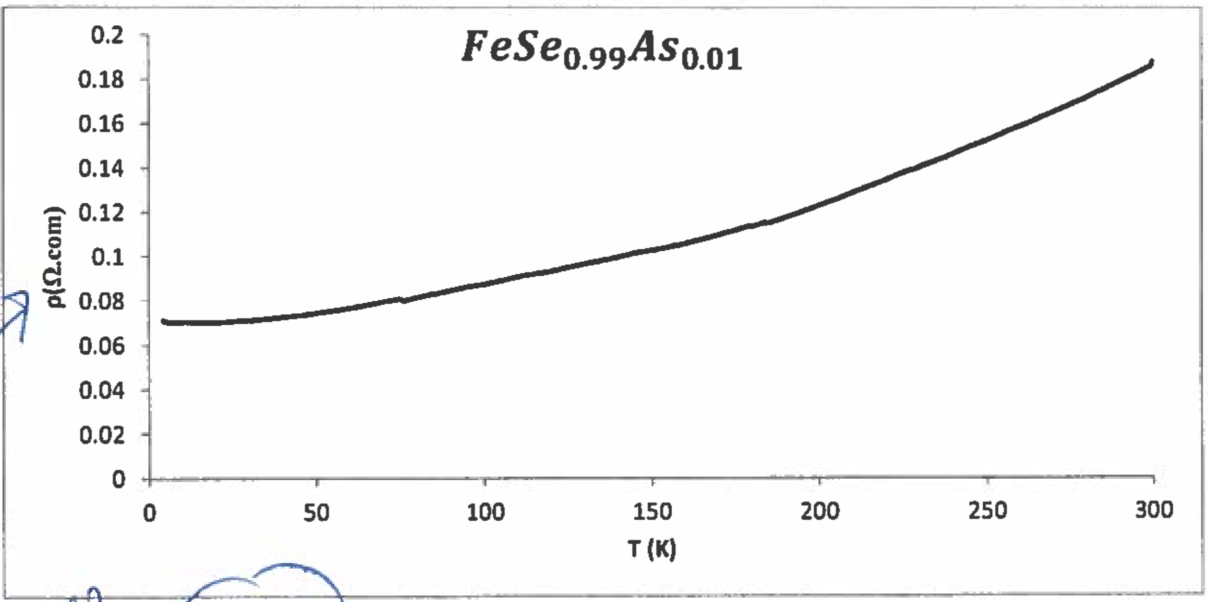

Figure 5: Resistance-Temperature behavior at x=0.01 (single crystal) cooling

Resistivity or Resistance and Why ??

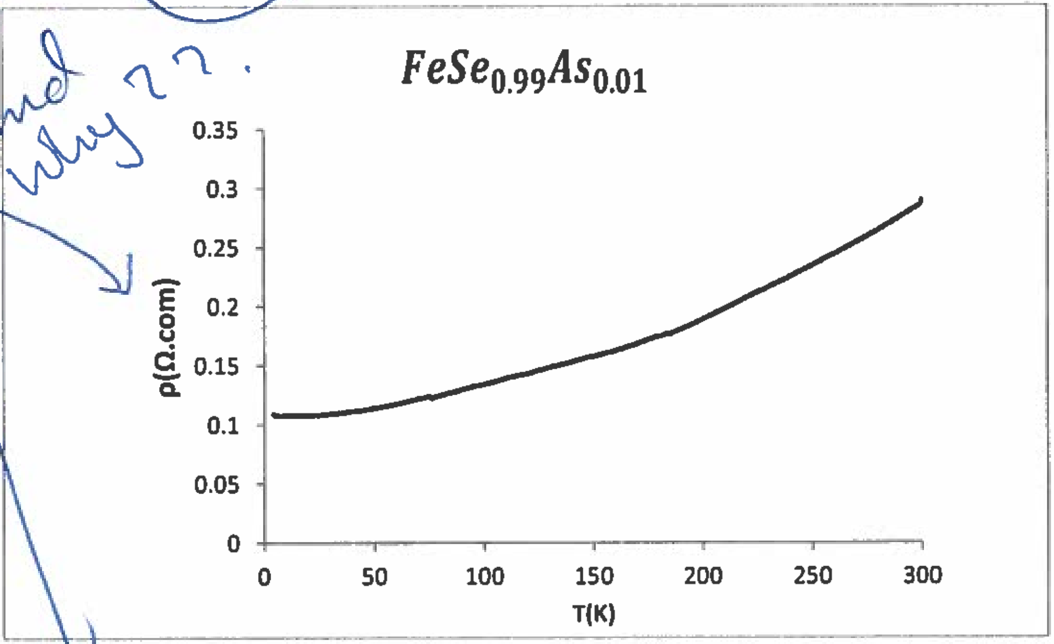

Figure 6: Resistance-Temperature behavior at x=0.01 (Polycrystal) cooling and heating

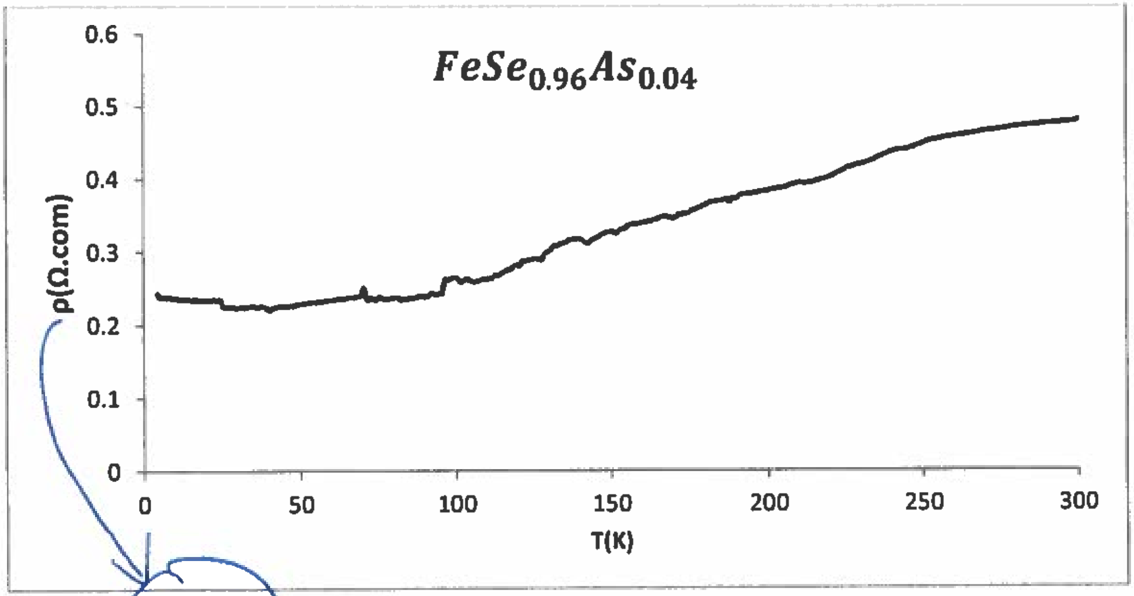

Figure 7: Resistance-Temperature behavior at x=0.04 (Polycrystal) cooling and heating

As we see in the last three figures, the behavior of R-T curve is different for each sample and concentration. For x=0.01single crystal, the resistivity dropped to around 0.07 ohms.cm, while for polycrystal the resistivity reached 0.12 ohms.cm. For the last sample, at x=0.04, the resistivity got to 0.24 ohms.cm at 4K. So, for lower arsenic concentration we had lower resistivity at 4K and that due to the effect of arsenic on the superconductivity of iron-based superconductors.

Conclusion

The superconductivity of $FeSe_{1-x}As_x$ have been studied for 3 different samples, two of them were at x=0.01 but one was single crystal and the other was polycrystal, the last sample was at x=0.04 single crystal. It has been found that each sample has its own transition temperature and they reached different low resistivity at 4K. So, the arsenic concentration affects the superconductivity and transition behavior of the Iron base superconductor.

References

[1] C. Bardeen, Leon, "Theory of Superconductivity", PH YSI Rev., vol. 108, pp. 1175-1204, 1957.

[2] C. Day, "Iron Based Superconductors" Phys. Today, August, 2009.

[3] Charles Kittle, Introduction to Solid State Physics, 8th edition.

[4] Neil Ashcroft and David Mermin, Solid State Physics, 1st edition.

[5] Michael T., Introduction to Superconductivity, 2nd edition.

[6] Stephen Blundell, Superconductivity: A very short introduction, 1st edition.

[7] Charles P.,H. Farach, Richard J., Ruslan P., Superconductivity, 2007.

limited number ?? one can add more easily!!

King Fahd University of Petroleum and Minerals
Department of Physics
Physics 503 - Term 142

Experiment #3 Report

Student Name : Zamzam Ibnu Sina

Student ID : 201408460

Code : E301

Evaluator : Dr. Dwaikat

	grades	Out of
Abstract	0.75	1
Introduction	4	5
Experimental details	5	6
Results and Discussion	7.75	9
Conclusion	1	1
References	1	1
Overall	1.5	2
Total	21	**25**

Prompt Gamma-ray Neutron Activation Analysis (PGNAA)

Graduate Laboratory (Phys - 503) term 142

Student Name : Zamzam Ibnu Siki
ID Number : g201408460

Advisor Name : Dr. Akhtar A. Naqvi

جامعة الملك فهد للبترول و المعادن
قسم الفيزياء
RECEIVED 10 MAY 2015 وارد
King Fahd University of Petroleum & Minerals
PHYSICS DEPT

Date of Submission :

10 May 2015

Physics Department

King Fahd University of Petroleum and Minerals

2015

Contents

1 Abstract

Detection of toxic element in water solution is required by many fields. This report demonstrates the mechanism of PGNAA technique in detecting and measuring the concentration of nickel contamination in water solution. Water solution containing 1.2, 2.8, 8.2, and 9.4 wt% of nickel were used to find the relation between nickel concentration and the number of detected gamma rays. Having this relation, we can approximate the concentration of nickel in nickel contaminated water solution.

2 Introduction

In performing elemental analysis of bulk sample, Prompt Gamma-ray Neutron Activation Analysis (PGNAA) has been widely used in many fields such as industrial, environmental, medical, civil engineering, and so on. This technique is ~~widely used because it~~ is a non-destructive method, and the chemical form and shape of the sample are relatively unimportant. Moreover, in situ analysis might be performed by utilizing portable neutron generator [1].

PGNAA is also commonly used to detect water contamination in many industries such as petroleum, pharmacy, agriculture, and many others. In this case, PGNAA technique was used to detect nickel contamination in water. Nickel is mostly used in fabrication of stainless steel products. Nickel also used in other industries such as rechargeable batteries, catalysts, foundry products, etc.

Most of the time, industrial wastes are in the form of liquid. If this industrial wastes, are not treated properly, they may have contaminated ground water. Some health effects side effects of having too large uptake quantities of nickel [2]:

- Higher chances of development of lung cancer, nose cancer, larynx cancer, and prostate cancer
- Lung embolism
- Respiratory failure
- Birth defects
- Asthma and chronic bronchitis
- Heart disorders

Therefore, nickel concentration levels monitoring in such industrial disposal is required.

'irradiating'

PGNAA is performed by continuously radiating the sample with neutrons. The constituent elements of the sample will absorb some of the neutrons and emit prompt gamma rays. The emitted gamma rays are then measured by the detector which will count the number of gamma rays and analyze their energies.

The analysis relies on unique elemental signatures. Each element emits a characteristic gamma ray energy as it returns to its stable state. Each element also has different tendency cross-section. to interact with neutrons. The gamma rays intensity is proportional to the number of atoms, which then can be used to calculate the concentration of an element in the analyzed sample. So based on this several consideration we can identify and quantify the elemental constituents of the sample [3].

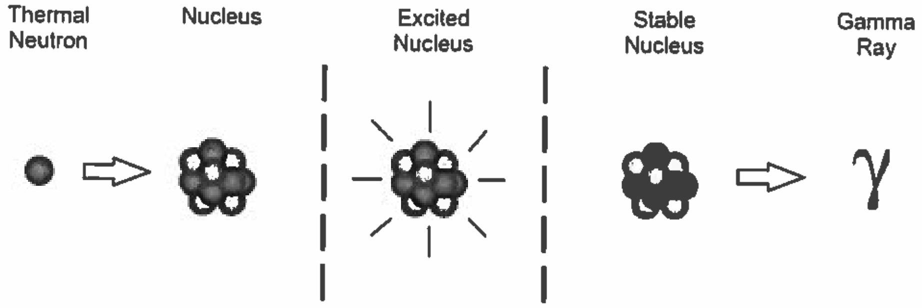

Figure 1: *Schematic representation of gamma rays production in thermal neutron capture (TNC) reactions. [3].*

The gamma rays production can be achieved via thermal neutron capture (TNC) reactions or fast neutron inelastic scattering (NIS) reactions. In this case, thermal neutron capture is chosen because the cross-section is high. This method is ideally suited for element with high cross section of thermal neutron capture such as mercury, cadmium, boron, etc [1]. ✓

The purpose of this experiment is to demonstrate PGNAA capability and mechanism to measure nickel concentration which is a toxic element in water solution.

3 Experimental Details

The experiments was performed using portable neutron generator type MP320 which produces a pulse beam of 2.5 MeV neutron. The neutron is generated through D(d,n) reaction using 70 μA beam of 70 keV deuteron. The deuteron pulse had a width of 5ns and a frequency of 250Hz. BGO (Bismuth Germanium Oxide) detector with 125 mm diameter and 125 mm height was used to count the gamma rays number and analyze their energy. BGO detector has high intrinsic efficiency at higher energy and very fast detection response. Moreover, BGO detector has strong neutron radiation resistance. However, BGO has poor conversion efficiency which ~~results in bad~~ energy resolution. Therefore, BGO is ideal for high energy and high rate gamma ray measurement that outweighing considerations of energy resolution [4].

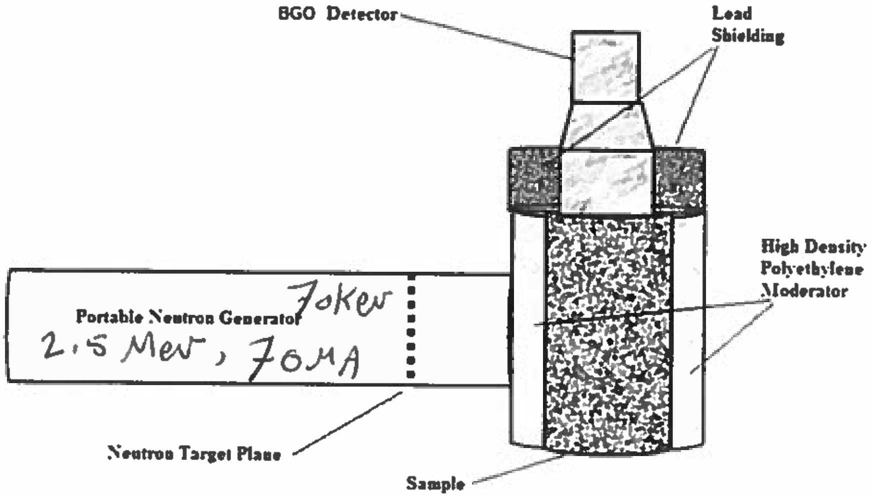

Figure 2: *Schematic diagram of the experimental setup. The main parts of the setup consists of the neutron generator, BGO detector, and polyethylene moderator. Moderator was used to reduce the neutron energy.*

Energy resolution is a parameter that indicate the detector capability to differentiate ✓ two or more gamma rays whose energy are very close to each other. This ~~properties~~ of

Property.

oc ~~these properties~~.

detector can be seen from the peak of the spectrum. Detectors with good energy resolution have sharp peak while the ones with bad energy resolution have broad peak.

Moderator was used to reduce the energy of fast neutron (2.5 MeV) to the energy of thermal neutron (2.5 meV). The moderator was placed adjacent to the neutron target plane of the portable neutron generator. The moderator has cylindrical cavity and the sample was placed inside it. 3 mm thick lead shielding and 50 mm thick neutron shielding are also used on the surrounding of the gamma ray detector to prevent unwanted gamma rays and neutron from reaching the detector. The neutron shielding was made of a mixture of paraffin and lithium carbonate mixed in equal weight proportions [5].

The samples used in this experiment can be seen in table 1. In this experiment, four water samples containing 1.2, 2.8, 8.2, and 9.4 wt% of nickel were used. These samples with known concentration were measured and it will be used to obtain relation between gamma rays number and the unknown concentration of nickel in the water sample.

Table 1: List of samples information that were used in this experiment.

Number	Chemical Solution	Molarity (mole)	Nickel Concentration (%)
1	NiBr	0.2	1.2
2	NiBr	0.5	2.8
3	$Ni(NO_3)_2$	1.4	8.2
4	$Ni(NO_3)_2$	1.6	9.4

The detector was connected to preamplifier to minimize the source of noise and convert the gamma rays to electrical signal which was send to an amplifier circuit in the control room. The amplifier circuit increases the power of the signal and an analogue to digital converter (ADC) converts the signal to digital number that represents the amount of gamma rays and linear gate stretcher was used to stretch a gated fast pulse to slow pulse. After that,it was connected to multichannel buffer which is connected to the PC where we can observe and record the data.

In this experiment, five measurements were performed. The first one is measurement without using any sample to obtain background spectrum, to calibrate the amplifier, and to obtain the relation between channel number and gamma rays energy using hydrogen peak. And then, the measurements with four samples were performed with different acquisition time for each samples. The acquisition times were decided spontaneously by observing the deviation in the spectra from the PC. When the deviation had reached less than 10 %, the measurement then was stopped.

4 Results and Discussion

The acquired data that was observed in the PC was showing the number of gamma rays in terms of channel number. A calibration was needed to obtain the relation between channel number and the energy of gamma rays. A calibration was performed by fitting the peak of known element to its energy. In this experiment, the peak of hydrogen was used. The hydrogen that was detected came from the polyethylene moderator.

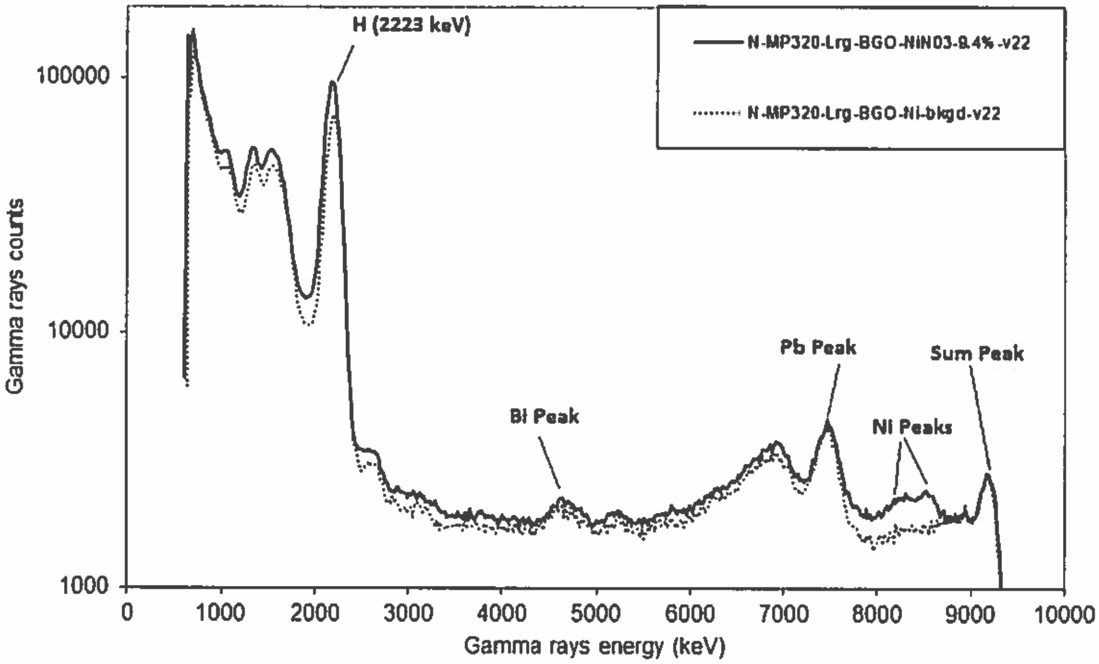

Figure 3: *Prompt gamma-ray experimental pulse height spectrum from a nickel solution sample. The background gamma-ray spectrum without the sample is superimposed to compare the sample influence on the spectrum and also to normalized the spectrum with nickel contamination.*

It ~~was~~ is known that the energy of hydrogen gamma rays are 2223 keV. From the raw data it was observed that hydrogen peak was located at channel number 112. From here, we can find the relation between channel number and the gamma rays energy. We obtained that, **1 channel number = 19.85 eV**. Having this relation, all spectrum with

point is not enough -

respect to the channel number were converted to spectrum with respect to the energy.

In figure 3, we can see all elements detected gamma rays spectra. It shows that the elements come not only from the sample but also from the from the detector (Pb, Bi) and the moderator. These other peaks that contributing to the spectra are considered as the background peaks. Background peaks were used to normalized each of the spectra because background peaks do not depend on the existence of the sample. In this case, the spectra from each sample with different concentration of nickel were normalized and then compared to each other (figure 4).

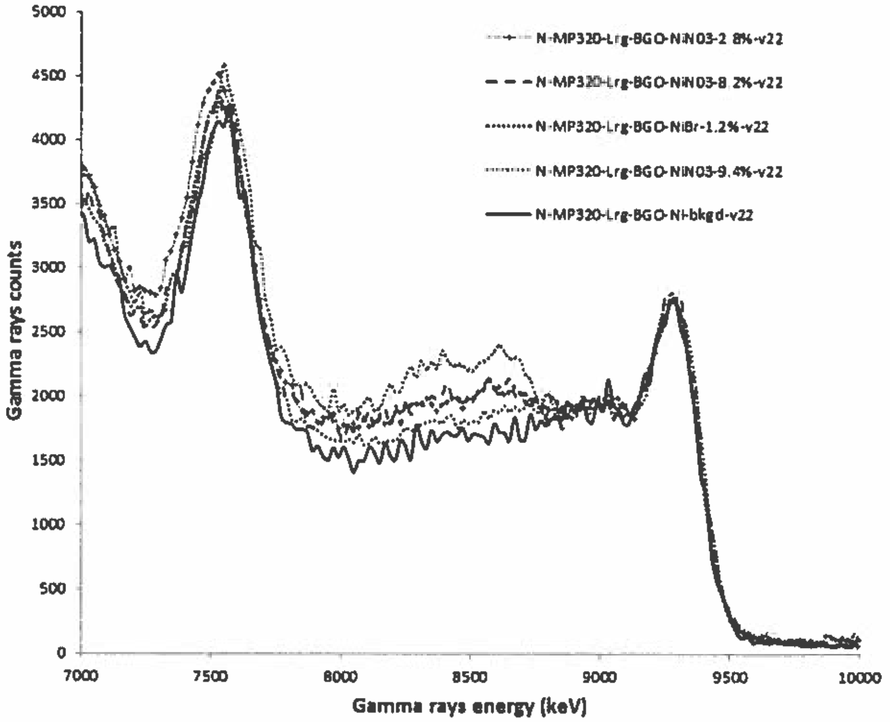

Figure 4: *Comparison of prompt gamma rays spectra from each samples containing 1.2, 2.8, 8.2, and 9.4 wt% nickel and the background (without sample). The area of interest is between the energy of 7700 keV until 9000 keV where we expected to see the peak of nickel.*

Our purpose here is to find the relation between the counts of gamma rays and the concentration of the nickel. It is known that the peaks of nickel can be found at energy about 8.5 MeV and 8.9 MeV. Because BGO detector was used in this experiment, which has bad energy resolution at high energy, these peaks of nickel cannot be clearly observed. Therefore, an area of interest between 7.7 MeV until 9 MeV was chosen to observe the sample influences to the spectra in this area.

In figure 4, we can see the difference spectra of nickel peaks for sample prepared with 1.2, 2.8, 8.2, and 9.4 wt% nickel concentration. The background spectrum is also superimposed to normalized each spectrum with nickel contamination. The total number of gamma rays in our area of interest is increasing when we have more nickel contamination in the sample.

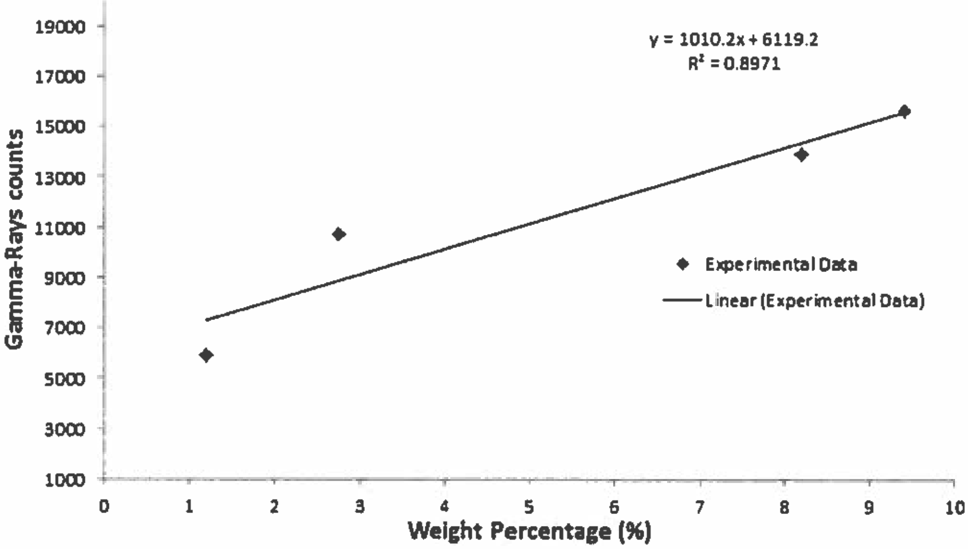

Figure 5: *Relation between total number of prompt gamma rays of the spectra with sample in our area of interest and the nickel concentration in the sample. The total number of prompt gamma rays here were generated by subtracting the background contribution from each of the spectra. The linear fitting was used for approximating the concentration of nickel when the number of prompt gamma rays is known.*

The relation between the total number of prompt gamma rays and the nickel concentration then was plotted (5). Linear fitting was also shown in the figure to approximate nickel concentration when the number of prompt gamma ray is known.

5 Conclusions

PGNAA technique has been used to find the relation between nickel concentration in water solution and the gamma rays number detected by BGO detector. The measurements were carried out with water samples containing 1.2, 2.8, 8.2 and 9.4 wt% of nickel.

It was found that higher concentration of nickel resulting more number of gamma rays were detected. The mathematical relation between nickel concentration and gamma rays number is approximated by linear fitting of the experimental data.

References

[1] Naqvi, A.A. et al, *Performance Evaluation of a Portable Neutron Generator for Prompt Gamma-Ray Application*, Arab J Sci Eng (2014) 39-531-539

[2] Nickel effect on environment, `http://www.lenntech.com/periodic/elements/ni.htm#Environmental%20effects%20of%20nickel`, 30 04 2015.

[3] PGNAA in industries, `http://acceleratingscience.com/mining/pgnaa-improves-process-and-quality-control-in-cement-production/`, 30 04 2015.

[4] Selecting Gamma Rays Detector, `http://www.nucsafe.com/cms/Selecting+Gamma+Detector/43.html`, 30 04 2015.

[5] Naqvi, A.A. et al, *Optimization of a prompt gamma setup for analysis of environmental samples*, J Radioanal Nucl Chem DOI 10.1007/s10967-012-2045-y

[6] Knoll, G. F, *Radiation Detection and Measurement*, 2000. John Wiley & Sons, Inc.

King Fahd University of Petroleum and Minerals
Department of Physics
Physics 503 - Term 142

Experiment #3 Report

Student Name : Mohamed Shemis

Student ID : 200991810

Code : E302

Evaluator : Dr. Naqvi

	grades	Out of
Abstract	1	1
Introduction	3	5 − 2 = ③
Experimental details	4	6 − 2 = ④
Results and Discussion	8	9 − 1 = ⑧
Conclusion	1	1
References	1	1
Overall	2	2
Total	18	~~25~~ [illegible] 20 ✓

① Report Points (after penality (−5)) = $\frac{18}{20}$

② Bonus Points for (Energy Resolution measurement Work) = +5

Total Points for reports = $\frac{18+5}{25} = \boxed{\frac{23}{25}}$

King Fahd University of Petroleum and Minerals
Physics Department
Physics 503 - Graduate Laboratory - Term 142

3rd report

Prompt Gamma-ray Neutron Activation Analysis of CrO_3 Water Samples Using BGO Detector and a Portable Neutron Generator

Extra Work

Penality for late starts = -5

Tot Points for report (for assigned task) = 20

Bonus Points = 5 for energy Resolution Measurement

Mohamed Shemis (g200991810)
Supervised by: Dr. Akhtar Abbas Naqvi
Co-ordinated by: Dr. AbdulAziz Al-Jalal

10/5/2015

Table of Contents

Abstract

High energy capture gamma rays (2-9 MeV) induced from 7.5, 11.4 and 16 % weight ratio of Cr/H_2O samples were tested. A portable pulsed neutron generator and a high density polyethylene moderator were used to produce thermal neutrons. A bismuth germinate $Bi_4Ge_3O_{12}$ (BGO) detector was used to detect the induced prompt gamma rays. Four chromium peaks at energies of 6646, 7100, 7274 and 7938 keV were observed in the spectrum. The integrated intensity of these four peaks plotted versus gamma ray energy, which is known as the calibration curve. The energy resolution was then computed for the prompt gamma rays peaks present in the spectra. A sharp decrease in it was observed at higher energies.

I. Introduction

Prompt Gamma-ray Neutron Activation analysis is an analytical technique used to determine the constituting elements concentrations. Prompt gamma-ray neutron activation analysis (PGNAA) is a non-destructive, in-situ technique that is capable of measuring multielements concentrations in bulk and liquid samples. PGNAA has wide applications in industry, mining quality control, building construction and concrete corrosion, and medical sciences and environmental sciences.

In this technique, the sample is first bombarded with neutron beams. The process of neutrons interaction with the material is called nuclear capture, in which elements nuclei are excited to higher states. Then, the elements nuclei relax and emit gamma rays in two processes, as shown in Figure 1. In the first process, prompt gamma-ray is emitted and the elements decay to the lowest energy state in about 10^{-14} - 10^{-9} seconds after excitation giving energy in the order of 1-10 MeV. Then, the nuclei become either stable or radioactive. The second process is a slow radioactive decay, and it produces beta particles and delayed gamma rays radiation. In Prompt Gamma Neutron activation Analysis (PGNAA), prompt gamma rays are used to determine the constituting elements and their concentrations. After that, prompt gamma rays energies and intensities are measured by a detector through the photoelectric effect. Then, prompt gamma rays energies and intensities are converted to an electrical signals and sent to the computer to be analyzed. Each element has finger-print gamma rays emission which were compared with the emitted gamma rays to test the element existence. Then, elements concentrations are determined from the emitted gamma rays peaks intensities. Good resolution detector is capable of distinguishing between the different gamma rays. High resolution detectors are required for samples with low energy prompt gamma-rays while intense neutron source is required for detection of elements with low neutron capture or scattering cross section. However, the interference between the sample and the detector increases the background noise and decreases the detector sensitivity.

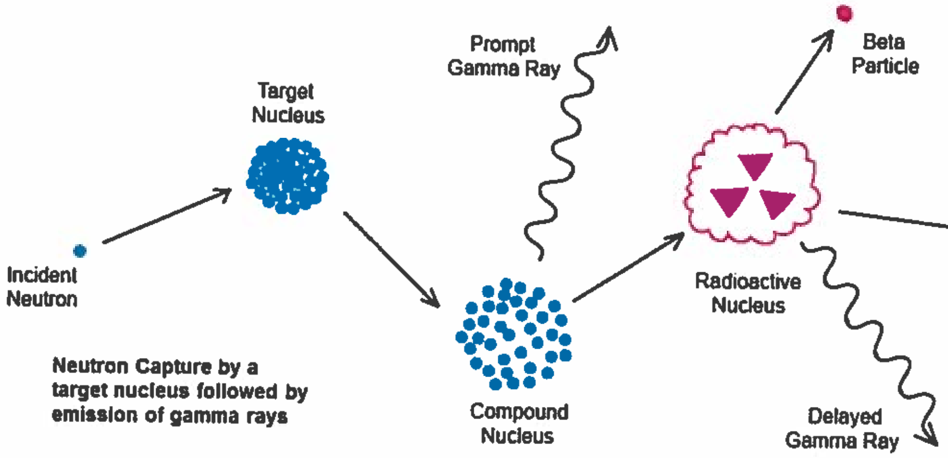

Figure 1. Nuclear decay Process and Prompt Gamma Ray Emission

II. Experimental Methods

A. Sample preparation

The prompt gamma-ray yields from chromium trioxide CrO_3 water samples were tested using PGNAA. Three one litter CrO_3 water solutions of Cr/H_2O weight ratio of 7.5, 11.4 and 16 % were prepared from 4 mol/L CrO_3 water solution by dilution. The experiment on each sample was run for about 90 minutes.

B. Experiment setup

The setup of the PGNAA experiment is shown in Figure 2-3. A portable neutron generator model MP320 was used to generate pulses of 2.5 MeV neutrons beam. A cylindrical modulator of high density polyethylene moderator to decelerate the generated neutrons and convert their energy to thermal energy. The moderator had a central cylindrical cavity of 12 cm diameter to accommodate a specimen and a thickness of 7 cm. The detector was covered from the sides with a 3mm thick lead layer in order to shield the detector from the undesired gamma-rays and neutrons coming from the environment. The axis of neutron beam coming from the neutron generator was perpendicular on to the moderator cylinder axis, while the detector longitudinal axis was along the moderator axis. The sample was inserted in the moderator such that the bottle axis is on the moderator cylinder axis. The BGO detector was coupled to a fast photomultiplier to amplify the output signal. Also detector had a built in integrated preamplifier to process the signals before sending to the computer. However, BGO detector has poor energy resolution, it is preferably used in neutron activation studies due to higher radiation hardness and larger photo peak-efficiency.

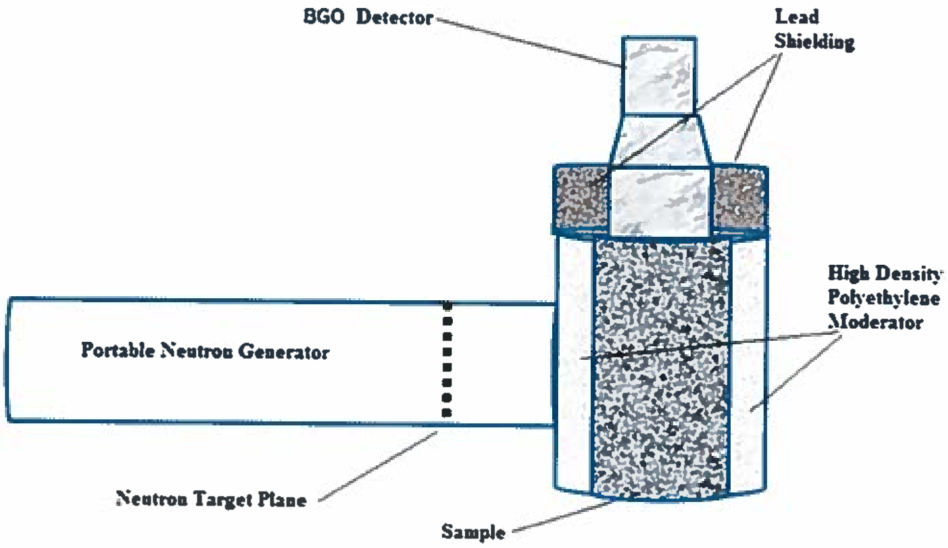

Figure 2: the PGNAA experiment setup

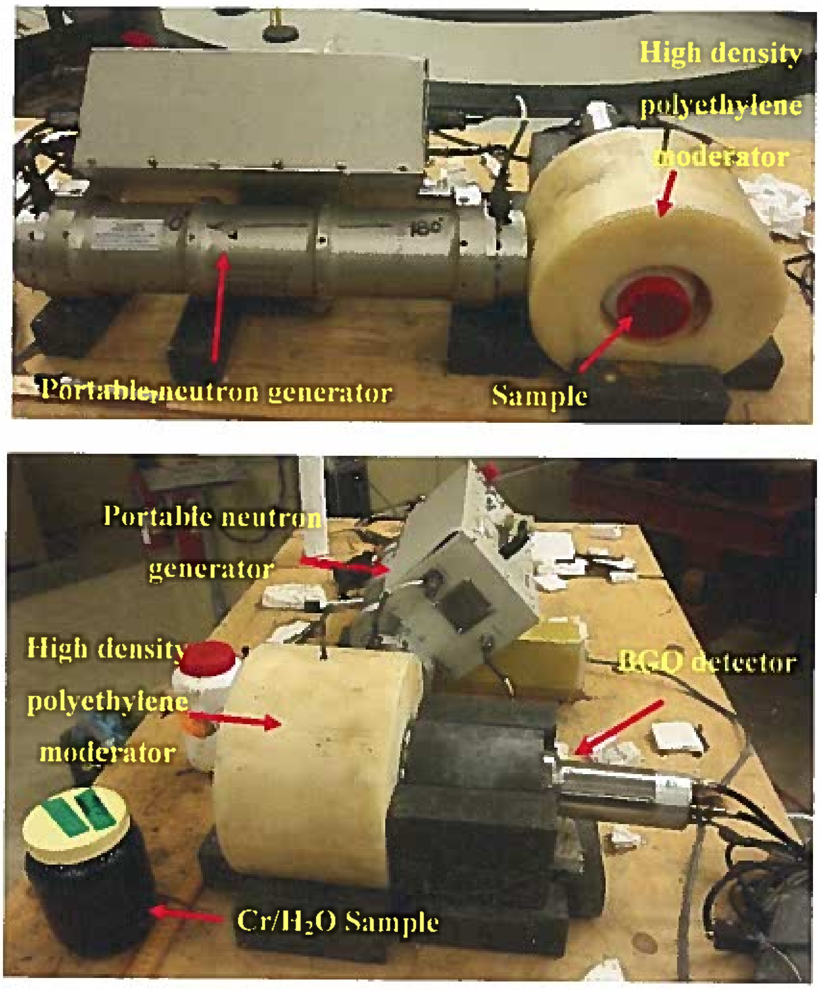

Figure 3: a real view of PGNAA experiment setup

C. *Excitation source*

Neutrons were produced in a portable neutron generator by the fusion of the accelerated deuterons with stationery deuterons, producing helium isotopes ^{3}He.

$$D + D \rightarrow n + {}^3He \qquad E_n = 2.5\ \text{MeV}$$

The portable neutron generator created a pulsed beam of 2.5 MeV neutrons from deuterons beam of 70 keV, 70 μA beam. The deuteron pulse had a width of 5 ns and a frequency of 250 Hz. Gamma-ray detectors vary in energy resolution varying over broad ranges. Bismuth germinate $Bi_4Ge_3O_{12}$ (BGO) detector has energy resolution of about ~ 10%.

III. Results and Discussion

First, the experiment was run with no sample inserted in the moderator to record the background spectrum. This step was important to differentiate between the sample gamma rays peaks and the BGO and noise peaks. Prompt Gamma rays were induced due to the thermal neutron capture in the sample and detector, and they were recorded through the photoelectric effect. A full spectrum of prompt gamma rays was recorded for each sample and the BGO detector background in the range 2000-9000 keV. Figure 4 shows the prompt gamma rays induced from a chromium trioxide solution with 16% Cr/H_2O weight ratio. The energy spectrum below 2000 KeV showed high background noise and thus was rejected. Table 1 shows the elements that correspond to the observed gamma rays peaks in the region 2000-9000 keV and the cross section area corresponding to each gamma ray peak. The right end gamma ray peak is the sum peak due to BGO detector. The spectrum showed peaks corresponding to the elements that exist in the BGO detector and the Cr/H_2O samples, namely Bismuth Bi, Germanium Ge, Hydrogen H and Chromium Cr.

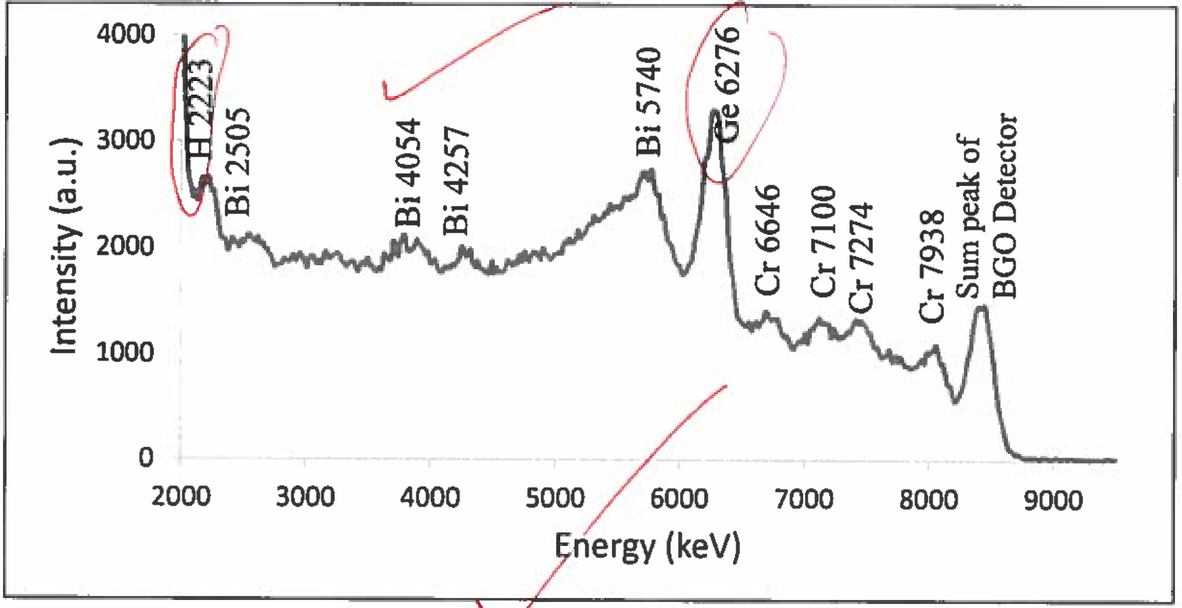

Figure 4: prompt gamma ray spectrum of Cr sample with weight ratio of 16 %.

Extra work

Table 1: prompt gamma rays peaks, their corresponding elements, cross section, FWHM and resolution

Element	Gamma ray energy (keV)	Cross section σ(Eγ) (barns)	FWHM KeV	Resolution FWHM/Eγ (%)
H	2223	0.3326	176	7.9
Bi	2505	0.0021	320	12.8
	4054	0.00136	337	8.3
	4257	0.0024	150	3.5
Fe	5920	0.227		
Ge	6276	0.021	205	3.3
Cr	6646	0.183	149	2.2
	7100	0.146	248	3.5
	7374	0.080	220	3.0
	7938	0.424	168	2.1

The intensity of the four peaks 6646, 7100, 7274 and 7938 keV shown in Figure 5 showed a difference after inserting Cr/H_2O samples with weight ratio of 7.5, 11.4 and 16 %, confirming their correspondence to Cr. The maximum concentration at which the detector is saturated was found to be around 20%. Then, the Cr four lines 6646, 7100, 7274 and 7938 keV were used for plotting the calibration curve. The integrated intensity between 6500 keV and 8200 keV is plotted versus Cr/H_2O weight ratio in Figure 6. The calibration equation showed that the intensity axis intercept $6.2*10^4$ is close to the recorded background integrated intensity $6.2*10^4$, 11% percentage difference, which indicates reliable results and correct peaks identification.

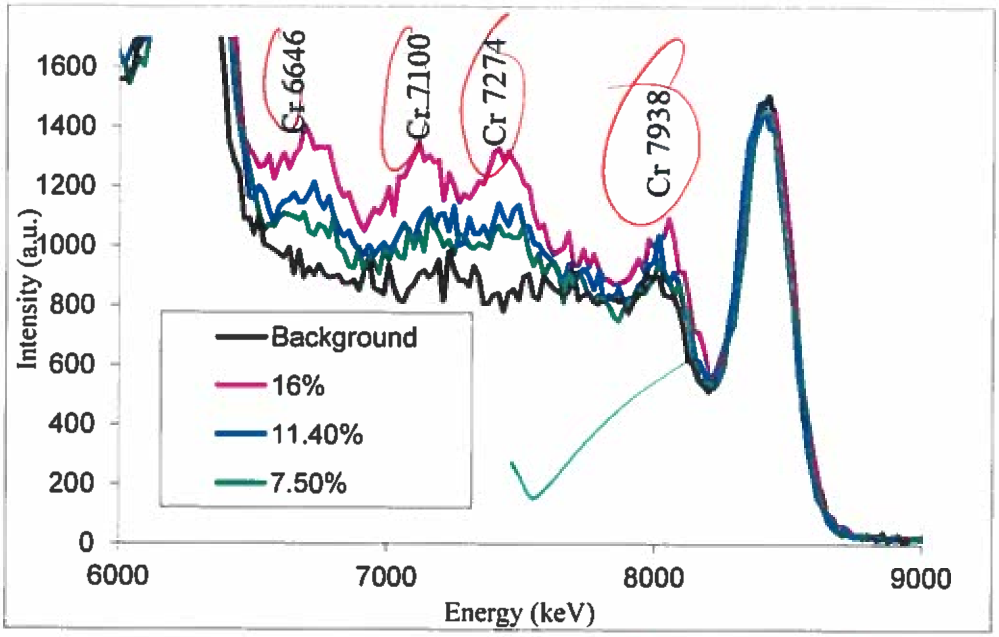

Figure 5: prompt gamma ray spectrum of Cr samples with ~~weight ratio of 16 %~~. 7.5, 11.4 & 16% Concentration (wt%)

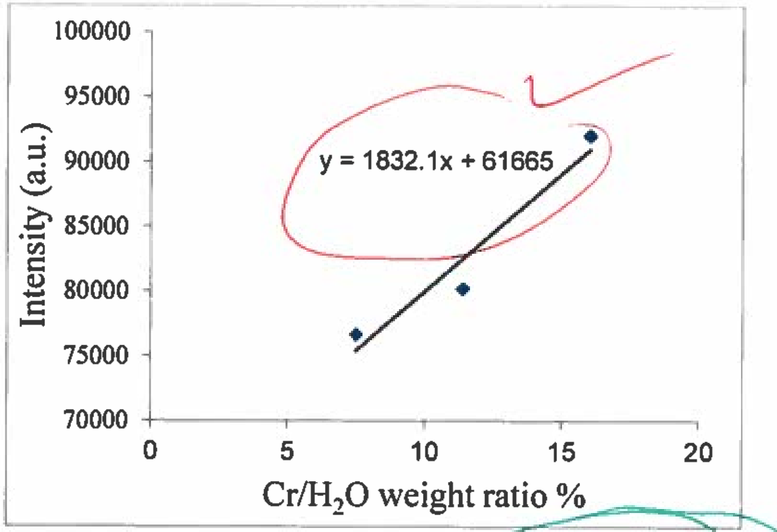

Figure 6: calibration curve of Cr gamma rays peaks integrated intensity in the region 6500-8200 keV. VS Concentrations

Figure 7 shows the energy resolution of the BGO detector defined as FWHM/Eγ for the identified prompt gamma rays peaks in Table 1. It is clear that the energy resolution sharply decreases at higher gamma rays energies.

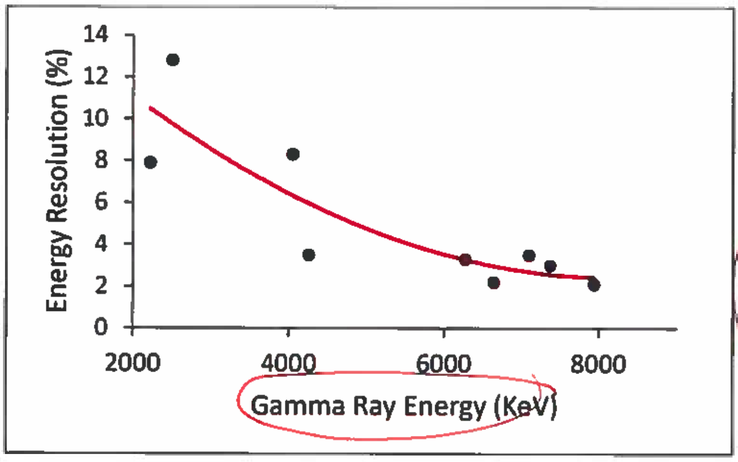

Extra Work

Figure 7: the energy resolution of the prompt gamma rays versus the gamma ray energy.

IV. Conclusion

In this experiment, prompt gamma rays neutron activation analysis was carried out for chromium trioxide samples with Cr/H_2O weight ratio of 7.5, 11.4 and 16 %. A portable pulsed neutron generator was used to excite the samples, and a high density polyethylene moderator was used to produce thermal neutrons and decelerate them. The induced prompt gamma rays due to thermal neutron capture of the sample was detected using a bismuth germinate $Bi_4Ge_3O_{12}$ (BGO) detector. The identified gamma rays peaks were corresponding to Bi, Ge and Cr. The four gamma rays peaks corresponding to Cr 6646, 7100, 7274 and 7938 keV were used for calibration; the integrated intensity of these four peaks were plotted versus Cr/H_2O weight ratio. The energy resolution of the observed peaks were calculated and showed a sharp decrease at higher energy prompt gamma rays.

References

1. A.A. Naqvi, Z. Kalakada, M.S. Al-Anezi, M. Raashid, Khateeb-ur-Rehman, M. Maslehuddin and M.A. Garwan, "Low energy prompt gamma-ray tests of a large volume BGO detector". Applied Radiation and Isotopes 70 (2012) 222–226.
2. A.A. Naqvi, M.S. Al-Anezi, Zameer Kalakada, A.A. Isab, M. Raashid, Faris Ahmed Al Matouq, Khateeb-ur-Rehman, F.Z. Khiari, M.A. Garwan, O.S.B. Al-Amoudi and M. Maslehuddin, "Detection efficiency of low levels of boron and cadmium with a LaBr3:Ce scintillation detector". Nuclear Instruments and Methods in Physics Research A 665 (2011) 74–79.
3. A. Naqvi, Faris A. Al-Matouq, F. Z. Khiari, Khateeb-ur-Rehman M. A. Gondal and A. A. Isab. "Optimization of a prompt gamma setup for analysis of environmental samples". J Radioanal Nucl Chem (2012).
4. A.A. Naqvi, M.S. Al-Anezi, Zameer Kalakada, Faris A. Al Matouq, M. Maslehuddin, M.A. Gondal, A.A. Isab, Khateeb-ur-Rehman and M. Dastageer. "Response tests of a LaCl3:Ce scintillation detector with low energy prompt gamma rays from boron and cadmium". Applied Radiation and Isotopes 70 (2012) 882–887.
5. A. A. Naqvi, Z. Kalakada, M. S. Al-Anezi, F. Al-Matouq, M. Maslehuddin O. S. B. Al-Amoudi. "Performance Evaluation of a Portable Neutron Generator for Prompt Gamma-Ray Applications". Arabian Journal for Science and Engineering 39(2014) 531-539.
6. A. A. Naqvi, M. M. Nagadi, and O. S. B. Al-Amoudi. "Prompt gamma analysis of chlorine in concrete for corrosion study." Applied radiation and isotopes 64 (2006) 283-289.
7. R. B. Firestone, H. D. Choi, R. M. Lindstrom, G. L. Molnar, S. F. Mughabghab, R. Paviotti-Corcuera, Zs Revay, A. Trkov, C. M. Zhou, and V. Zerkin. "Database of prompt gamma rays from slow neutron capture for elemental analysis." Lawrence Berkeley National Laboratory (2004).

King Fahd University of Petroleum and Minerals
Department of Physics
Physics 503 - Term 142

Experiment #1 Report

Student Name : Ibsal Assi

Student ID : 201403420

Code : E303

Evaluator : Dr. Faiz

	grades	Out of
Abstract	0.5	1
Introduction	5	5
Experimental details	4	6
Results and Discussion	6	9
Conclusion	0.5	1
References	1	1
Overall	1	2
Total	18	**25**

H α

جامعة الملك فهد للبترول والمعادن
قسم الفيزياء
RECEIVED
08 MAR 2015
وارد
King Fahd University of Petroleum & Minerals
PHYSICS DEPT

Department of Physics

PHYS503: Graduate Lab

Term: 142

Gamma Ray Spectroscopy and the Measurement of Potassium Concentration in KH_2PO_4 sample

Done by:

Mr. Ibsal Assi

ID#: 201403420

Under the supervision of:

Dr. Nidal Dwaikat

Date of Submission:

8th of March, 2015.

Contents

Abstract

NaI (Tl) detector has been used to find percentage of potassium K-40 in KH_4PO_4. Two standard sources of Cs-137 and Co-60 were used to calibrate the NaI(Tl) and then a sample is used to calculate the percentage of potassium that composed in it through peak analysis. We found that there's 7.25 grams of K-40 in the 250 gram sample of KH2PO4.

Page #'s missing

Introduction

1.1: Radiation

We live in a universe in which radiation is part of everyday life. Natural radiation is ubiquitous in our environment and each of us is exposed to radiation every day. Radiation sources can be divided into natural and man-made sources. Naturally occurring radioisotopes are found in soil, rocks, and in water and food as a product of reactions with soil and rocks. The most important natural isotopes that occur in air, in drinking water and in food are the isotopes of hydrogen (tritium: ^{3}H), carbon (^{14}C), potassium (^{40}K), polonium (^{210}Po), radon (^{222}Rn), radium (^{226}Ra and ^{228}Ra), and uranium (^{238}U) [1–4]

1.2: Gamma Ray interaction with matter:

Gamma rays interact with matter through three main ways. At first,

Photoelectric Absorption which take place for low energetic γ-photons (several keVs) and high atomic number materials. Secondly, **Pair Production** (Electron and positron) which predominates for low Z materials (Z: Atomic Number) and high energetic gamma particles (5-10 MeVs). Lastly, **Compton Scattering** which happens between both extremes and the most probably to happen. Figure [1] describes those interactions mentioned above.

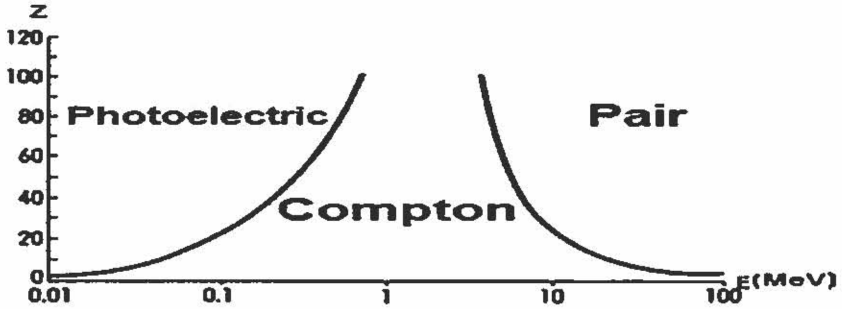

Figure [1]: Gamma Ray interaction mechanisms with matter versus the atomic number of the target.[*]

To begin, the photoelectric effect is one of those interaction mechanisms at which the γ-particle hit the material and then a bound electron will be ejected with energy given by equation [[1]] below:

$E_e = E_\gamma - \Phi$ .... [[1]] where E_γ is the energy of the incident photon and Φ is the work function of the specific material

The second type of interactions is called Compton Scattering which happens between a free (unbounded) electron which causes a scattering of the gamma particle and recoiling of the free electron, the energy gained by this electron is given by equation [[2]] below:

$$E_e = E_\gamma - E_{\gamma'} = hf\,\frac{\left(\frac{hf}{mc^2}\right)(1-\cos(\theta))}{1+\left(\frac{hf}{mc^2}\right)(1-\cos(\theta))} \text{.............. [[2]]}$$

Where h is blank's constant, f is the frequency of the incident gamma ray, c the speed of light and θ is the recoiling angle of the recoiled electron which varies from 0 to Pi which causes a continuum energy spectrum.

The last interaction mechanism, which's the pair production, happens when gamma particle with enough energy travels near the nucleus of the absorbed material turns into an electron and positron. That case happens very fast since the positron is an unstable particle and the energy will be released back to the system. The annihilation photon in some cases will be absorbed by the material which results in a peak called *single escape peak* appears on the pulse height spectrum.

The total energy of the pairs can be calculated through equation [[3]]:

$$\mathrm{E}_{e-} + \mathrm{E}_{e+} = \mathrm{hf} - 2mc^2 \text{ .... [[3]]}$$

1.3: Objectives

The main targets of this experiment are: Using Gamma spectroscopy to analyze unknown samples and determine what does it compose of through the analysis of the energies of gamma radiation using spectroscopy system like NaI(TI) detector system which we used in this experiment. Also, Be familiar with spectral analysis and the spectroscopy techniques at the sodium iodide level.

Experimental Setup and Procedure

2.1: NaI detector apparatus

In 1948, it was reported that there was a large scintillation phenomenon caused by adding doped Thallium (Tl) into a crystal of Sodium Iodide (NaI), that was the beginning of manufacturing of NaI detector. Our NaI(Tl) crystal is of size 5x5 inches and it consists of the NaI(Tl) crystal, light pipe, photocathode, and lastly the photomultiplier tube (PMT). Figure [2] below shows a schematic diagram of the NaI(Tl) detector.

o

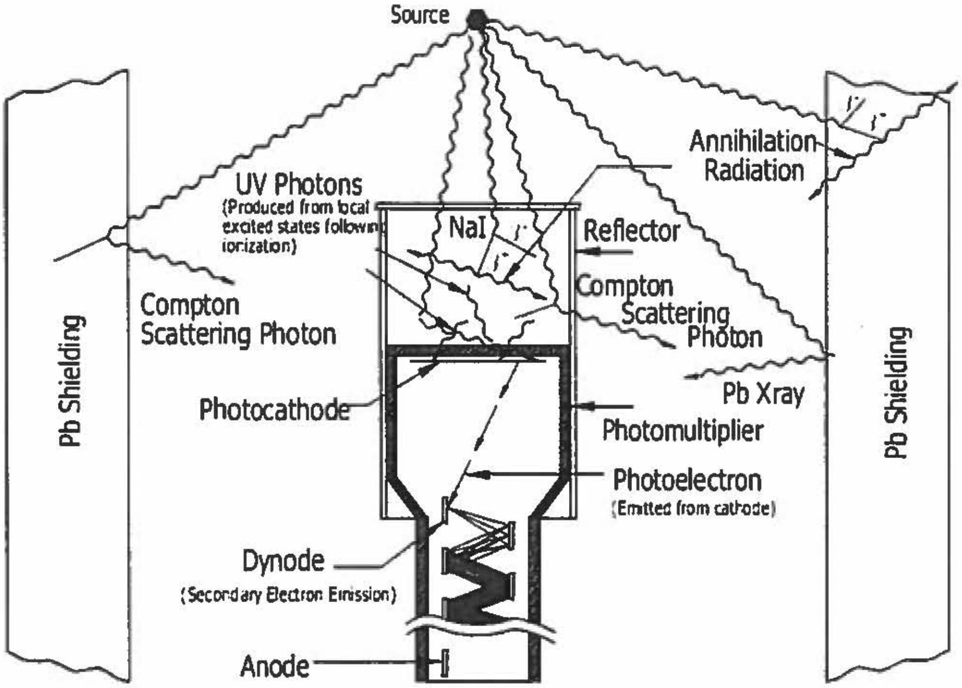

Figure [2]: NaI(Tl) detector shielded with lead blocks. [2]

When the photon emitted from the source towards the crystal it frees an electron from the crystal (Photoelectron) and after de-excitation a photon will travel directly to the photocathode as shown in figure [2]. An electron will be produced and then will enter the region called ***photomultiplier tube*** which takes an electron from the Dynode and accelerated through those Dynodes. In each acceleration process more electrons do travel to the final destination at the anode as described in the last figure.

The process of increasing the number of electrons will continue and the final number of electrons will be in the order of ten thousands or even more. The amount of charge arrived at the anode is proportional to the number of electrons left the photocathode and by the photoelectric effect this will be proportional to the energy deposited in the crystal by gamma ray. The charges now will leave the anode directly to the ***Preamplifier*** which prepares the electric signal to further amplification through the amplifier. The preamplifier is placed close to the detector to reduce the noise and the interference of the signals. The ***Amplifier*** will amplify the signal and shape it and then transfer it directly to the ***Multichannel Analyzer***which converts the analog signal to digital (ADC) and then take the signal to the PC to analyze it through the software.

The sample is placed close to the detector then the systemshielded by lead blocks.Then we analyzed the spectrum for some period of time. Then we removed the sample and analyze the spectrum of the background for the same period of time which helps us to figure out the percentage amount of Potassium in the sample through some analysis which will be mentioned in the main part.

The figure below shows the NaI spectroscopy system used in this experiment:

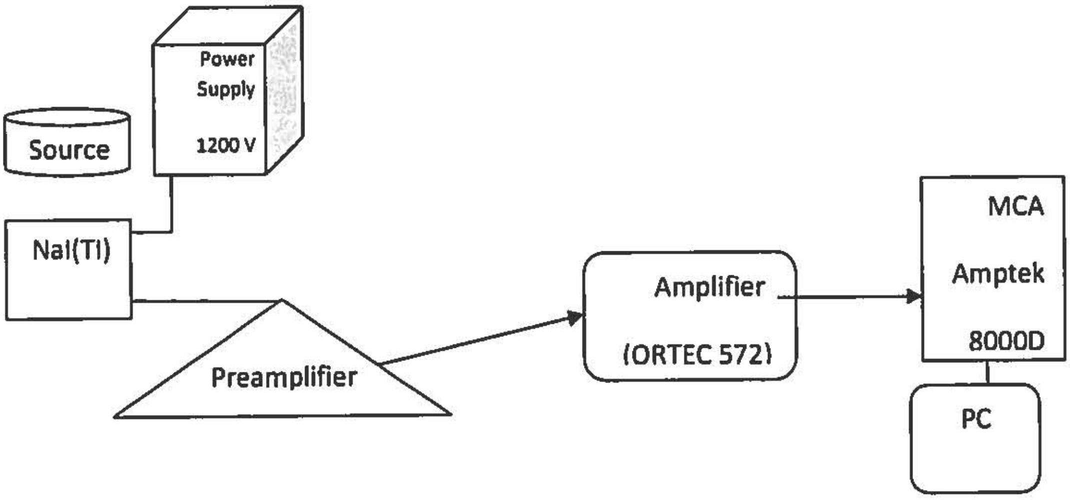

Figure [3]: The apparatus of the experiment from the source to the PC

2.2 Method Used:

1- The electronic parts connected together as shown in figure [3]. Cs-137 standard source has been used to find the operational voltage. We changed the voltage from

850 volts till 1250 volts to find the best resolution which was at 1200 V (operational voltage)(highest resolution)

2- Next, two standard sources have been placed separately and study their individual spectrum alone and that's a part of the energy calibration which mentioned in the next part. in each of them, the source placed close to the detector then the system shielded and the spectrum has been studied over some period of time. For the Cesium, for example, we adjusted the fine gain of the amplifier so that the peak will be centered at 600 in 2048 channel system.

3- The spectral size have been changed using the MCA to see how the peaks and their resolution are affected by the spectrum size.

4- The sample has been placed close to the detector and the system shielded and left for 1800 seconds and a clear spectrum has been seen. Then after, the sample has been taken away and records of the detector spectrum without the sample taken (background).

2.3: Sample Preparation:

A sample of Potassium Dihydrogen Phosphate was used to measure the concentration of potassium K-40 in the sample using NaI(Tl) detector.

Calibrations, results and comments

3.1: Resolution and the Operational Voltage

Move to next page

Resolution is a measure of the degree of broadening and defined as the ration between the *full width at half maxima (FWHM)* to the pulse height (centroid), see equation [[4]] below:

$$R=\frac{FWHM}{Centroid}x100\% \text{ ……………. [[4]]}$$

The operational voltage has been determined at which the peak has highest resolution. The following table shows the voltage readings versus the resolution:

Input Voltage (Volts)	R
950	7.03%
1000	6.79%
1050	6.55%
1100	6.38%
1150	5.85%
1200	5.68%

Table [1]: The input voltage versus the resolution. Operational voltage is 1200V

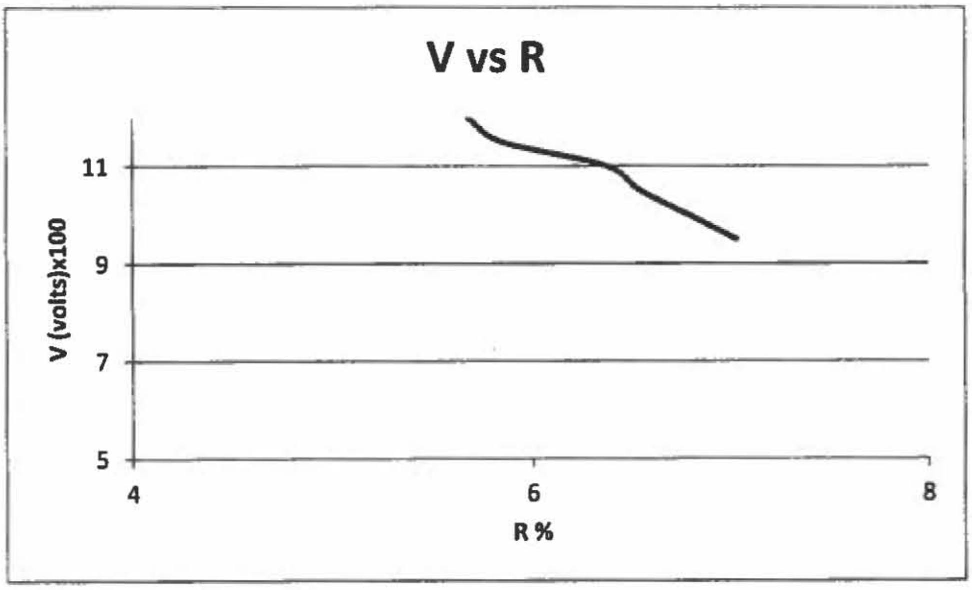

Figure [4]: The input voltage versus the resolution

Figure [4.5] shows the effect of spectrum size on the resolution

?

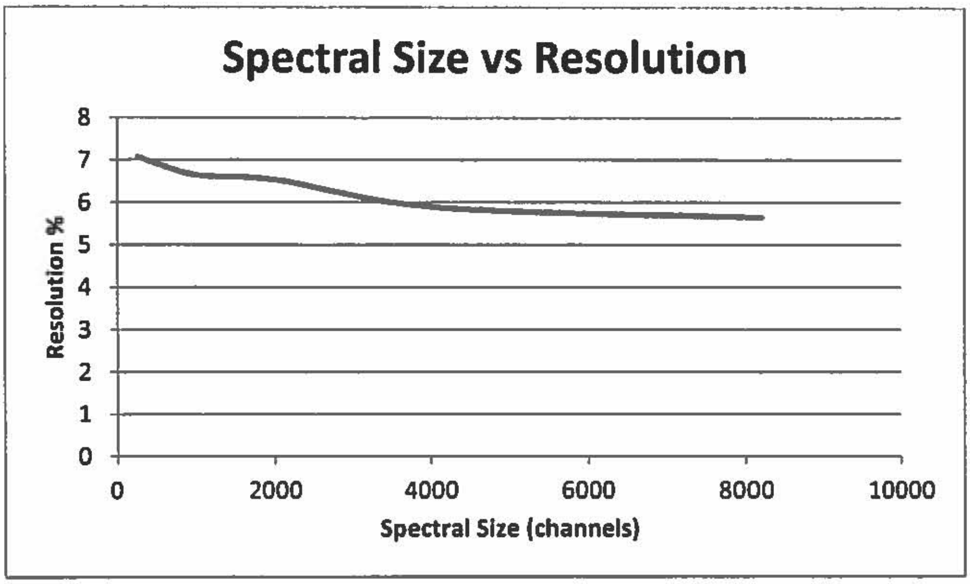

Figure [4.5]: Spectral size versus the resolution

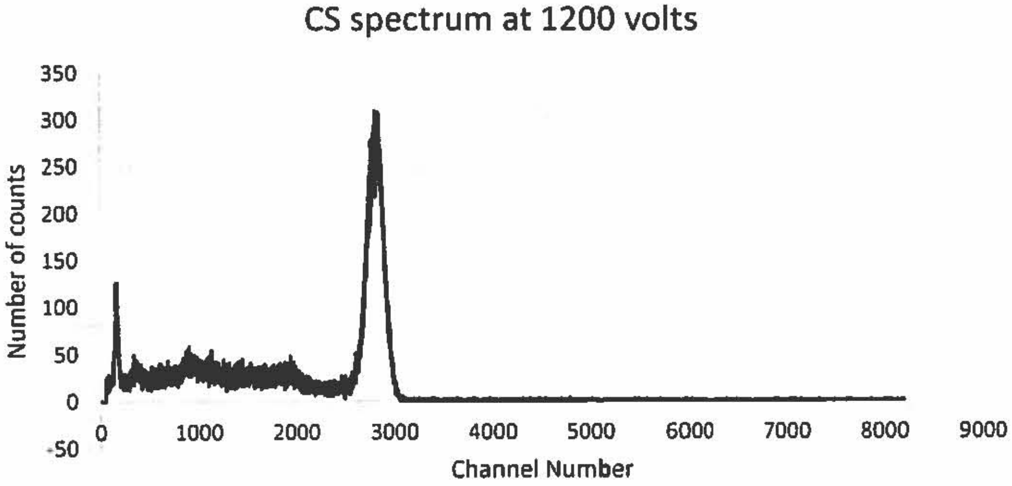

Figure [5]: The spectrum of Cs at the operational voltage (highest resolution)

3.2: Energy Calibration of NaI(Tl):

Setup calibration is an important step in spectral analysis since the system does not read the data directly and that's like a reference frame in the language of mathematics. Calibration can be done through known sources, in our case we used 137_{Cs} and 60_{CO} as known sources to calibrate the system. The first source has one peak at 0.662MeV and the second has two peaks at 1.173MeV and 1.332MeV respectively.

Figure [5] shows the calibration curve of the standard sources:

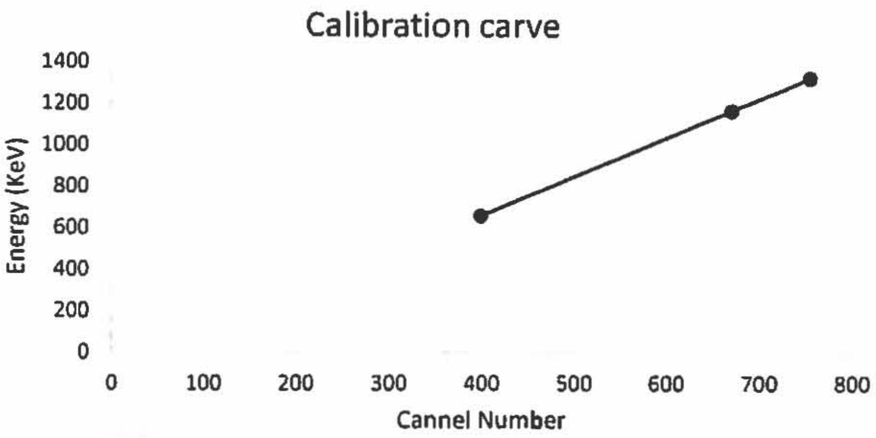

Figure [5]: Calibration curve. Equation: E=1.88521*Channel-90.8217

Table [2] shows the calculated values of the energy and the real ones:

Source	Calculated Energy (keV)	Actual Energy (keV)
Cs137	661.72	662
Co60[1]	117.35	117.3
Co60[2]	133.108	133.2

Table [2]: Energy values of the sources.

Lastly, figures [6] and [7] shows the spectrums of Cs and Co respectively:

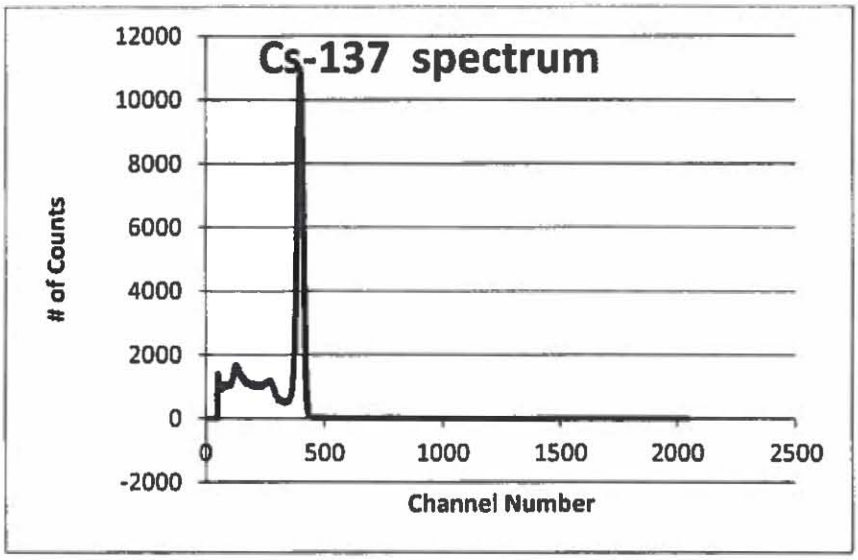

Figure [6]: Cs spectrum

What is the difference
between this figure and
the previous Cs-Spectrum figure?

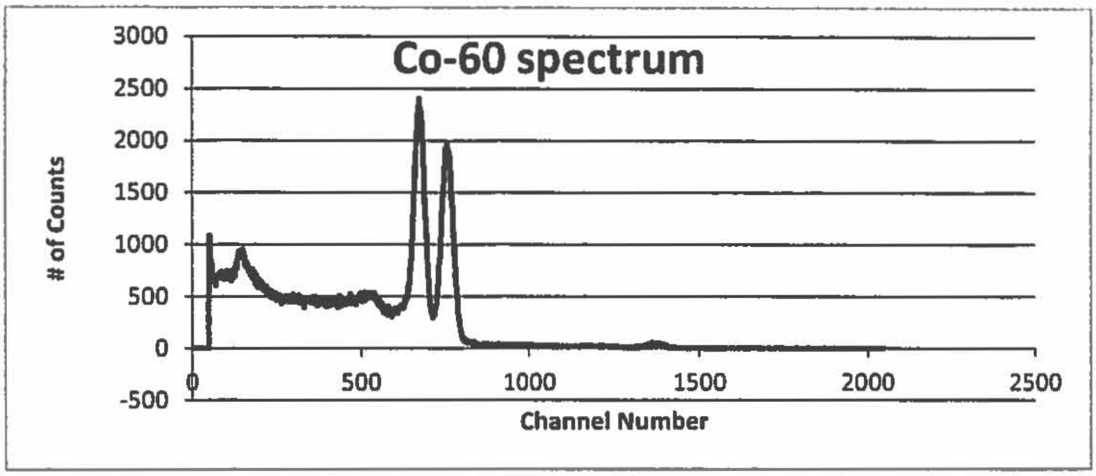

Figure [7]: Spectrum of cobalt.

3.3: K-40 concentration in Standard source

Figures [8] and [9] shows the spectrums of the source and the background, respectively:

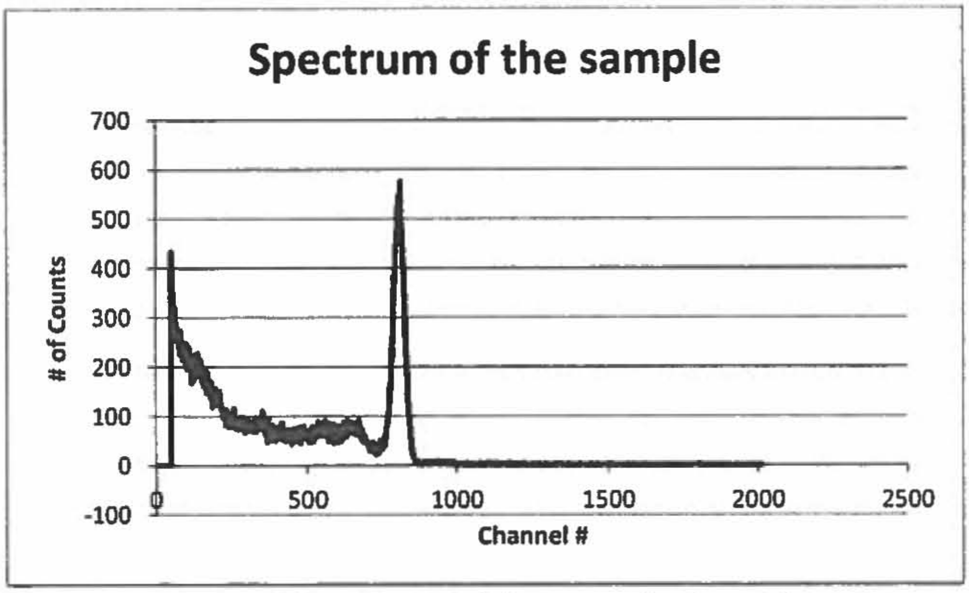

Figure [8]: Spectrum of the source (un-known)

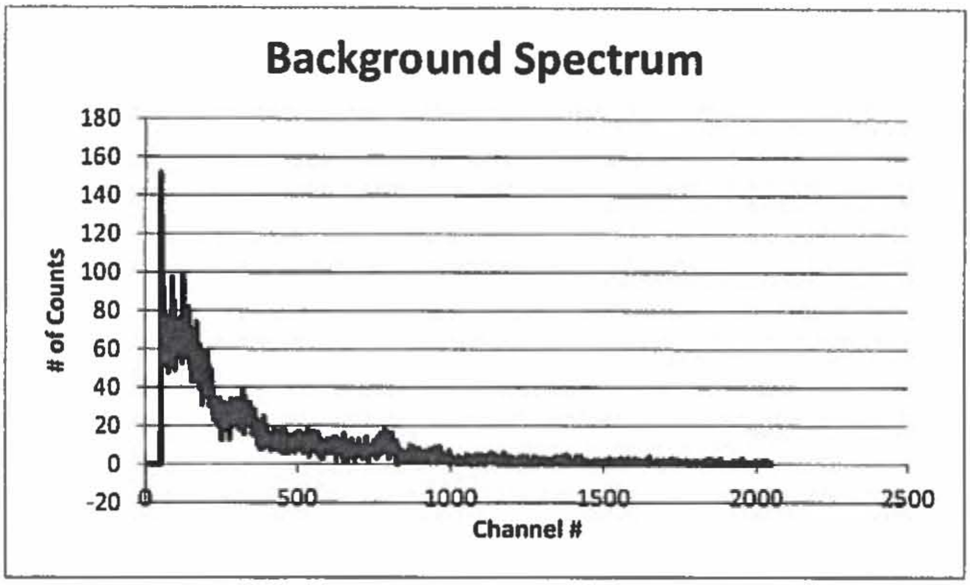

Figure [9]: Background Spectrum

A 250 g of Sodium Dihydrogen Phosphate sample has been used to calculate the % of Potassium (K-40). The peak was at the channel 806.6 as shown in figure [8] which's the potassium peak, in the next figure the potassium peak from the background shown at same position (Energy of 1430 keV). ??

not clear

The activity of the sample can be calculated using the absolute method:

$$A_U = \frac{C_U - C_b}{t\,\varepsilon\, f} \text{ .... [[5]]}$$

? where did you use this eq^n?

Where: A_U is the activity of the sample, C's are the number of counts, t is the time of measurement, ε is the efficiency of the peak, and f is the decay fraction.

Calculations

Molecular weight of the sample=136.09 g/mole

Relative content of K40=0.012%, Half time=1.28x10^9 $years$

The activity then becomes A=227.3 kBq.

?

The calibration factor= $K_f = \frac{Activity}{Counting\ Rate} = \frac{227.3*1000}{12.41} = 18316 Bq.s$

not clear

K40 counting rate=0.036 (1/s) → A(K40)=rate*K_f=660 Bq

Now,

Atomic weight of Potassium= 39.01 g/mole

→ Potassium portion is 71.7 grams

The specific activity=$\frac{A}{m}$=9.2Bq/g

Thus, the % of potassium is: $\frac{92}{3170}$

? Not clear

3.4: Results and Comments:

* Operational Voltage: 1200 V

* Calibration Equation: $Energy = 1.88521 * Channel\# - 90.8217$

* K-40 concentration was around 3% of the sample which's 7.25 g out of 250 g sample.

The amount of K-40 in the sample was small compared to the weight of the sample. Using NaI(TI) detector it was easy to calculate the percentage of K-40 through studying the spectrum of the sample and focusing on the potassium peak.

Conclusion:

Two standard source of Cs and Co has been used to calibrate the system and a sample used to measure the percentage of potassium in it through the NaI(Tl) detector system. NaI(Tl) can be used to analyze samples and find the concentration of the elements that compositedin the sample through the idea of energy study (spectroscopy). Mention your findings here -

REFERENCES

1. Akiko Kitajima et al., Monitoring low-radioactivity caesium in Fukushima waters, Environ. Sci.: Processes Impacts, 16 (2014) 28.
2. Claus Grupen, Introduction to Radiation Protection, copyright © Springer-Verlag Berlin Heidelberg (2010) pp. 172-174.
3. A. Baeza, A. Salas, J. Guillén , A. Muñoz-Serrano, Association of naturally occurring radionuclides in sludges from Drinking Water Treatment Plants previously optimized for their removal, Chemosphere 97 (2014) 108.
4. Ndéye Marième Wade-Gueye, Chronic exposure to natural uranium via drinking water affects bone in growing rats, Biochimica et Biophysica Acta 1820 (2012) 1121